

CERN-EP/2016-227
2017/05/11

CMS-TOP-16-008

Measurement of differential cross sections for top quark pair production using the lepton+jets final state in proton-proton collisions at 13 TeV

The CMS Collaboration*

Abstract

Differential and double-differential cross sections for the production of top quark pairs in proton-proton collisions at 13 TeV are measured as a function of jet multiplicity and of kinematic variables of the top quarks and the top quark-antiquark system. This analysis is based on data collected by the CMS experiment at the LHC corresponding to an integrated luminosity of 2.3 fb^{-1} . The measurements are performed in the lepton+jets decay channels with a single muon or electron in the final state. The differential cross sections are presented at particle level, within a phase space close to the experimental acceptance, and at parton level in the full phase space. The results are compared to several standard model predictions.

Published in Physical Review D as doi:10.1103/PhysRevD.95.092001.

arXiv:1610.04191v2 [hep-ex] 10 May 2017

1 Introduction

Studying the differential production cross sections of top quark pairs ($t\bar{t}$) at high energies is a crucial ingredient in testing the standard model and searching for sources of new physics, which could alter the production rate. In particular, the differential $t\bar{t}$ cross sections probe predictions of quantum chromodynamics (QCD) and facilitate the comparisons of the data with state-of-the-art calculations. In addition, some of the measured distributions, especially distributions of invariant mass and rapidity of the $t\bar{t}$ system, can be used to improve our understanding of parton distribution functions (PDFs).

A measurement of the $t\bar{t}$ differential and double-differential production cross sections as a function of jet multiplicity and of kinematic variables of the top quarks and the $t\bar{t}$ system is presented. The measurement is based on proton-proton collision data at a center-of-mass energy of 13 TeV corresponding to an integrated luminosity of 2.3 fb^{-1} [1]. The data were recorded by the CMS experiment at the CERN LHC in 2015. This measurement makes use of the $t\bar{t}$ decay into the ℓ +jets ($\ell = e, \mu$) final state, where, after the decay of each top quark into a bottom quark and a W boson, one of the W bosons decays hadronically and the other one leptonically. The τ lepton decay mode is not considered here as signal. The differential cross sections are presented as a function of the transverse momentum p_T and the absolute rapidity $|y|$ of the hadronically (t_h) and the leptonically (t_ℓ) decaying top quarks; as a function of p_T , $|y|$, and mass M of the $t\bar{t}$ system. The cross section is also measured as a function of the number of additional jets in the event. In addition, the differential cross sections as a function of $p_T(t_h)$ and $p_T(t\bar{t})$ are measured in bins of jet multiplicity and double-differential cross sections for the following combinations of variables are determined: $|y(t_h)|$ vs. $p_T(t_h)$, $M(t\bar{t})$ vs. $|y(t\bar{t})|$, and $p_T(t\bar{t})$ vs. $M(t\bar{t})$.

This measurement continues a series of differential $t\bar{t}$ production cross section measurements in proton-proton collisions at the LHC. Previous measurements at 7 TeV [2, 3] and 8 TeV [4–8] have been performed in various $t\bar{t}$ decay channels.

The differential cross sections are presented in two different ways, at particle level and at parton level. For the particle-level measurement a proxy of the top quark is defined based on experimentally accessible quantities like jets, which consist of quasi-stable particles with a mean lifetime greater than 30 ps. These are described by theoretical calculations that, in contrast to pure matrix-element calculations, involve parton shower and hadronization models. These objects are required to match closely the experimental acceptance. A detailed definition is given in Section 3. Such an approach has the advantage that it reduces theoretical uncertainties in the experimental results by avoiding theory-based extrapolations from the experimentally accessible portion of the phase space to the full range, and from jets to partons. However, such results cannot be compared to parton-level calculations.

For the measurement at parton level, the top quarks are defined directly before decaying into a bottom quark and a W boson. For this analysis the parton-level $t\bar{t}$ system is calculated at next-to-leading order (NLO) and combined with a simulation of the parton shower. No restriction of the phase space is applied for parton-level top quarks.

The experimental signature is the same for both measurements and consists of two jets coming from the hadronization of b quarks (b jets), two jets from a hadronically decaying W boson, a transverse momentum imbalance associated with the neutrino, and a single isolated muon or electron.

This paper is organized as follows: In Section 2 we provide a description of the signal and background simulations, followed by the definition of the particle-level top quarks in Section 3. After a short overview of the CMS detector and the particle reconstruction in Section 4, we

describe the object and event selections in Sections 5 and 6, respectively. Section 7 contains a detailed description of the reconstruction of the $t\bar{t}$ system. Details on the background estimation and the unfolding are presented in Sections 8 and 9. After a discussion on systematic uncertainties in Section 10, the results are finally presented in Section 11.

2 Signal and background modeling

The Monte Carlo programs POWHEG [9–12] (v2) and MADGRAPH5_aMC@NLO [13] (v2.2.2) (MG5_aMC@NLO) are used to simulate $t\bar{t}$ events. They include NLO QCD matrix element calculations that are combined with the parton shower simulation of PYTHIA [14, 15] (v8.205) (PYTHIA8) using the tune CUETP8M1 [16]. In addition, MG5_aMC@NLO is used to produce simulations of $t\bar{t}$ events with additional partons. In one simulation all processes of up to three additional partons are calculated at leading order (LO) and combined with the PYTHIA8 parton shower simulation using the MLM [17] algorithm. In another simulation all processes of up to two additional partons are calculated at NLO and combined with the PYTHIA8 parton shower simulation using the FxFx [18] algorithm. The default parametrization of the PDF used in all simulations is NNPDF30_nlo_as_0118 [19]. A top quark mass $m_t = 172.5 \text{ GeV}$ is used. When compared to the data, simulations are normalized to an inclusive $t\bar{t}$ production cross section of $832^{+40}_{-46} \text{ pb}$ [20]. This value is calculated with next-to-NLO (NNLO) precision including the resummation of next-to-next-to-leading-logarithmic (NNLL) soft gluon terms. Its given uncertainty is due to the choice of hadronization/factorization scales and PDF.

In all simulations, event weights are calculated that represent the usage of the uncertainty eigenvector sets of the PDF. There are also event weights available that represent the changes of factorization and renormalization scales by a factor of two or one half. These additional weights allow for the calculation of systematic uncertainties due to the PDF and the scale choices. For additional uncertainty estimations we use POWHEG+PYTHIA8 simulations with top quark masses of 171.5 and 173.5 GeV, with parton shower scales varied up and down by a factor of two, and a simulation with POWHEG combined with HERWIG++ [21] (v2.7.1) using the tune EE5C [22].

The main backgrounds are produced using the same techniques. The MG5_aMC@NLO generator is used for the simulation of W boson production in association with jets, t -channel single top quark production, and Drell–Yan (DY) production in association with jets. The POWHEG generator is used for the simulation of single top quark associated production with a W boson (tW) and PYTHIA8 is used for multijet production. In all cases the parton shower and the hadronization are described by PYTHIA8. The W boson and DY backgrounds are normalized to their NNLO cross sections [23]. The single top quark processes are normalized to NLO calculations [24, 25], and the multijet simulation is normalized to the LO calculation [15].

The detector response is simulated using GEANT4 [26]. Afterwards, the same reconstruction algorithms that are applied to the data are used. Multiple proton-proton interactions per bunch crossing (pileup) are included in the simulation. To correct the simulation to be in agreement with the pileup conditions observed during the data taking, the average number of pileup events per bunch crossing is calculated for the measured instantaneous luminosity. The simulated events are weighted, depending on their number of pileup interactions, to reproduce the measured pileup distribution.

3 Particle-level top quark definition

The following list describes the definitions of objects constructed from quasi-stable particles, obtained from the predictions of $t\bar{t}$ event generators before any detector simulation. These objects are further used to define the particle-level top quarks.

- Muons and electrons that do not have their origin in a decay of a hadron are selected and their momenta are corrected for the final-state radiation effects. The anti- k_T jet algorithm [27, 28] with a distance parameter of 0.1 is used to cluster the leptons and photons not originating from hadron decays. Those photons that are clustered together with a selected lepton are assumed to have been radiated by the lepton and their momenta are added to the lepton momentum. However, the lepton is only selected if the original p_T is at least half of their corrected p_T .
- All neutrinos that do not have their origin in a decay of a hadron are selected.
- Jets are clustered by the anti- k_T jet algorithm with a distance parameter of 0.4. All quasi-stable particles are considered, excluding the selected neutrinos and leptons together with their radiated photons.
- b jets at particle level are defined as those jets that contain a b hadron. As a result of the short lifetime of b hadrons, only their decay products should be considered for the jet clustering. However, to allow their association to a jet, the b hadrons are also included with their momenta scaled down to a negligible value. This preserves the information of their directions, but they have no impact on the jet clustering itself.

Based on the invariant masses M of these objects, we construct a pair of particle-level top quarks in the ℓ +jets final state. Events with exactly one muon or electron with $p_T > 30$ GeV and an absolute pseudorapidity $|\eta| < 2.5$ are selected. We take the sum of the four-momenta of all selected neutrinos as the neutrino momentum p_ν from the leptonically decaying top quark and find the permutation of jets that minimizes the quantity

$$K^2 = [M(p_\nu + p_\ell + p_{b_\ell}) - m_t]^2 + [M(p_{j_1} + p_{j_2}) - m_W]^2 + [M(p_{j_1} + p_{j_2} + p_{b_h}) - m_t]^2, \quad (1)$$

where $p_{j_{1/2}}$ are the four-momenta of two light-flavor jet candidates, $p_{b_{\ell/h}}$ are the four-momenta of two b-jet candidates, p_ℓ is the four-momentum of the lepton, and $m_W = 80.4$ GeV is the mass of the W boson. All jets with $p_T > 25$ GeV and $|\eta| < 2.5$ are considered. At least four jets are required, of which at least two must be b jets. If there are more than two b jets, we allow b jets as decay products of the proxy for the hadronically decaying W boson. Due to a limited efficiency of the b jet identification at detector level this improves the agreement between the reconstructed top quarks and the particle-level top quarks. The remaining jets with the same kinematic selection are considered as additional jets at particle level.

It should be remarked that events with a hadronic and a leptonic particle-level top quark are not required to be ℓ +jets events at the parton level. As an example, in Fig. 1 the relation between the $p_T(t_h)$ values at particle and parton level is shown.

4 The CMS detector

The central feature of the CMS detector is a superconducting solenoid of 6 m internal diameter, providing a magnetic field of 3.8 T. Within the solenoid volume are a silicon pixel and strip tracker, a lead tungstate crystal electromagnetic calorimeter (ECAL), and a brass and scintillator hadron calorimeter (HCAL), each composed of a barrel and two endcap sections. Forward calorimeters extend the η coverage provided by the barrel and endcap detectors. Muons

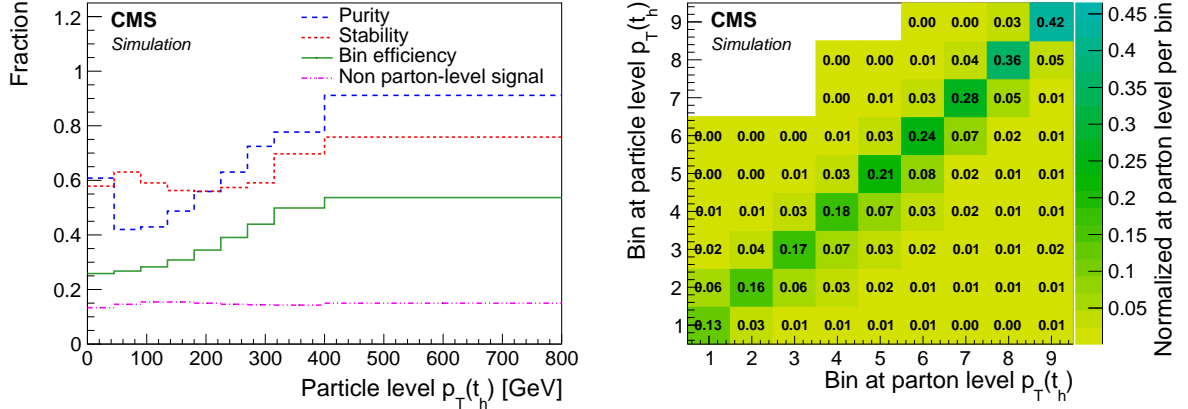


Figure 1: Comparison between the $p_T(t_h)$ at particle and parton level, extracted from the POWHEG+PYTHIA8 simulation. Left: fraction of parton-level top quarks in the same bin at particle level (purity), fraction of particle-level top quarks in the same bin at parton level (stability), ratio of the number of particle- to parton-level top quarks, and fraction of events with a particle-level top quark pair that are not considered as signal events at parton level. Right: bin migrations between particle and parton level. The p_T range of the bins can be taken from the left panel. Each column is normalized to the number of events per column at parton level in the full phase space.

are measured in gas-ionization detectors embedded in the steel flux-return yoke outside the solenoid. A more detailed description of the CMS detector, together with a definition of the coordinate system and relevant kinematic variables, can be found in Ref. [29].

The particle-flow (PF) event algorithm [30, 31] reconstructs and identifies each individual particle with an optimized combination of information from the various elements of the CMS detector. The energy of photons is directly obtained from the ECAL measurement, corrected for zero-suppression effects. The energy of electrons is determined from a combination of the electron momentum at the primary interaction vertex as determined by the tracker, the energy of the corresponding ECAL cluster, and the energy sum of all bremsstrahlung photons spatially compatible with originating from the electron track. The energy of muons is obtained from the curvature of the corresponding track. The energy of charged hadrons is determined from a combination of their momentum measured in the tracker and the matching ECAL and HCAL energy deposits, corrected for zero-suppression effects and for the response function of the calorimeters to hadronic showers. Finally, the energy of neutral hadrons is obtained from the corresponding corrected ECAL and HCAL energy.

5 Physics object reconstruction

This analysis depends on the reconstruction and identification of muons, electrons, jets, and missing transverse momentum associated with a neutrino. Only leptons are selected that are compatible with originating from the primary vertex, defined as the vertex at the beam position with the highest sum of p_T^2 of the associated tracks. Leptons from $t\bar{t}$ decays are typically isolated, i.e., separated in $\Delta R = \sqrt{(\Delta\phi)^2 + (\Delta\eta)^2}$ from other particles. A requirement on the lepton isolation is used to reject leptons produced in decays of hadrons.

The muon isolation variable is defined as the sum of the p_T of all tracks, except for the muon track, originating from the $t\bar{t}$ interaction vertex within a cone of $\Delta R = 0.3$. It is required to be less than 5% of the muon p_T . The muon reconstruction and selection [32] efficiency is measured

in the data using tag-and-probe techniques [33]. Depending on the p_T and η of the muon it is 90–95%.

For electrons the isolation variable is the sum of the p_T of neutral hadrons, charged hadrons, and photon PF candidates in a cone of $\Delta R = 0.3$ around the electron. Contributions of the electron to the isolation variable are suppressed excluding a small region around the electron. This isolation variable is required to be smaller than 7% of the electron p_T . An event-by-event correction is applied that maintains a constant electron isolation efficiency with respect to the number of pileup interactions [34]. The measured reconstruction and identification [35] efficiency for electrons is 70–85% with a p_T and η dependence.

Jets are reconstructed from PF objects clustered using the anti- k_T jet algorithm with a distance parameter of 0.4 using the FASTJET package [28]. Charged particles originating from a vertex of a pileup interaction are excluded. The total energy of the jets is corrected for energy depositions from pileup. In addition, p_T - and η -dependent corrections are applied to correct for detector response effects [36]. Those jets identified as isolated muons or electrons are removed from consideration.

For the identification of b jets the combined secondary vertex algorithm [37] is used. It provides a discriminant between light-flavor and b jets based on the combined information of secondary vertices and the impact parameter of tracks at the primary vertex. A jet is identified as b jet if the associated value of the discriminant exceeds a threshold criterion. Two threshold criteria are used: a tight threshold with an efficiency of about 70% and a light-flavor jet rejection probability of 95%, and a loose one with an efficiency of about 80% and a rejection probability of 85%.

The missing transverse momentum \vec{p}_T^{miss} is calculated as the negative of the vectorial sum of transverse momenta of all PF candidates in the event. Jet energy corrections are also propagated to improve the measurement of \vec{p}_T^{miss} .

6 Event selection

Events are selected if they pass single-lepton triggers. These require $p_T > 22$ GeV for electrons and $p_T > 20$ GeV for muons, as well as various quality and isolation criteria.

To reduce the background contributions and optimize the $t\bar{t}$ reconstruction additional, more stringent, requirements on the events are imposed. Events with exactly one muon or electron with $p_T > 30$ GeV and $|\eta| < 2.1$ are selected. No additional muons or electrons with $p_T > 15$ GeV and $|\eta| < 2.4$ are allowed. In addition to the lepton, at least four jets with $p_T > 30$ GeV and $|\eta| < 2.4$ are required. At least two of these jets must be tagged as b jets. At least one jet has to fulfill the tight b-jet identification criterion while for the second b jet only the loose criterion is required. At least one of the two jets with the highest value of the b tagging discriminant and at least one of the remaining jets are required to have $p_T > 35$ GeV.

We compare several kinematic distributions of the muon and electron channels to the simulation to verify that there are no unexpected differences. The ratios of the measured to the expected event yields in the two channels agree within the uncertainty in the lepton reconstruction and selection efficiencies. In the remaining steps of the analysis the two channels are combined by adding their distributions.

7 Reconstruction of the top quark-antiquark system

The goal of the $t\bar{t}$ reconstruction is the correct identification of reconstructed objects as parton- or particle-level top quark decay products. To test the performance of the reconstruction algorithm an assignment between detector level and particle- (parton-) level objects is needed. For the particle-level measurement this relationship is straightforward. Reconstructed leptons and jets can be matched spatially to corresponding objects at the particle level. For the parton-level measurement we need to define how to match the four initial quarks from a $t\bar{t}$ decay with reconstructed jets. This is not free of ambiguities since a quark does generally not lead to a single jet. One quark might shower into several jets or multiple quarks might be clustered into one jet if they are not well separated. We introduce an unambiguous matching criterion that matches the reconstructed jet with the highest p_T within $\Delta R = 0.4$ to a quark from the $t\bar{t}$ decay. If two quarks are matched with the same jet, the event has a merged topology and is considered as “not reconstructible” in the context of this analysis.

The same matching criterion is also used to assign particle-level jets to the $t\bar{t}$ decay products at parton level. Those particle-level jets with $p_T > 25$ GeV and $|\eta| < 2.5$, which are not assigned to one of the initial quarks, are considered as additional jets at parton level.

For the reconstruction of the top quark-antiquark system all possible permutations of jets that assign reconstructed jets to the decay products of the $t\bar{t}$ system are tested and a likelihood that a certain permutation is correct is evaluated. Permutations are considered only if the two jets with the highest b tagging probabilities are the two b-jet candidates. In addition, the p_T of at least one b-jet candidate and at least one jet candidate from the W boson decay have to be above 35 GeV. In each event the permutation with the highest probability is selected. The likelihoods are evaluated separately for the particle- and the parton-level measurements.

The first reconstruction step involves the determination of the neutrino four-momentum p_ν . This is performed using the algorithm described in Ref. [38]. The idea is to find all possible solutions for the three components of the neutrino momentum using the two mass constraints $(p_\nu + p_\ell)^2 = m_W^2$ and $(p_\nu + p_\ell + p_{b_\ell})^2 = m_t^2$. Each equation describes an ellipsoid in the three-dimensional momentum space of the neutrino. The intersection of these two ellipsoids is usually an ellipse. We select p_ν as the point on the ellipse for which the distance $D_{\nu,\min}$ between the ellipse projection onto the transverse plane and \vec{p}_T^{miss} is minimal. This algorithm leads to a unique solution for the longitudinal neutrino momentum and an improved resolution for the transverse component. The minimum distance $D_{\nu,\min}$ can also be used to identify the correct b_ℓ . In the cases with an invariant mass of the lepton and the b_ℓ candidate above m_t no solution can be found and we continue with the next permutation.

The likelihood λ is maximized to select the best permutation of jets. It uses constraints of the top quark and W boson masses on the hadronic side and the $D_{\nu,\min}$ value from the neutrino reconstruction, and is defined through

$$-\log(\lambda) = -\log(P_m(m_2, m_3)) - \log(P_\nu(D_{\nu,\min})), \quad (2)$$

where P_m is the two-dimensional probability distribution of the invariant masses of correctly reconstructed W bosons and top quarks. This probability is calculated for the invariant mass of the two jets m_2 tested as the W boson decay products, and the invariant mass of the three jets m_3 tested as the decay products of the hadronically decaying top quark. The distributions for the correct jet assignments, taken from the POWHEG+PYTHIA8 simulation and normalized to unity, are shown in Fig. 2 for the particle- and parton-level measurements. Permutations with probabilities of less than 0.1% of the highest value are rejected. This part of the likelihood is sensitive to the correct reconstruction of the hadronically decaying top quark, modulo a

permutation of the two jets from the W boson, but none of the measured kinematic variables will be affected by this ambiguity.

The probability P_ν describes the distribution of $D_{\nu,\min}$ for a correctly selected b_ℓ . In Fig. 2 the normalized distributions of $D_{\nu,\min}$ for b_ℓ and for other jets are shown. On average, the distance $D_{\nu,\min}$ for correctly selected b_ℓ is smaller and has a lower tail compared to the distance obtained for other jets. Permutations with values of $D_{\nu,\min} > 150$ GeV are rejected since they are very unlikely to originate from a correct b_ℓ association. This part of the likelihood is sensitive to the correct reconstruction of the leptonically decaying top quark.

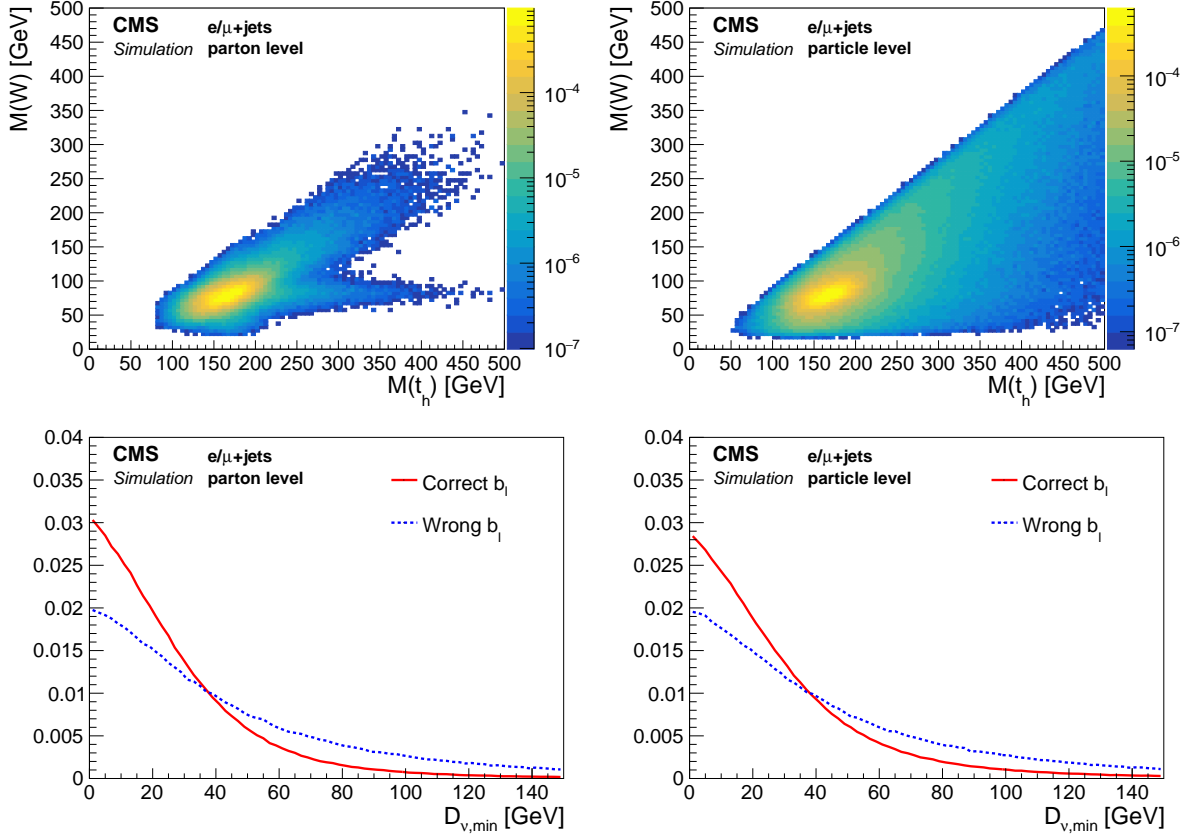


Figure 2: Top: normalized two-dimensional mass distribution of the correct reconstructed hadronically decaying W bosons $M(W)$ and the correct reconstructed top quarks $M(t_h)$ for the parton- (left) and the particle- (right) level measurements. Bottom: normalized distributions of the distance $D_{\nu,\min}$ for correctly and wrongly selected b jets from the leptonically decaying top quarks. The distributions are taken from the POWHEG+PYTHIA8 $t\bar{t}$ simulation.

The likelihood λ combines the probabilities from the reconstruction of the hadronically and leptonically decaying top quarks and provides information on reconstructing the whole $t\bar{t}$ system. The performance of the reconstruction algorithm is tested using the three $t\bar{t}$ simulations generated with POWHEG combined with PYTHIA8 or HERWIG++, and MG5_aMC@NLO+PYTHIA8 where we use the input distributions P_m and P_ν from POWHEG+PYTHIA8. The efficiency of the reconstruction algorithm is defined as the probability that the most likely permutation, as identified through the maximization of the likelihood λ , is the correct one, given that all decay products from the $t\bar{t}$ decay are reconstructed and selected. These efficiencies as a function of the jet multiplicity are shown in Fig. 3. Since the number of permutations increases drastically with the number of jets, it is more likely to select a wrong permutation if there are additional jets. The small differences observed in different simulations are taken into account for the un-

certainty estimations. We observe a lower reconstruction efficiency for the particle-level measurement. This is caused by the weaker mass constraints for a particle-level top quark, where, in contrast to the parton-level top quark, exact matches to the top quark and W boson masses are not required. This can be seen in the mass distributions of Fig. 2 and the likelihood distributions in Fig. 4. Here the signal simulation is divided into the following categories: correctly reconstructed $t\bar{t}$ systems ($t\bar{t}$ right reco), events where all decay products are available, but the algorithm failed to identify the correct permutation ($t\bar{t}$ wrong reco), ℓ +jets $t\bar{t}$ events where at least one decay product is missing ($t\bar{t}$ not reconstructible), and nonsignal $t\bar{t}$ events ($t\bar{t}$ background). However, the lower reconstruction efficiency of the particle-level top quark is compensated by the higher number of reconstructible events.

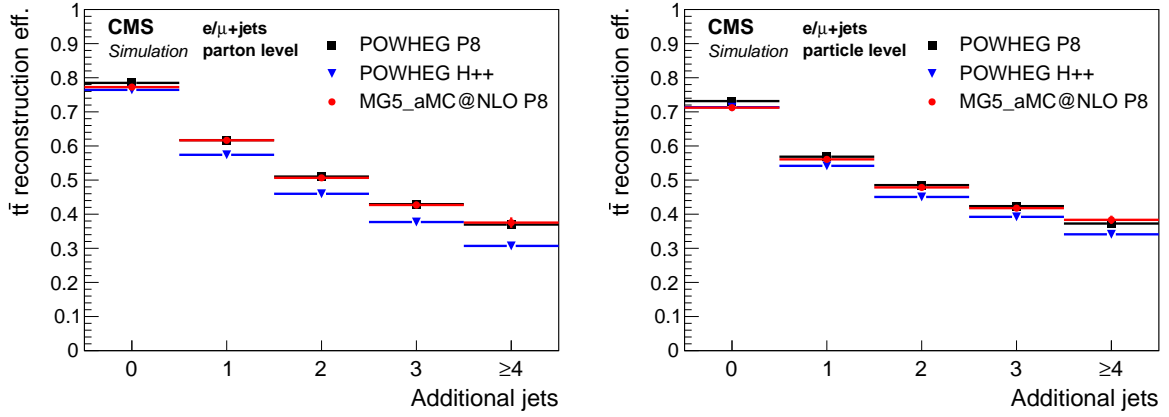


Figure 3: Reconstruction efficiency of the $t\bar{t}$ system as a function of the number of additional jets for the parton- (left) and particle- (right) level measurements calculated based on the simulations with POWHEG+PYTHIA8 (P8), POWHEG+HERWIG++ (H++), and MG5_aMC@NLO+PYTHIA8.

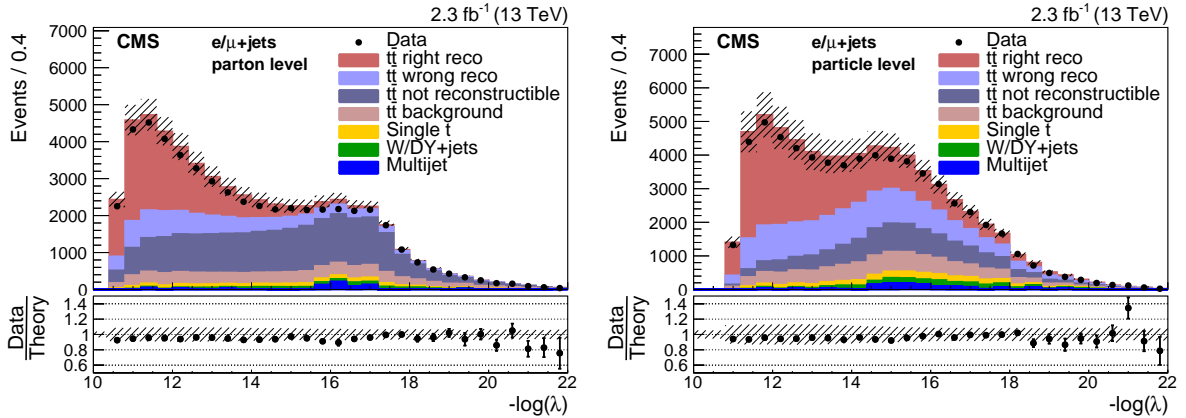


Figure 4: Distribution of the negative log-likelihood for the selected best permutation in the parton- (left) and the particle- (right) level measurements in data and simulations. The simulation of POWHEG+PYTHIA8 is used to describe the $t\bar{t}$ production. Experimental (cf. Section 10) and statistical uncertainties (hatched area) are shown for the total simulated yield, which is normalized to the measured integrated luminosity. The ratios of data to the sum of the expected yields are provided at the bottom of each panel.

In Fig. 5 the distributions of p_T and $|y|$ of the reconstructed hadronically decaying top quarks for the parton- and particle-level measurements are compared to the simulation. In Fig. 6 the distributions of $p_T(t\bar{t})$, $|y(t\bar{t})|$, $M(t\bar{t})$, and the number of additional jets are shown. In general,

good agreement is observed between the data and the simulation though the overall yield in the data is slightly lower, but within the experimental uncertainties. The observed jet multiplicities are lower than predicted.

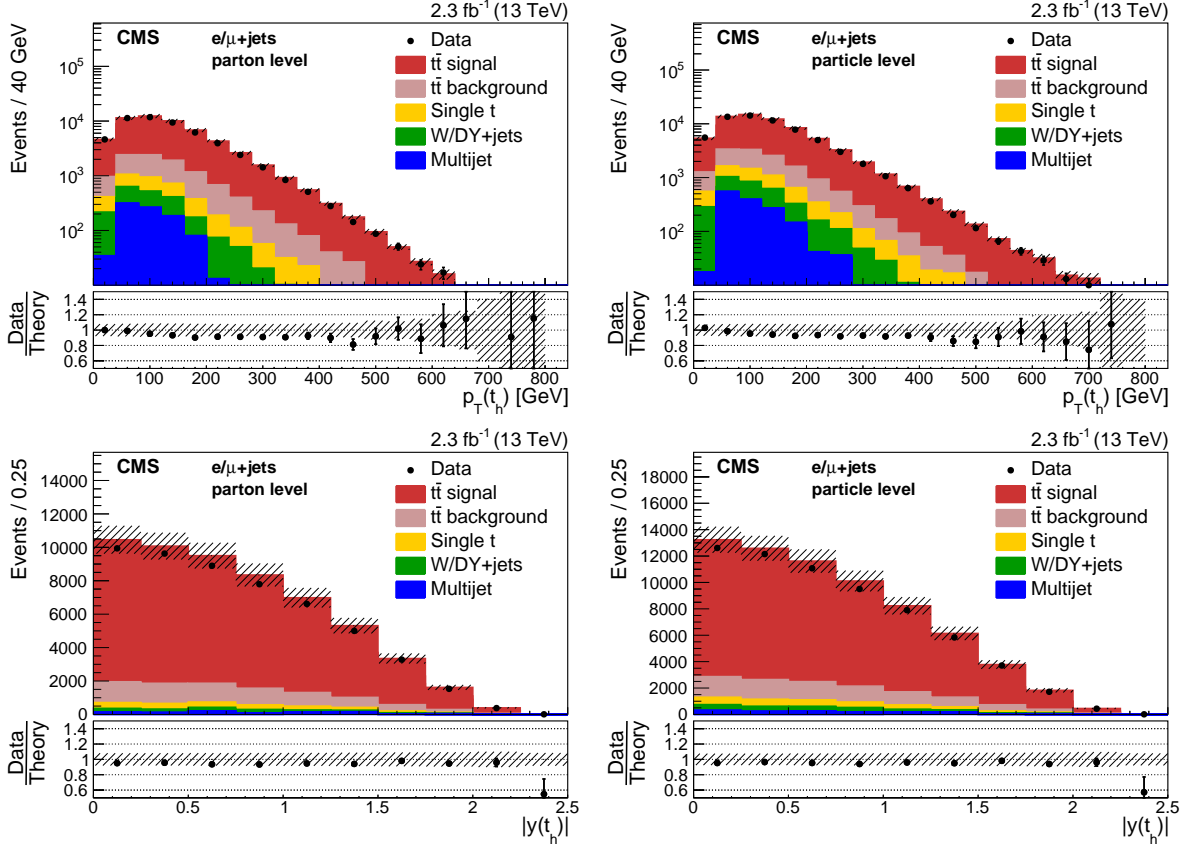


Figure 5: Comparisons of the reconstructed $p_T(t_h)$ (top) and $|y(t_h)|$ (bottom) in data and simulations for the parton (left) and the particle (right) level. The simulation of POWHEG+PYTHIA8 is used to describe the $t\bar{t}$ production. Experimental (cf. Section 10) and statistical uncertainties (hatched area) are shown for the total simulated yield, which is normalized according to the measured integrated luminosity. The ratios of data to the expected yields are given at the bottom of each panel.

8 Background subtraction

After the event selection and $t\bar{t}$ reconstruction about 65 000 (53 000) events are observed in the particle- (parton-) level measurements. A small contribution of about 9% of single top quark, DY, W boson, and multijet events is expected. These have to be estimated and subtracted from the selected data.

The background from single top quark production is subtracted based on its simulation. Its overall contribution corresponds to about 4% of the selected data. Single top quark production cross sections are calculated with precisions of a few percent [24, 25]. Since the calculations have a limited reliability after $t\bar{t}$ selection we assume an overall uncertainty of 50%. However, this conservative estimate has negligible impact on the final results and their accuracy.

The simulations of multijet, DY, and W boson production contain limited numbers of events after the full selection. We extract the shapes of the distributions of these backgrounds from

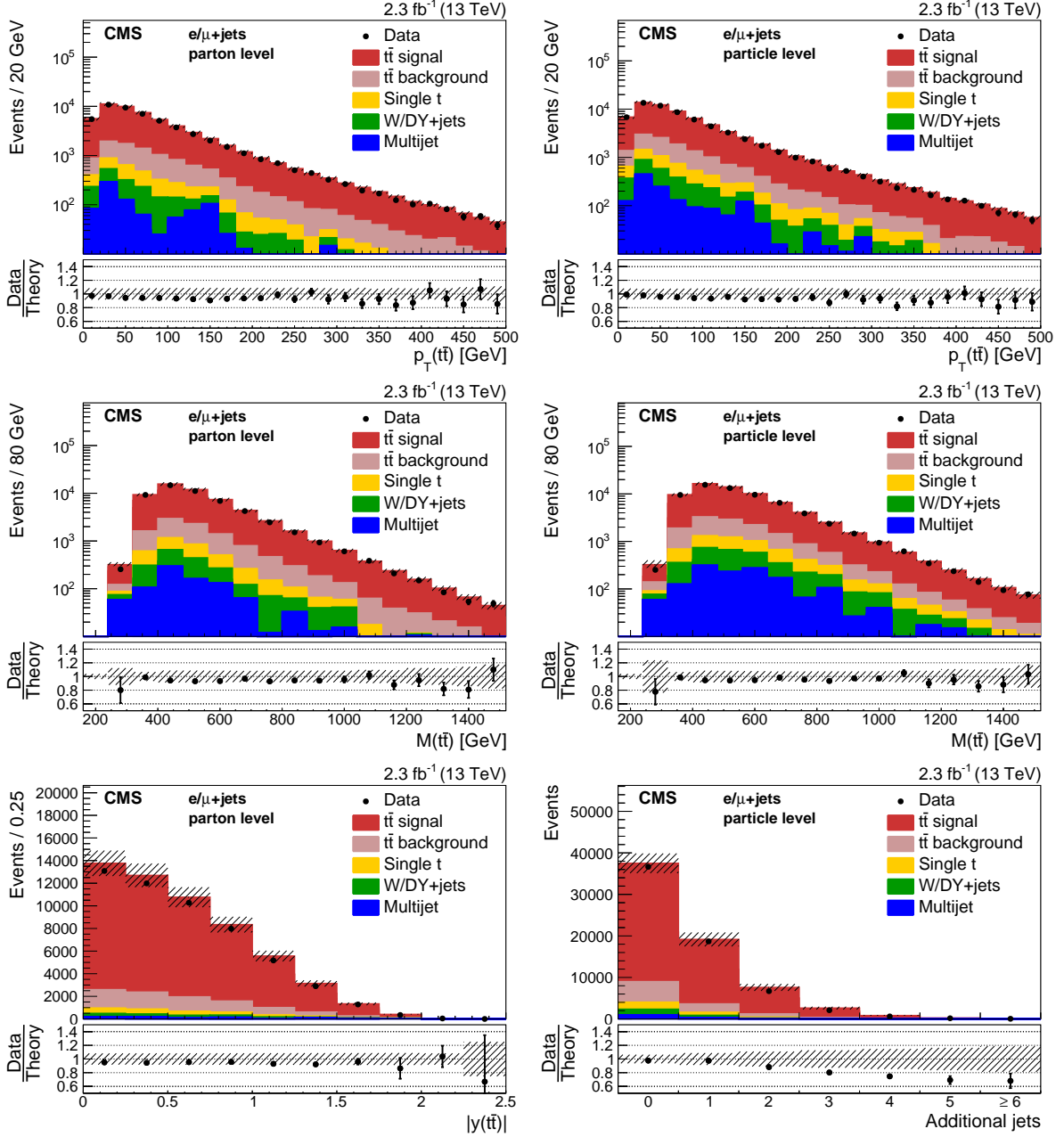


Figure 6: Comparisons of the reconstructed distributions of $p_T(t\bar{t})$ (top) and $M(t\bar{t})$ (middle) for the parton- (left) and the particle- (right) level measurements in data and simulations. Bottom: distributions of $|y(t\bar{t})|$ (left) and the number of additional jets (right). The simulation of POWHEG+PYTHIA8 is used to describe the $t\bar{t}$ production. Experimental (cf. Section 10) and statistical uncertainties (hatched area) are shown for the total simulated yield, which is normalized according to the measured integrated luminosity. The ratios of data to the expected yields are given at the bottom of each panel.

a control region in the data, similar to the signal region, but requiring no b-tagged jet in the event. In this selection the contribution of $t\bar{t}$ events is estimated to be about 15%. The remaining fraction consists of multijet, DY, and W boson events. The reconstruction algorithm is exactly the same as for the signal selection. To estimate the shape dependency in the control region on the selection we vary the selection threshold of the b tagging discriminant. This changes the top quark contribution and the flavor composition, however, we find the observed shape variation to be negligible. For the background subtraction, the distributions extracted from the control region are normalized to the yield of multijet, DY, and W boson events predicted by the simulation in the signal region. In the control region the expected and measured event yields agree within their statistical uncertainties. Taking into account the statistical uncertainty of the normalization factor and the shape differences between the signal and control regions in the simulation, we estimate an overall uncertainty of 20% in this background estimation. The overall contribution to the selected data is about 5%.

For the parton-level measurement, special care has to be taken with the contribution of nonsignal $t\bar{t}$ events, i.e., dilepton, all-jets, and τ +jets events. For the particle-level measurement care is needed with all $t\bar{t}$ events for which no pair of particle-level top quarks exists. The behavior of this background depends on the $t\bar{t}$ cross section and a subtraction according to the expected value can result in a bias of the measurement, especially if large differences between the simulation and the data are observed. However, the shapes of the distributions show an agreement within uncertainties between data and simulation and we subtract the predicted relative fractions from the remaining event yields.

9 Unfolding

For the unfolding, the iterative D'Agostini method [39] is used. The migration matrices and the acceptances are needed as input. The migration matrix relates the quantities at particle (parton) level and at detector level. It accounts for the effects from the parton shower and hadronization as well as the detector response, where the former has a large impact on the parton-level measurement. For the central results the migration matrices and the acceptances are taken from the POWHEG+PYTHIA8 simulation and other simulations are used to estimate the uncertainties. The binning in the unfolding is optimized based on the resolution in the simulation. We utilize for the minimal bin widths that, according to the resolution, at least 50% of the events are reconstructed in the correct bin.

The iterative D'Agostini method takes the number of iterations as an input parameter to control the level of regularization. A small number of iterations corresponds to a large regularization, which may bias the unfolded results. The level of regularization and hence the bias decreases with the number of iterations – but with the drawback of increasing variances in the unfolded spectra. To optimize the number of iterations, we chose the criterion that the compatibility between a model and the unfolded data at particle (parton) level is the same as the compatibility between the folded model and the data at detector level. The compatibilities are determined by χ^2 tests at both levels based on all available simulations and several modified spectra obtained by reweighting the $p_T(t)$, $|y(t)|$, or $p_T(t\bar{t})$ distributions in the POWHEG+PYTHIA8 simulation. The reweighted spectra are chosen in such a way that they cover the observed differences between the data and the unmodified simulation.

We find the above criterion fulfilled for the number of iterations such that a second χ^2 test between the detector-level spectrum with its statistical uncertainty and the refolded spectrum exceeds a probability of 99.9%. The refolded spectrum is obtained by inverting the unfolding step. This consists of a multiplication with the response matrix and does not need any regular-

ization.

For the two-dimensional measurements with n bins in one and m bins in the other quantity the D'Agostini unfolding can be generalized using a vector of $n \cdot m$ entries of the form: $b_{1,1}, b_{2,1} \dots b_{n,1}, \dots b_{1,m}, b_{2,m} \dots b_{n,m}$ with a corresponding $(n \cdot m) \times (n \cdot m)$ migration matrix. The number of iterations is optimized in the same way.

10 Systematic uncertainties

We study several sources of experimental and theoretical uncertainty. Uncertainties in the jet and \vec{p}_T^{miss} calibrations, in the pileup modeling, in the b tagging and lepton selection efficiencies, and in the integrated luminosity measurement fall into the first category.

Uncertainties in the jet energy calibration are estimated by shifting the energies of jets in the simulation up and down by their p_T - and η -dependent uncertainties of 3–7% [36]. At the same time \vec{p}_T^{miss} is recalculated according to the rescaled jet energies. The recomputed backgrounds, response matrices, and acceptances are used to unfold the data. The observed differences between these and the original results are taken as an uncertainty in the unfolded event yields. The same technique is used to calculate the impact of the uncertainties in the jet energy resolution, the uncertainty in \vec{p}_T^{miss} not related to the jet energy calibration, in the b tagging, and in the pileup modeling.

The b tagging efficiency in the simulation is corrected using scale factors determined from the data [37]. These have an uncertainty of about 2–5% depending on the p_T of the b jet.

The effect on the measurement due to the uncertainty in the modeling of pileup in the simulation is estimated by varying the average number of pileup events per bunch crossing by 5% and reweighting the simulated events accordingly.

The trigger, reconstruction, and identification efficiencies of leptons are evaluated with tag-and-probe techniques using Z boson dilepton decays [33]. The uncertainties in the scale factors, which are used to correct the simulation to match the data, take into account the different lepton selection efficiencies in events with high jet multiplicities. The overall uncertainty in the lepton reconstruction and selection efficiencies is 3%.

The relative uncertainty in the integrated luminosity measurement is 2.3% [1].

Uncertainties in the PDFs, the choice of factorization and renormalization scales, the modeling of the parton shower and hadronization, the effect of different NLO event generation methods, and the top quark mass fall into the second category of theoretical uncertainties.

The effects of these uncertainties are estimated either by using the various event weights introduced in Section 2, e.g., in the case of PDFs, factorization scale, and renormalization scale, or by using a different $t\bar{t}$ signal simulation. The POWHEG simulation combined with HERWIG++ is used to estimate the effect of different parton shower and hadronization models. In addition, POWHEG+PYTHIA8 samples with a parton shower scale varied by a factor of two are used to study the parton shower modeling uncertainties. The result obtained with MG5_aMC@NLO is used to estimate the effect of different NLO event generation methods. The effect due to uncertainties in the top quark mass is estimated using simulations with altered top quark masses. We quote as uncertainty the cross section differences observed for a top quark mass variation of 1 GeV around the central value of 172.5 GeV used in the central simulation.

The background predictions, response matrices, and acceptances obtained from these simula-

tions are used to unfold the data. The observed deviations with respect to the original result are quoted as an uncertainty in the unfolded event yield.

For the PDF uncertainty only the variation in the acceptance is taken into account while variations due to migrations between bins are neglected. It is calculated according to the uncertainties in the NNPDF30_nlo_as_0118 [19] parametrization. In addition, the uncertainties obtained using the PDF sets derived with varied values of the strong coupling constant $\alpha_s = 0.117$ and 0.119 are considered.

An overview of the uncertainties in the differential cross sections is provided in Table 1, where the typical ranges of uncertainties in the bins are shown. In the double-differential measurements the jet energy scale uncertainty is about 15% in bins of high jet multiplicities and the dominant uncertainties due to hadronization modeling and NLO calculation reach up to 30% for the parton-level measurements.

Table 1: Overview of the uncertainties in the differential cross section measurements at particle and at parton level. Typical ranges of uncertainties in the bins are shown.

Source	Particle level [%]	Parton level [%]
Statistical uncertainty	1–5	1–5
Jet energy scale	5–8	6–8
Jet energy resolution	<1	<1
\vec{p}_T^{miss} (non jet)	<1	<1
b tagging	2–3	2–3
Pileup	<1	<1
Lepton selection	3	3
Luminosity	2.3	2.3
Background	1–3	1–3
PDF	<1	<1
Fact./ren. scale	<1	<1
Parton shower scale	2–5	2–9
POWHEG+PYTHIA8 vs. HERWIG++	1–5	1–12
NLO event generation	1–5	1–10
m_t	1–2	1–3

11 Cross section results

The cross section σ in each bin is calculated as the ratio of the unfolded signal yield and the integrated luminosity. These are further divided by the bin width (the product of the two bin widths) to obtain the single- (double-) differential results.

The measured differential cross sections are compared to the predictions of POWHEG and MG5_aMC@NLO, each combined with the parton shower simulations of PYTHIA8 and HERWIG++. In addition, the $t\bar{t}$ multiparton simulations of MG5_aMC@NLO at LO and NLO with a PYTHIA8 parton shower are shown in Fig. 7 (8) as a function of the top quark p_T and $|y|$ at parton (particle) level. In Figs. 9 and 10 the cross sections as a function of kinematic variables of the $t\bar{t}$ system and the number of additional jets are compared to the same theoretical predictions.

In Fig. 11 the parton-level results are compared to theoretical predictions of various accuracies. The first is an approximate NNLO [40] QCD calculation using the CT14NNLO [41] PDF and

$m_t = 172.5$ GeV. The factorization and renormalization scales are fixed at m_t . The second is an approximate next-to-NNLO (NNNLO) [42, 43] QCD calculation using the MSTW2008nnlo [44] PDF, $m_t = 172.5$ GeV and factorization and renormalization scales fixed at m_t . The third combines the NLO QCD calculation with an improved NNLL QCD calculation (NLO+NNLL') [45] using the MSTW2008nnlo PDF, $m_t = 173.2$ GeV, and the renormalization and factorization scales of $M_T = \sqrt{m_t^2 + p_T^2(t)}$ for the $p_T(t)$ calculation and $M(t\bar{t})/2$ for the $M(t\bar{t})$ calculation. The fourth is a full NNLO [46] QCD calculation using the NNPDF3.0 PDF, $m_t = 173.3$ GeV, and the renormalization and factorization scales of $M_T/2$ for the $p_T(t)$ calculation and one-fourth of the sum of the p_T of all partons for the other distributions. The displayed uncertainties come from varying the scales up and down by a factor of two. Only the uncertainties in the approximate NNLO calculation include PDF uncertainties and a m_t variation of 1 GeV.

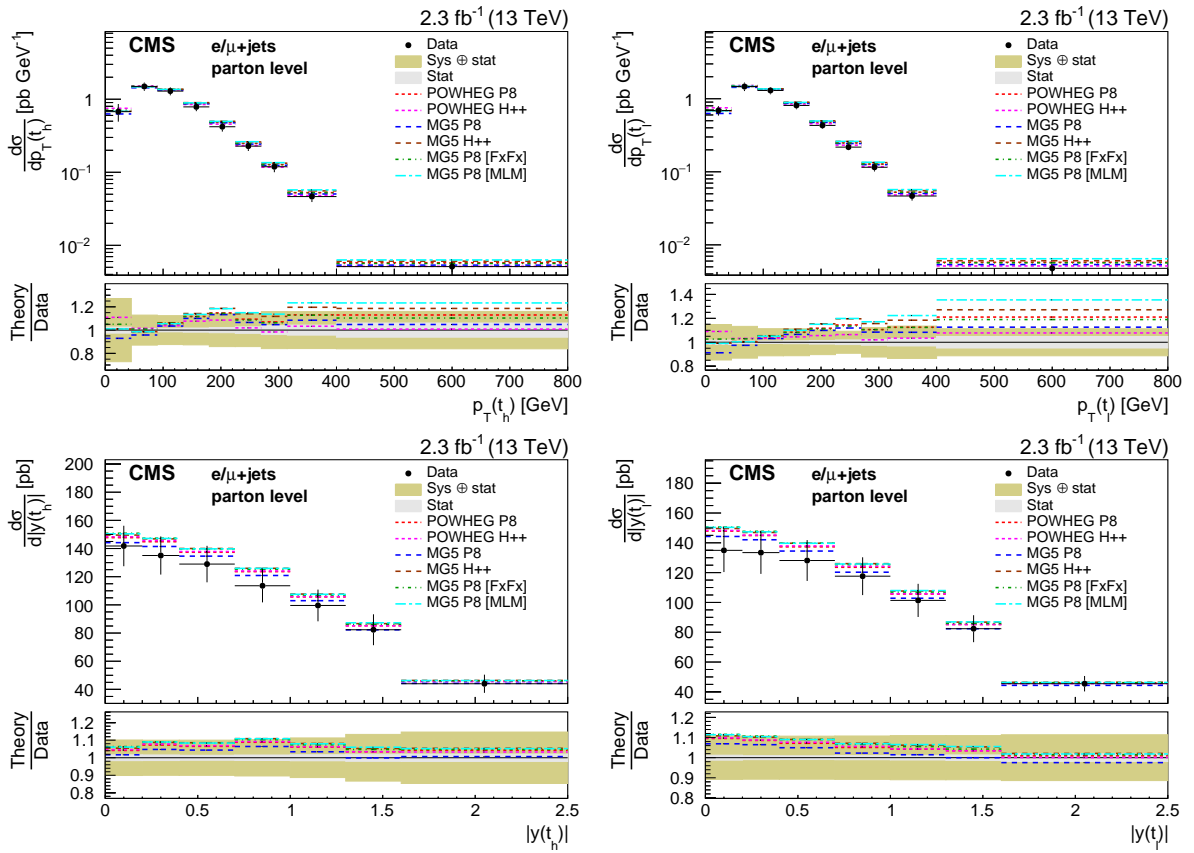


Figure 7: Differential cross sections at parton level as a function of $p_T(t)$ (top) and $|y(t)|$ (bottom) measured separately for the hadronically (left) and leptonically (right) decaying top quarks. The cross sections are compared to the predictions of POWHEG and MG5_aMC@NLO (MG5) combined with PYTHIA8 (P8) or HERWIG++ (H++) and the multiparton simulations MG5_aMC@NLO+PYTHIA8 MLM and MG5_aMC@NLO+PYTHIA8 FxFx. The ratios of the various predictions to the measured cross sections are shown at the bottom of each panel together with the statistical and systematic uncertainties of the measurement.

The differential cross sections as a function of $p_T(t_h)$ and $p_T(t\bar{t})$ in bins of the number of additional jets are shown in Fig. 12 (13) at parton (particle) level. The double-differential cross sections as a function of $|y(t_h)|$ vs. $p_T(t_h)$, $M(t\bar{t})$ vs. $|y(t\bar{t})|$, and $p_T(t\bar{t})$ vs. $M(t\bar{t})$ are shown at parton level in Figs. 14–15 and at particle level in Figs. 16–17. The results are compared to the predictions of the event generators. All cross section values together with their statistical and systematic uncertainties are listed in Appendices A and B for the parton- and particle-level

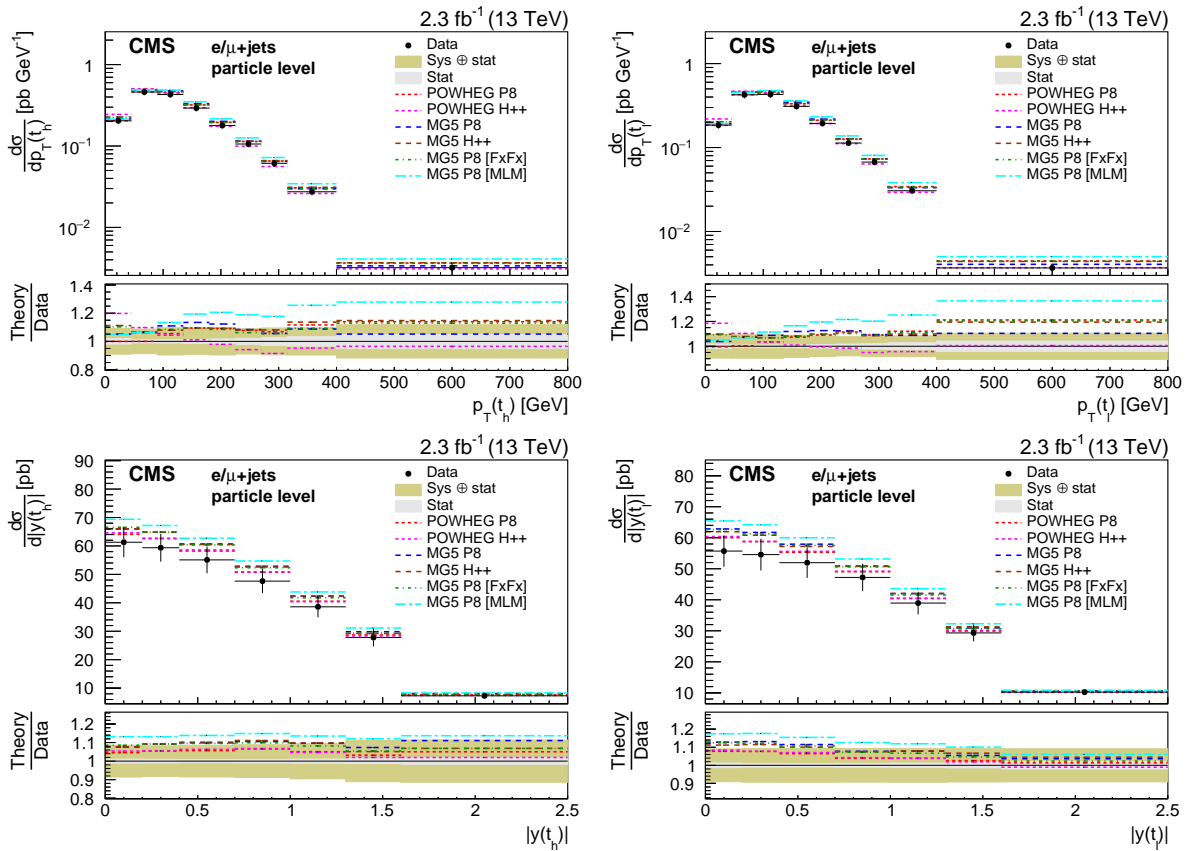


Figure 8: Differential cross sections at particle level as a function of $p_T(t)$ (top) and $|y(t)|$ (bottom) measured separately for the hadronically (left) and leptonically (right) decaying particle-level top quarks. The cross sections are compared to the predictions of POWHEG and MG5_aMC@NLO (MG5) combined with PYTHIA8 (P8) or HERWIG++ (H++) and the multiparton simulations MG5_aMC@NLO+PYTHIA8 MLM and MG5_aMC@NLO+PYTHIA8 FxFx. The ratios of the various predictions to the measured cross sections are shown at the bottom of each panel together with the statistical and systematic uncertainties of the measurement.

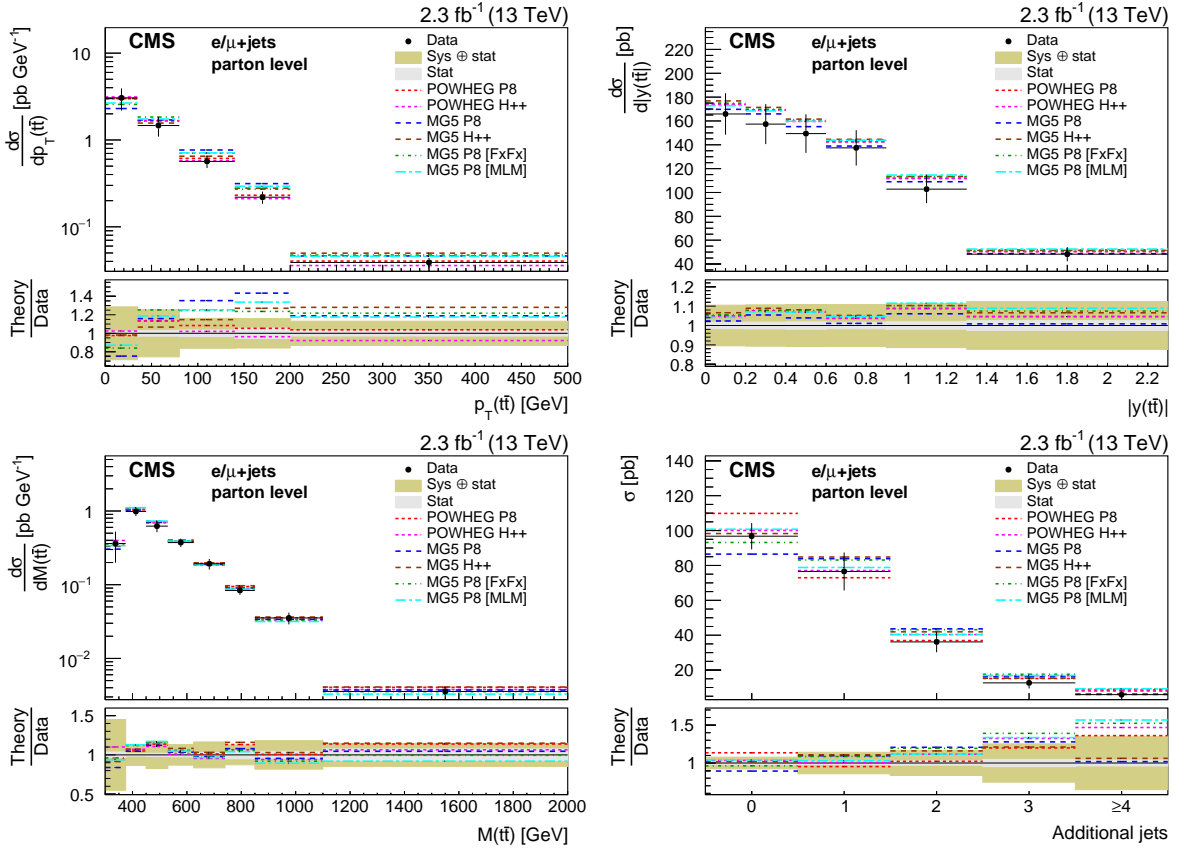


Figure 9: Differential cross sections at parton level as a function of $p_T(\bar{t}\bar{t})$, $|y(\bar{t}\bar{t})|$, $M(\bar{t}\bar{t})$, and cross sections as a function of the number of additional jets compared to the predictions of POWHEG and MG5_aMC@NLO (MG5) combined with PYTHIA8 (P8) or HERWIG++ (H++) and the multiparton simulations MG5_aMC@NLO+PYTHIA8 MLM and MG5_aMC@NLO+PYTHIA8 FxFx. The ratios of the various predictions to the measured cross sections are shown at the bottom of each panel together with the statistical and systematic uncertainties of the measurement.

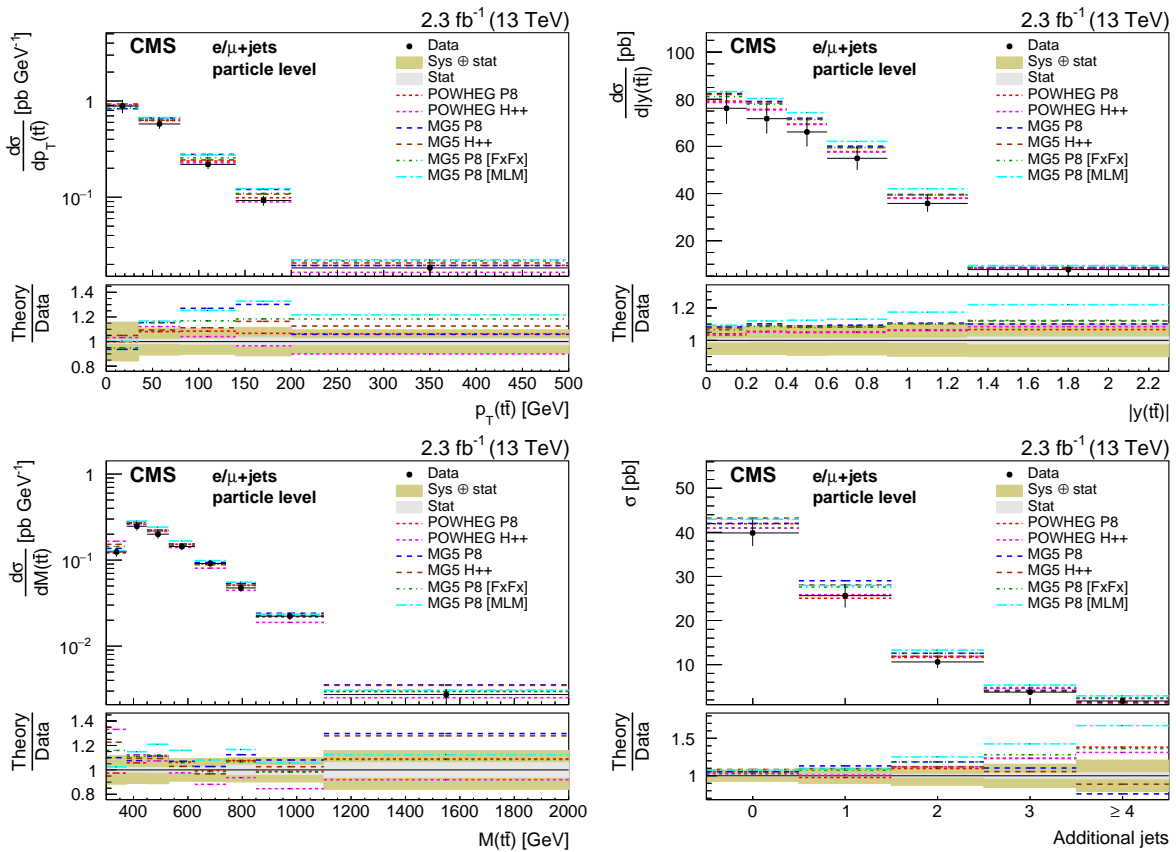


Figure 10: Differential cross sections at particle level as a function of $p_T(\bar{t}\bar{t})$, $|y(\bar{t}\bar{t})|$, $M(\bar{t}\bar{t})$, and cross sections as a function of the number of additional jets compared to the predictions of POWHEG and MG5_aMC@NLO (MG5) combined with PYTHIA8 (P8) or HERWIG++ (H++) and the multiparton simulations MG5_aMC@NLO+PYTHIA8 MLM and MG5_aMC@NLO+PYTHIA8 FxFx. The ratios of the various predictions to the measured cross sections are shown at the bottom of each panel together with the statistical and systematic uncertainties of the measurement.

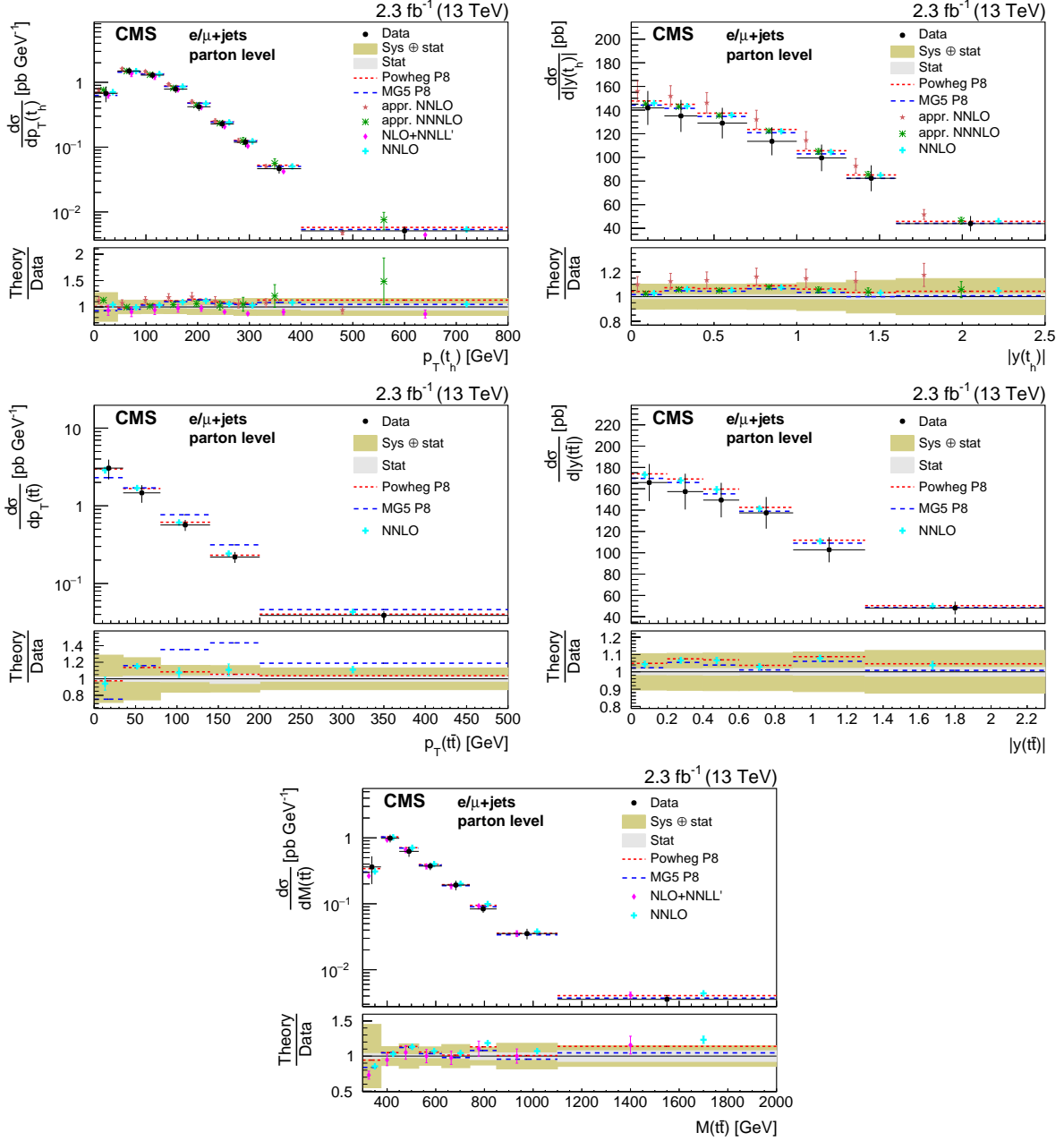


Figure 11: Differential cross sections at parton level as a function of $p_T(t)$, $|y(t)|$, $p_T(\bar{t}\bar{t})$, $|y(\bar{t}\bar{t})|$, and $M(\bar{t}\bar{t})$ compared to the available predictions of an approximate NNLO calculation [40], an approximate NNNLO calculation [42, 43], a NLO+NNLL' calculation [45], and a full NNLO calculation [46]. For these models uncertainties due to the choices of scales are shown. To improve the visibility the theoretical predictions are horizontally shifted. The ratios of the various predictions to the measured cross sections are shown at the bottom of each panel together with the statistical and systematic uncertainties of the measurement.

measurements, respectively.

The precision of the measurement is limited by systematic uncertainties, dominated by jet energy scale uncertainties on the experimental side and parton shower and hadronization modeling uncertainties on the theoretical side. As expected, the theoretical uncertainties are reduced in the particle-level measurements since these are less dependent on theory-based extrapolations.

We evaluate the level of agreement between the measured differential cross sections and the various theoretical predictions using χ^2 tests. In these tests we take into account the full covariance matrix obtained from the unfolding procedure for the statistical uncertainty. For each of the studied systematic uncertainties we assume a full correlation among all bins. No uncertainties in the theoretical predictions are considered for this comparison. However, these uncertainties are known to be large. Typically, differences between the various models are used to assess their uncertainties. From the χ^2 values and the numbers of degrees of freedom, which corresponds to the number of bins in the distributions, the p-values are calculated. The results are shown in Table 2 for the parton-level and in Table 3 for the particle-level measurements.

The observed cross sections are slightly lower than expected. However, taking into account the systematic uncertainties, that are highly correlated among the bins, there is no significant deviation. In general, the measured distributions are in agreement with the predictions of the event generators with some exceptions in the $p_T(\bar{t}\bar{t})$ and $M(\bar{t}\bar{t})$ distributions. The jet multiplicities are lower than predicted by almost all simulations. The measured p_T of the top quarks is slightly softer than predicted. Such an effect has already been observed in previous measurements [2–5]. However, the comparison between the HERWIG++ and PYTHIA8 simulations together with the same matrix-element calculations show the large impact of the parton shower and hadronization modeling. The parton-level results are well described by the matrix-element calculations. Especially, the soft p_T of the top quarks is predicted by the NNLO and NLO+NNLL' QCD calculation.

12 Summary

Measurements of the differential and double-differential cross sections for $\bar{t}\bar{t}$ production in proton-proton collisions at 13 TeV have been presented. The data correspond to an integrated luminosity of 2.3 fb^{-1} recorded by the CMS experiment. The $\bar{t}\bar{t}$ production cross section is measured in the lepton+jets channel as a function of transverse momentum p_T and rapidity $|y|$ of the top quarks; p_T , $|y|$, and invariant mass of the $\bar{t}\bar{t}$ system; and the number of additional jets. The measurement at parton level is dominated by the uncertainties in the parton shower and hadronization modeling. The dependence on these theoretical models is reduced for the particle-level measurement, for which the experimental uncertainties of jet energy calibration and b tagging efficiency are dominant.

The results are compared to several standard model predictions that use different methods and approximations for their calculations. In general, the measured cross sections are slightly lower than predicted, but within the uncertainty compatible with the expectation. The measured distributions are in agreement with the predictions of the event generators with some exceptions in the $p_T(\bar{t}\bar{t})$ and $M(\bar{t}\bar{t})$ distributions. The number of additional jets is lower and the measured p_T of the top quarks is slightly softer than predicted by most of the event generators. A softer p_T of the top quarks has already been observed in previous measurements and is predicted by the NNLO and the NLO+NNLL' QCD calculation.

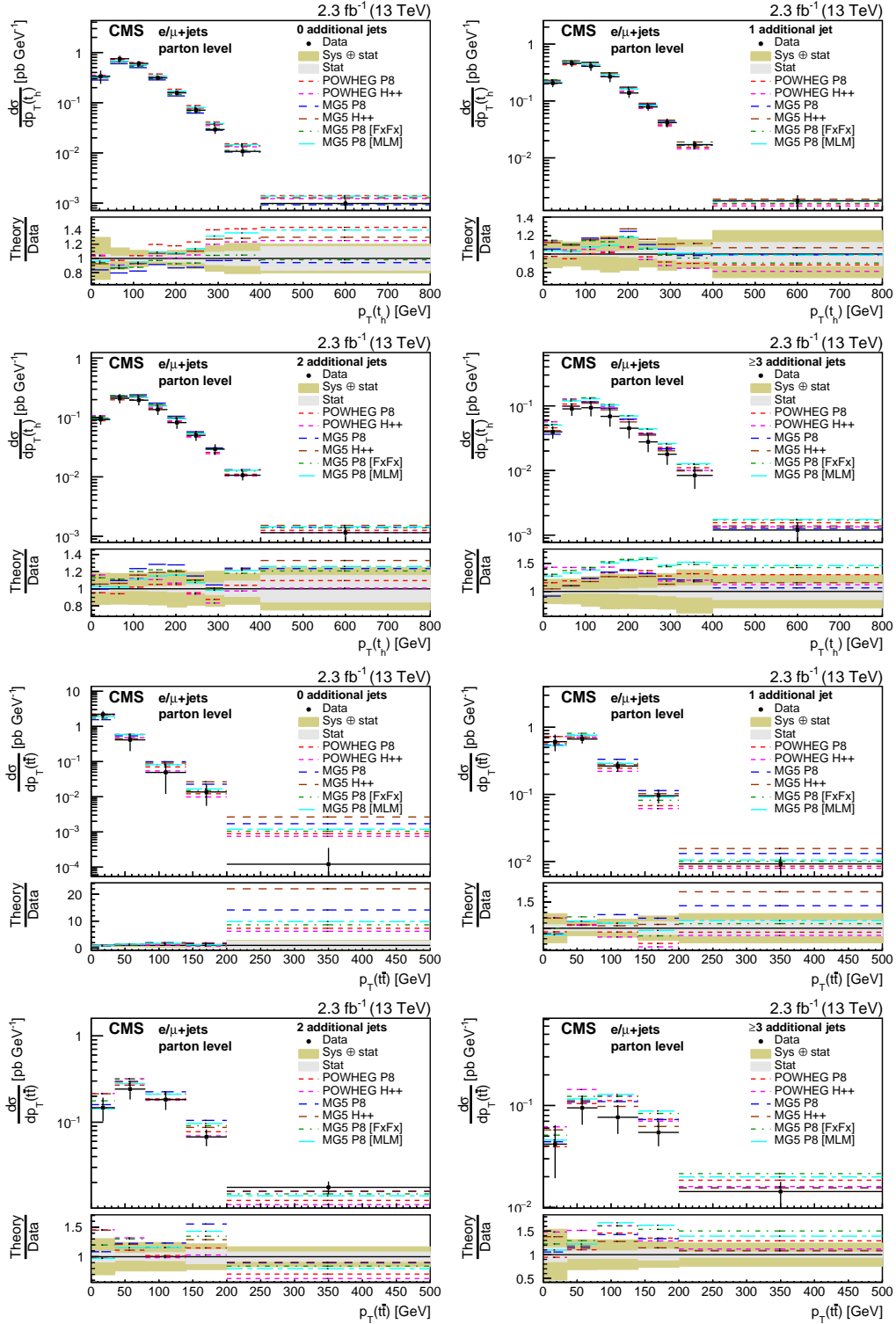


Figure 12: Differential cross sections at parton level as a function of $p_T(t_h)$ (upper two rows) and $p_T(t\bar{t})$ (lower two rows) in bins of the number of additional jets. The measurements are compared to the predictions of POWHEG and MG5_aMC@NLO (MG5) combined with PYTHIA8 (P8) or HERWIG++ (H++) and the multiparton simulations MG5_aMC@NLO+PYTHIA8 MLM and MG5_aMC@NLO+PYTHIA8 FxFx. The ratios of the predictions to the measured cross sections are shown at the bottom of each panel together with the statistical and systematic uncertainties of the measurement.

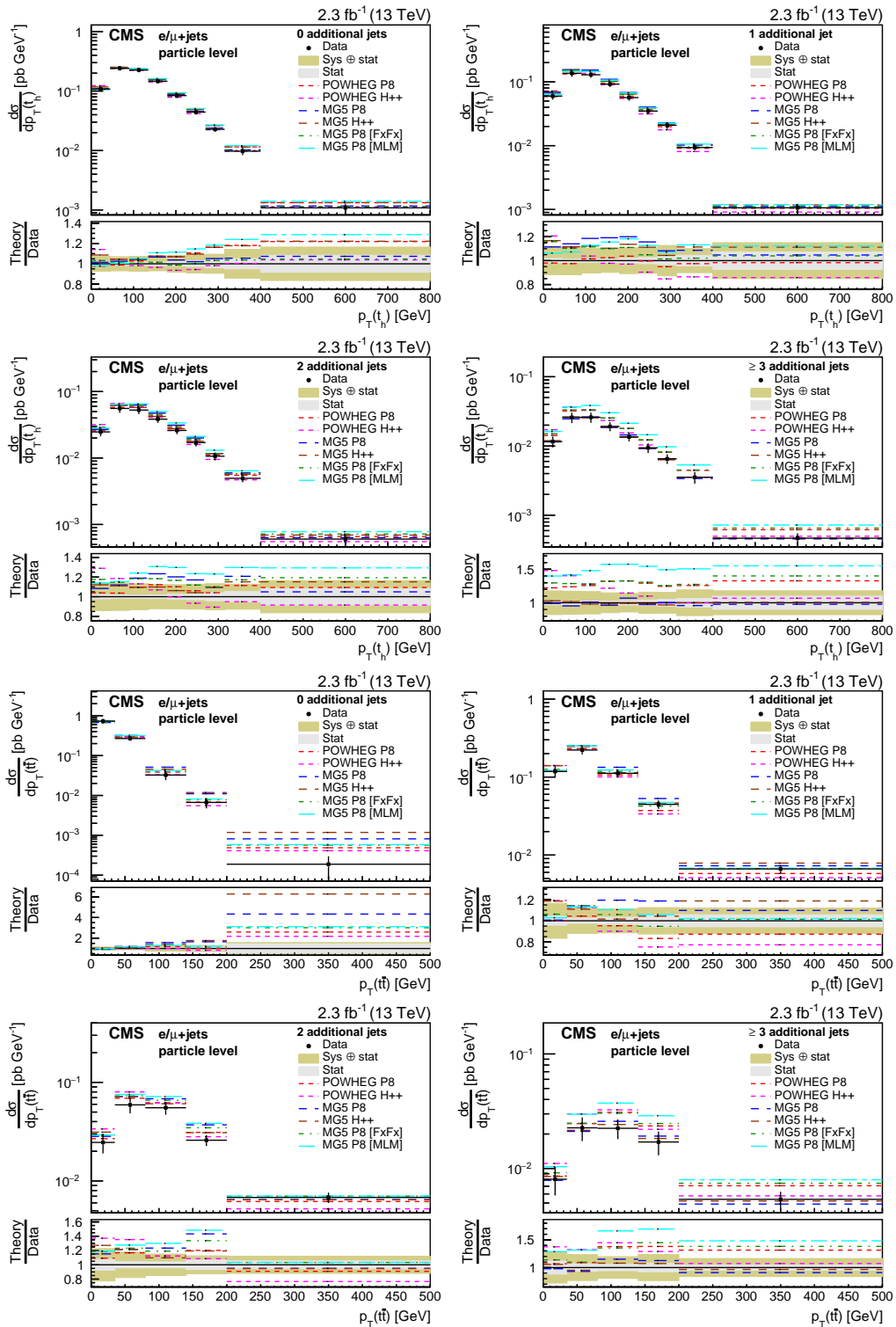


Figure 13: Differential cross sections at particle level as a function of $p_T(t_h)$ (upper two rows) and $p_T(t_{\bar{t}})$ (lower two rows) in bins of the number of additional jets. The measurements are compared to the predictions of POWHEG and MG5_aMC@NLO (MG5) combined with PYTHIA8 (P8) or HERWIG++ (H++) and the multiparton simulations MG5_aMC@NLO+PYTHIA8 MLM and MG5_aMC@NLO+PYTHIA8 FxFx. The ratios of the predictions to the measured cross sections are shown at the bottom of each panel together with the statistical and systematic uncertainties of the measurement.

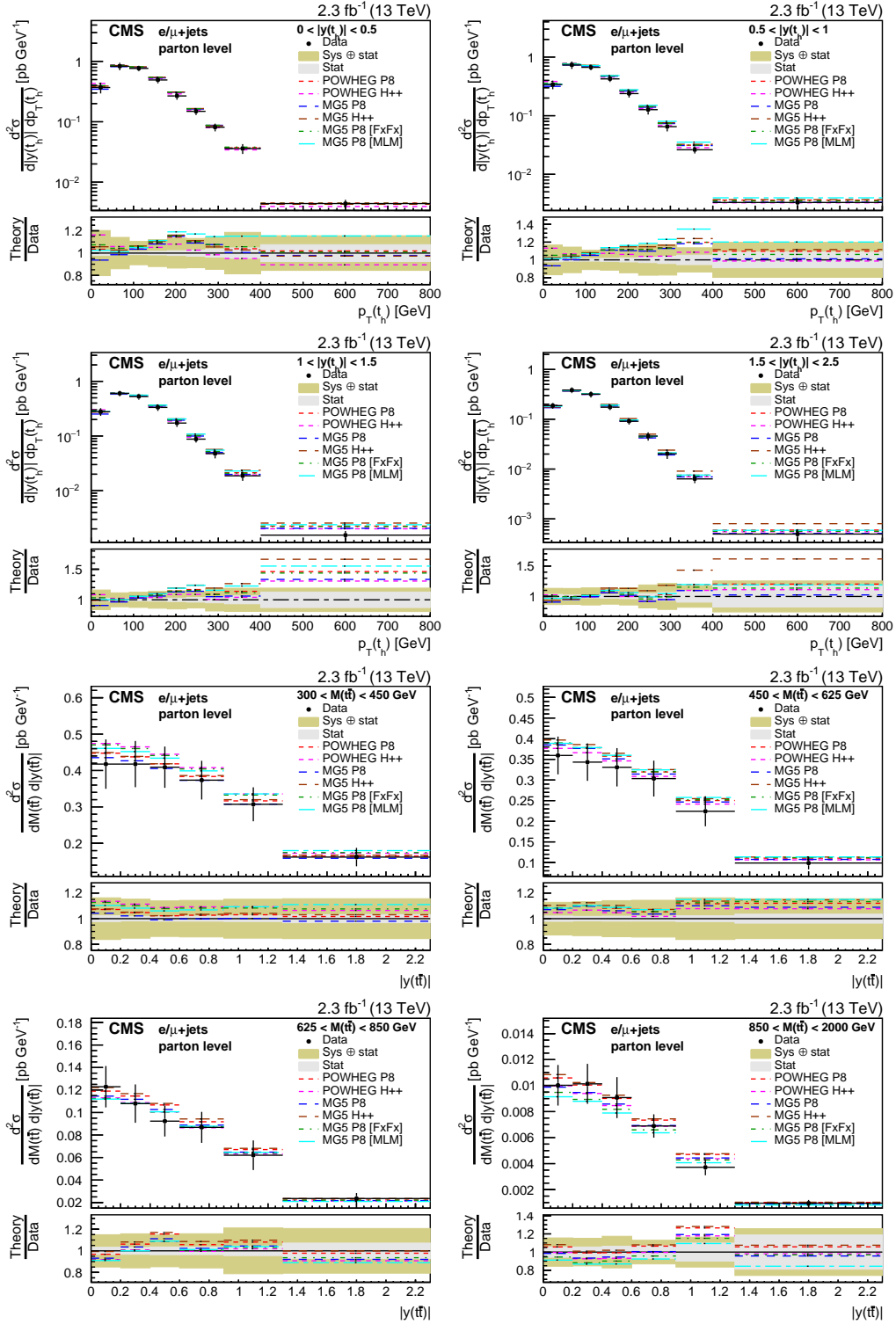


Figure 14: Double-differential cross sections at parton level as a function of $|y(t_h)|$ vs. $p_T(t_h)$ (upper two rows) and $M(t\bar{t})$ vs. $|y(t\bar{t})|$ (lower two rows). The measurements are compared to the predictions of POWHEG and MG5_aMC@NLO (MG5) combined with PYTHIA8 (P8) or HERWIG++ (H++) and the multiparton simulations MG5_aMC@NLO+PYTHIA8 MLM and MG5_aMC@NLO+PYTHIA8 FxFx. The ratios of the predictions to the measured cross sections are shown at the bottom of each panel together with the statistical and systematic uncertainties of the measurement.

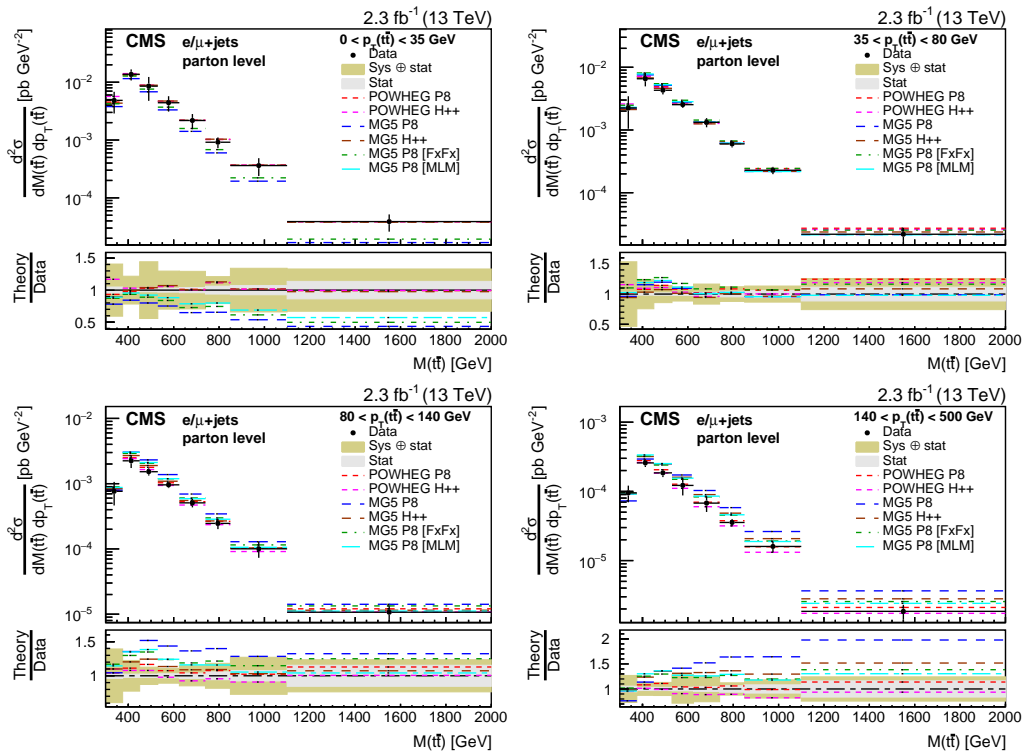


Figure 15: Double-differential cross section at parton level as a function of $p_T(\bar{t})$ vs. $M(\bar{t}\bar{t})$. The measurements are compared to the predictions of POWHEG and MG5_aMC@NLO (MG5) combined with PYTHIA8 (P8) or HERWIG++ (H++) and the multiparton simulations MG5_aMC@NLO+PYTHIA8 MLM and MG5_aMC@NLO+PYTHIA8 FxFx. The ratios of the predictions to the measured cross sections are shown at the bottom of each panel together with the statistical and systematic uncertainties of the measurement.

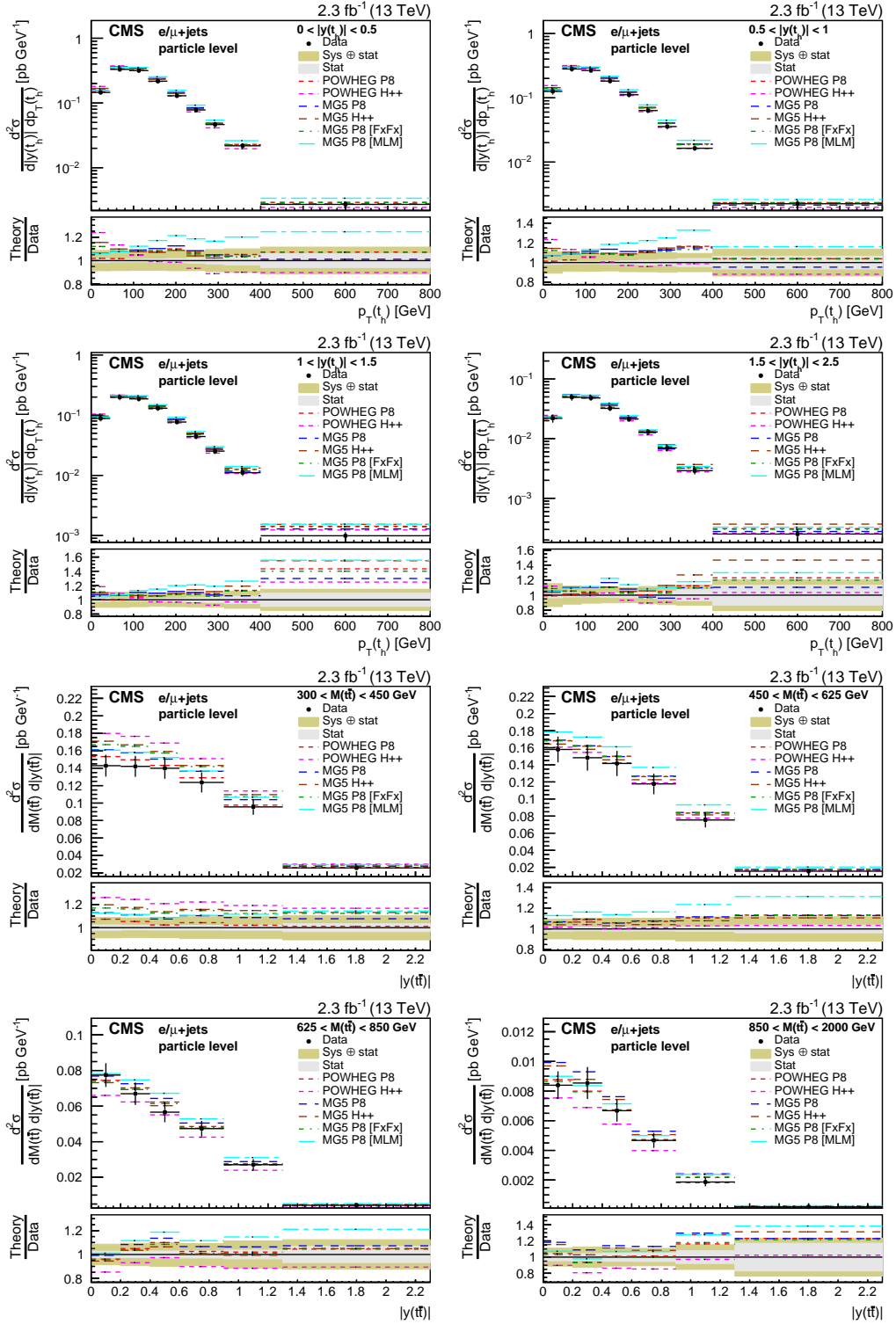


Figure 16: Double-differential cross sections at particle level as a function of $|y(t_h)|$ vs. $p_T(t_h)$ (upper two rows) and $M(t\bar{t})$ vs. $|y(t\bar{t})|$ (lower two rows). The measurements are compared to the predictions of POWHEG and MG5_aMC@NLO (MG5) combined with PYTHIA8 (P8) or HERWIG++ (H++) and the multiparton simulations MG5_aMC@NLO+PYTHIA8 MLM and MG5_aMC@NLO+PYTHIA8 FxFx. The ratios of the predictions to the measured cross sections are shown at the bottom of each panel together with the statistical and systematic uncertainties of the measurement.

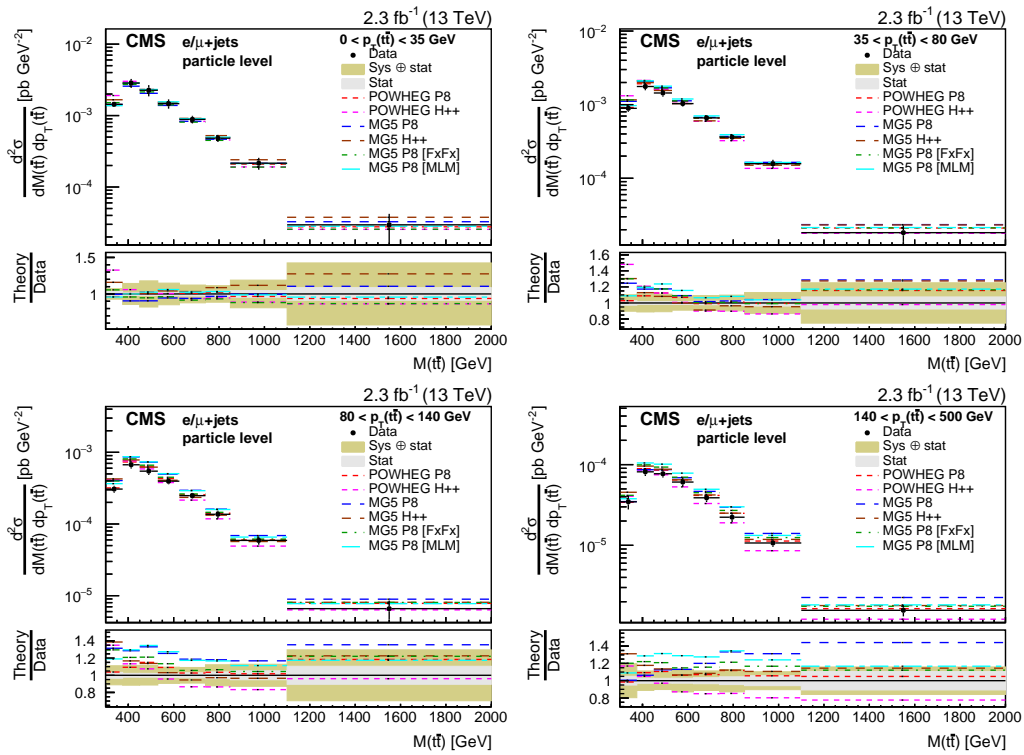


Figure 17: Double-differential cross section at particle level as a function of $p_T(\bar{t})$ vs. $M(\bar{t}\bar{t})$. The measurements are compared to the predictions of POWHEG and MG5_aMC@NLO (MG5) combined with PYTHIA8 (P8) or HERWIG++ (H++) and the multiparton simulations MG5_aMC@NLO+PYTHIA8 MLM and MG5_aMC@NLO+PYTHIA8 FxFx. The ratios of the predictions to the measured cross sections are shown at the bottom of each panel together with the statistical and systematic uncertainties of the measurement.

Table 2: Comparison between the measured distributions at parton level and the predictions of POWHEG and MG5_aMC@NLO combined with PYTHIA8 (P8) or HERWIG++ (H++) and the multiparton simulations MG5_aMC@NLO MLM and MG5_aMC@NLO FxFx, as well as the predictions of an approximate NNNLO calculation [42, 43], a NLO+NNLL' calculation [45], and a full NNLO calculation [46]. We list the results of the χ^2 tests together with the numbers of degrees of freedom (dof) and the corresponding p-values. For the comparison no uncertainties in the theoretical predictions are taken into account.

Distribution	χ^2/dof	p-value	χ^2/dof	p-value	χ^2/dof	p-value
	POWHEG+P8		POWHEG+H++		MG5_aMC@NLO+P8 MLM	
	Order: NLO		Order: NLO		Order: LO, up to 3 add. partons	
$p_T(t_h)$	10.7/9	0.295	8.01/9	0.533	19.0/9	0.025
$ y(t_h) $	3.91/7	0.790	4.33/7	0.741	4.49/7	0.721
$p_T(t_\ell)$	14.9/9	0.093	9.03/9	0.435	41.8/9	< 0.01
$ y(t_\ell) $	11.4/7	0.121	13.1/7	0.070	12.0/7	0.100
$M(t\bar{t})$	5.61/8	0.691	10.9/8	0.206	45.0/8	< 0.01
$p_T(t\bar{t})$	0.941/5	0.967	4.34/5	0.501	16.8/5	< 0.01
$ y(t\bar{t}) $	1.95/6	0.924	2.04/6	0.916	5.55/6	0.476
Additional jets	8.22/5	0.145	6.88/5	0.230	5.82/5	0.324
Additional jets vs. $p_T(t\bar{t})$	85.3/20	< 0.01	132/20	< 0.01	135/20	< 0.01
Additional jets vs. $p_T(t_h)$	89.0/36	< 0.01	43.1/36	0.193	71.7/36	< 0.01
$ y(t_h) $ vs. $p_T(t_h)$	55.3/36	0.021	52.4/36	0.038	60.7/36	< 0.01
$M(t\bar{t})$ vs. $ y(t\bar{t}) $	19.3/24	0.734	18.3/24	0.788	49.4/24	< 0.01
$p_T(t\bar{t})$ vs. $M(t\bar{t})$	14.5/32	0.997	26.2/32	0.755	100/32	< 0.01
	MG5_aMC@NLO+P8		MG5_aMC@NLO+H++		MG5_aMC@NLO+P8 FxFx	
	Order: NLO		Order: NLO		Order: NLO, up to 2 add. partons	
$p_T(t_h)$	8.68/9	0.467	15.3/9	0.084	9.35/9	0.406
$ y(t_h) $	4.11/7	0.767	5.42/7	0.608	3.91/7	0.790
$p_T(t_\ell)$	13.0/9	0.162	26.8/9	< 0.01	11.7/9	0.228
$ y(t_\ell) $	14.3/7	0.046	10.7/7	0.151	16.4/7	0.022
$M(t\bar{t})$	9.91/8	0.271	5.93/8	0.655	28.0/8	< 0.01
$p_T(t\bar{t})$	31.1/5	< 0.01	24.6/5	< 0.01	18.4/5	< 0.01
$ y(t\bar{t}) $	1.97/6	0.923	2.04/6	0.916	2.49/6	0.870
Additional jets	21.5/5	< 0.01	4.21/5	0.520	7.98/5	0.158
Additional jets vs. $p_T(t\bar{t})$	319/20	< 0.01	259/20	< 0.01	121/20	< 0.01
Additional jets vs. $p_T(t_h)$	90.9/36	< 0.01	45.0/36	0.145	52.5/36	0.037
$ y(t_h) $ vs. $p_T(t_h)$	73.1/36	< 0.01	111/36	< 0.01	48.1/36	0.086
$M(t\bar{t})$ vs. $ y(t\bar{t}) $	26.1/24	0.347	17.8/24	0.811	36.7/24	0.047
$p_T(t\bar{t})$ vs. $M(t\bar{t})$	229/32	< 0.01	71.5/32	< 0.01	97.6/32	< 0.01
	appr. NNLO		appr. NNNLO		NLO+NNLL'	
$p_T(t_h)$	14.3/9	0.111	36.7/9	< 0.01	6.29/9	0.710
$ y(t_h) $	5.30/7	0.623	2.59/7	0.920	—	—
$p_T(t_\ell)$	12.1/9	0.209	92.1/9	< 0.01	3.06/9	0.962
$ y(t_\ell) $	3.77/7	0.805	4.34/7	0.739	—	—
$M(t\bar{t})$	—	—	—	—	6.70/8	0.569
	NNLO					
$p_T(t_h)$	5.78/9	0.762				
$ y(t_h) $	2.20/7	0.948				
$p_T(t_\ell)$	5.54/9	0.785				
$ y(t_\ell) $	6.48/7	0.485				
$M(t\bar{t})$	5.88/8	0.660				
$p_T(t\bar{t})$	3.50/5	0.623				
$ y(t\bar{t}) $	1.42/6	0.965				

Table 3: Comparison between the measured distributions at particle level and the predictions of POWHEG and MG5_aMC@NLO combined with PYTHIA8 (P8) or HERWIG++ (H++) and the multiparton simulations MG5_aMC@NLO MLM and MG5_aMC@NLO FxFx. We list the results of the χ^2 tests together with the numbers of degrees of freedom (dof) and the corresponding p-values. For the comparison no uncertainties in the theoretical predictions are taken into account.

Distribution	χ^2/dof	p-value	χ^2/dof	p-value	χ^2/dof	p-value
	POWHEG+P8		POWHEG+H++		MG5_aMC@NLO+P8 MLM	
	Order: NLO		Order: NLO		Order: LO, up to 3 add. partons	
$p_T(t_h)$	14.2/9	0.115	24.0/9	< 0.01	32.8/9	< 0.01
$ y(t_h) $	3.47/7	0.838	5.66/7	0.579	6.64/7	0.468
$p_T(t_\ell)$	20.8/9	0.013	38.2/9	< 0.01	49.7/9	< 0.01
$ y(t_\ell) $	6.37/7	0.497	9.69/7	0.207	16.1/7	0.025
$M(t\bar{t})$	9.03/8	0.340	148/8	< 0.01	12.0/8	0.151
$p_T(t\bar{t})$	2.15/5	0.829	29.4/5	< 0.01	49.2/5	< 0.01
$ y(t\bar{t}) $	0.869/6	0.990	2.06/6	0.914	13.2/6	0.040
Additional jets	28.2/5	< 0.01	17.2/5	< 0.01	36.8/5	< 0.01
Additional jets vs. $p_T(t\bar{t})$	70.7/20	< 0.01	86.1/20	< 0.01	161/20	< 0.01
Additional jets vs. $p_T(t_h)$	91.6/36	< 0.01	200/36	< 0.01	162/36	< 0.01
$ y(t_h) $ vs. $p_T(t_h)$	56.2/36	0.017	197/36	< 0.01	114/36	< 0.01
$M(t\bar{t})$ vs. $ y(t\bar{t}) $	26.6/24	0.324	263/24	< 0.01	38.1/24	0.034
$p_T(t\bar{t})$ vs. $M(t\bar{t})$	13.4/32	0.998	459/32	< 0.01	89.0/32	< 0.01
	MG5_aMC@NLO+P8		MG5_aMC@NLO+H++		MG5_aMC@NLO+P8 FxFx	
	Order: NLO		Order: NLO		Order: NLO, up to 2 add. partons	
$p_T(t_h)$	11.9/9	0.221	5.51/9	0.788	4.17/9	0.900
$ y(t_h) $	7.34/7	0.394	10.6/7	0.156	5.93/7	0.547
$p_T(t_\ell)$	11.0/9	0.274	6.37/9	0.702	6.51/9	0.688
$ y(t_\ell) $	12.3/7	0.092	6.04/7	0.535	14.3/7	0.047
$M(t\bar{t})$	9.57/8	0.296	28.7/8	< 0.01	28.5/8	< 0.01
$p_T(t\bar{t})$	37.1/5	< 0.01	7.92/5	0.161	29.6/5	< 0.01
$ y(t\bar{t}) $	1.75/6	0.942	1.98/6	0.922	2.87/6	0.825
Additional jets	29.6/5	< 0.01	12.2/5	0.032	11.6/5	0.041
Additional jets vs. $p_T(t\bar{t})$	197/20	< 0.01	163/20	< 0.01	85.3/20	< 0.01
Additional jets vs. $p_T(t_h)$	151/36	< 0.01	57.7/36	0.012	40.4/36	0.282
$ y(t_h) $ vs. $p_T(t_h)$	36.6/36	0.441	82.5/36	< 0.01	42.2/36	0.222
$M(t\bar{t})$ vs. $ y(t\bar{t}) $	21.4/24	0.612	47.9/24	< 0.01	52.3/24	< 0.01
$p_T(t\bar{t})$ vs. $M(t\bar{t})$	119/32	< 0.01	164/32	< 0.01	107/32	< 0.01

Acknowledgments

We congratulate our colleagues in the CERN accelerator departments for the excellent performance of the LHC and thank the technical and administrative staffs at CERN and at other CMS institutes for their contributions to the success of the CMS effort. In addition, we gratefully acknowledge the computing centers and personnel of the Worldwide LHC Computing Grid for delivering so effectively the computing infrastructure essential to our analyses. Finally, we acknowledge the enduring support for the construction and operation of the LHC and the CMS detector provided by the following funding agencies: the Austrian Federal Ministry of Science, Research and Economy and the Austrian Science Fund; the Belgian Fonds de la Recherche Scientifique, and Fonds voor Wetenschappelijk Onderzoek; the Brazilian Funding Agencies (CNPq, CAPES, FAPERJ, and FAPESP); the Bulgarian Ministry of Education and Science; CERN; the Chinese Academy of Sciences, Ministry of Science and Technology, and National Natural Science Foundation of China; the Colombian Funding Agency (COLCIENCIAS); the Croatian Ministry of Science, Education and Sport, and the Croatian Science Foundation; the Research Promotion Foundation, Cyprus; the Secretariat for Higher Education, Science, Technology and Innovation, Ecuador; the Ministry of Education and Research, Estonian Research Council via IUT23-4 and IUT23-6 and European Regional Development Fund, Estonia; the Academy of Finland, Finnish Ministry of Education and Culture, and Helsinki Institute of Physics; the Institut National de Physique Nucléaire et de Physique des Particules / CNRS, and Commissariat à l'Énergie Atomique et aux Énergies Alternatives / CEA, France; the Bundesministerium für Bildung und Forschung, Deutsche Forschungsgemeinschaft, and Helmholtz-Gemeinschaft Deutscher Forschungszentren, Germany; the General Secretariat for Research and Technology, Greece; the National Scientific Research Foundation, and National Innovation Office, Hungary; the Department of Atomic Energy and the Department of Science and Technology, India; the Institute for Studies in Theoretical Physics and Mathematics, Iran; the Science Foundation, Ireland; the Istituto Nazionale di Fisica Nucleare, Italy; the Ministry of Science, ICT and Future Planning, and National Research Foundation (NRF), Republic of Korea; the Lithuanian Academy of Sciences; the Ministry of Education, and University of Malaya (Malaysia); the Mexican Funding Agencies (BUAP, CINVESTAV, CONACYT, LNS, SEP, and UASLP-FAI); the Ministry of Business, Innovation and Employment, New Zealand; the Pakistan Atomic Energy Commission; the Ministry of Science and Higher Education and the National Science Centre, Poland; the Fundação para a Ciência e a Tecnologia, Portugal; JINR, Dubna; the Ministry of Education and Science of the Russian Federation, the Federal Agency of Atomic Energy of the Russian Federation, Russian Academy of Sciences, and the Russian Foundation for Basic Research; the Ministry of Education, Science and Technological Development of Serbia; the Secretaría de Estado de Investigación, Desarrollo e Innovación and Programa Consolider-Ingenio 2010, Spain; the Swiss Funding Agencies (ETH Board, ETH Zurich, PSI, SNF, UniZH, Canton Zurich, and SER); the Ministry of Science and Technology, Taipei; the Thailand Center of Excellence in Physics, the Institute for the Promotion of Teaching Science and Technology of Thailand, Special Task Force for Activating Research and the National Science and Technology Development Agency of Thailand; the Scientific and Technical Research Council of Turkey, and Turkish Atomic Energy Authority; the National Academy of Sciences of Ukraine, and State Fund for Fundamental Researches, Ukraine; the Science and Technology Facilities Council, UK; the US Department of Energy, and the US National Science Foundation.

Individuals have received support from the Marie-Curie program and the European Research Council and EPLANET (European Union); the Leventis Foundation; the A. P. Sloan Foundation; the Alexander von Humboldt Foundation; the Belgian Federal Science Policy Office; the Fonds pour la Formation à la Recherche dans l'Industrie et dans l'Agriculture (FRRIA-Belgium);

the Agentschap voor Innovatie door Wetenschap en Technologie (IWT-Belgium); the Ministry of Education, Youth and Sports (MEYS) of the Czech Republic; the Council of Science and Industrial Research, India; the HOMING PLUS program of the Foundation for Polish Science, cofinanced from European Union, Regional Development Fund, the Mobility Plus program of the Ministry of Science and Higher Education, the National Science Center (Poland), contracts Harmonia 2014/14/M/ST2/00428, Opus 2013/11/B/ST2/04202, 2014/13/B/ST2/02543 and 2014/15/B/ST2/03998, Sonata-bis 2012/07/E/ST2/01406; the Thalys and Aristeia programs cofinanced by EU-ESF and the Greek NSRF; the National Priorities Research Program by Qatar National Research Fund; the Programa Clarín-COFUND del Principado de Asturias; the Rachadapisek Sompot Fund for Postdoctoral Fellowship, Chulalongkorn University and the Chulalongkorn Academic into Its 2nd Century Project Advancement Project (Thailand); and the Welch Foundation, contract C-1845.

References

- [1] CMS Collaboration, “CMS Luminosity Measurement for the 2015 Data Taking Period”, CMS Physics Analysis Summary CMS-PAS-LUM-15-001, 2017.
- [2] CMS Collaboration, “Measurement of differential top-quark pair production cross sections in pp collisions at $\sqrt{s} = 7$ TeV”, *Eur. Phys. J. C* **73** (2013) 2339, doi:10.1140/epjc/s10052-013-2339-4, arXiv:1211.2220.
- [3] ATLAS Collaboration, “Differential top-antitop cross-section measurements as a function of observables constructed from final-state particles using pp collisions at $\sqrt{s} = 7$ TeV in the ATLAS detector”, *JHEP* **06** (2015) 100, doi:10.1007/JHEP06(2015)100, arXiv:1502.05923.
- [4] CMS Collaboration, “Measurement of the differential cross section for top quark pair production in pp collisions at $\sqrt{s} = 8$ TeV”, *Eur. Phys. J. C* **75** (2015) 542, doi:10.1140/epjc/s10052-015-3709-x, arXiv:1505.04480.
- [5] ATLAS Collaboration, “Measurements of top-quark pair differential cross-sections in the lepton+jets channel in pp collisions at $\sqrt{s} = 8$ TeV using the ATLAS detector”, *Eur. Phys. J. C* **76** (2016) 538, doi:10.1140/epjc/s10052-016-4366-4, arXiv:1511.04716.
- [6] ATLAS Collaboration, “Measurement of the differential cross-section of highly boosted top quarks as a function of their transverse momentum in $\sqrt{s} = 8$ TeV proton-proton collisions using the ATLAS detector”, *Phys. Rev. D* **93** (2016) 032009, doi:10.1103/PhysRevD.93.032009, arXiv:1510.03818.
- [7] CMS Collaboration, “Measurement of the $t\bar{t}$ production cross section in the all-jets final state in pp collisions at $\sqrt{s} = 8$ TeV”, *Eur. Phys. J. C* **76** (2016) 128, doi:10.1140/epjc/s10052-016-3956-5, arXiv:1509.06076.
- [8] CMS Collaboration, “Measurement of the integrated and differential $t\bar{t}$ production cross sections for high- p_T top quarks in pp collisions at $\sqrt{s} = 8$ TeV”, *Phys. Rev. D* **94** (2016) 072002, doi:10.1103/PhysRevD.94.072002, arXiv:1605.00116.
- [9] P. Nason, “A new method for combining NLO QCD with shower Monte Carlo algorithms”, *JHEP* **11** (2004) 040, doi:10.1088/1126-6708/2004/11/040, arXiv:hep-ph/0409146.
- [10] S. Frixione, P. Nason, and C. Oleari, “Matching NLO QCD computations with Parton Shower simulations: the POWHEG method”, *JHEP* **11** (2007) 070, doi:10.1088/1126-6708/2007/11/070, arXiv:0709.2092.
- [11] S. Alioli, P. Nason, C. Oleari, and E. Re, “A general framework for implementing NLO calculations in shower Monte Carlo programs: the POWHEG BOX”, *JHEP* **06** (2010) 043, doi:10.1007/JHEP06(2010)043, arXiv:1002.2581.
- [12] J. M. Campbell, R. K. Ellis, P. Nason, and E. Re, “Top-pair production and decay at NLO matched with parton showers”, *JHEP* **04** (2015) 114, doi:10.1007/JHEP04(2015)114, arXiv:1412.1828.
- [13] J. Alwall et al., “The automated computation of tree-level and next-to-leading order differential cross sections, and their matching to parton shower simulations”, *JHEP* **07** (2014) 079, doi:10.1007/JHEP07(2014)079, arXiv:1405.0301.

- [14] T. Sjöstrand, S. Mrenna, and P. Skands, “PYTHIA 6.4 physics and manual”, *JHEP* **05** (2006) 026, doi:10.1088/1126-6708/2006/05/026, arXiv:hep-ph/0603175.
- [15] T. Sjöstrand, S. Mrenna, and P. Z. Skands, “A brief introduction to PYTHIA 8.1”, *Comput. Phys. Commun.* **178** (2008) 852, doi:10.1016/j.cpc.2008.01.036, arXiv:0710.3820.
- [16] P. Skands, S. Carrazza, and J. Rojo, “Tuning PYTHIA 8.1: the Monash 2013 Tune”, *Eur. Phys. J. C* **74** (2014) 3024, doi:10.1140/epjc/s10052-014-3024-y, arXiv:1404.5630.
- [17] J. Alwall et al., “Comparative study of various algorithms for the merging of parton showers and matrix elements in hadronic collisions”, *Eur. Phys. J. C* **53** (2008) 473, doi:10.1140/epjc/s10052-007-0490-5, arXiv:0706.2569.
- [18] R. Frederix and S. Frixione, “Merging meets matching in MC@NLO”, *JHEP* **12** (2012) 061, doi:10.1007/JHEP12(2012)061, arXiv:1209.6215.
- [19] NNPDF Collaboration, “Parton distributions for the LHC Run II”, *JHEP* **04** (2015) 040, doi:10.1007/JHEP04(2015)040, arXiv:1410.8849.
- [20] M. Czakon and A. Mitov, “Top++: A Program for the Calculation of the Top-Pair Cross-Section at Hadron Colliders”, *Comput. Phys. Commun.* **185** (2014) 2930, doi:10.1016/j.cpc.2014.06.021, arXiv:1112.5675.
- [21] M. Bähr et al., “Herwig++ physics and manual”, *Eur. Phys. J. C* **58** (2008) 639, doi:10.1140/epjc/s10052-008-0798-9, arXiv:0803.0883.
- [22] M. H. Seymour and A. Siodmok, “Constraining MPI models using σ_{eff} and recent Tevatron and LHC Underlying Event data”, *JHEP* **10** (2013) 113, doi:10.1007/JHEP10(2013)113, arXiv:1307.5015.
- [23] Y. Li and F. Petriello, “Combining QCD and electroweak corrections to dilepton production in FEWZ”, *Phys. Rev. D* **86** (2012) 094034, doi:10.1103/PhysRevD.86.094034, arXiv:1208.5967.
- [24] P. Kant et al., “HatHor for single top-quark production: Updated predictions and uncertainty estimates for single top-quark production in hadronic collisions”, *Comput. Phys. Commun.* **191** (2015) 74, doi:10.1016/j.cpc.2015.02.001, arXiv:1406.4403.
- [25] N. Kidonakis, “NNLL threshold resummation for top-pair and single-top production”, *Phys. Part. Nucl.* **45** (2014) 714, doi:10.1134/S1063779614040091, arXiv:1210.7813.
- [26] J. Allison et al., “Geant4 developments and applications”, *IEEE Trans. Nucl. Sci.* **53** (2006) 270, doi:10.1109/TNS.2006.869826.
- [27] M. Cacciari, G. P. Salam, and G. Soyez, “The anti- k_t jet clustering algorithm”, *JHEP* **04** (2008) 063, doi:10.1088/1126-6708/2008/04/063, arXiv:0802.1189.
- [28] M. Cacciari, G. P. Salam, and G. Soyez, “FastJet user manual”, *Eur. Phys. J. C* **72** (2012) 1896, doi:10.1140/epjc/s10052-012-1896-2, arXiv:1111.6097.

- [29] CMS Collaboration, “The CMS experiment at the CERN LHC”, *JINST* **3** (2008) S08004, doi:10.1088/1748-0221/3/08/S08004.
- [30] CMS Collaboration, “Particle-flow event reconstruction in CMS and performance for jets, taus, and E_T^{miss} ”, CMS Physics Analysis Summary CMS-PAS-PFT-09-001, 2009.
- [31] CMS Collaboration, “Commissioning of the particle-flow event reconstruction with the first LHC collisions recorded in the CMS detector”, CMS Physics Analysis Summary CMS-PAS-PFT-10-001, 2010.
- [32] CMS Collaboration, “Performance of CMS muon reconstruction in pp collision events at $\sqrt{s} = 7$ TeV”, *JINST* **7** (2012) P10002, doi:10.1088/1748-0221/7/10/P10002, arXiv:1206.4071.
- [33] CMS Collaboration, “Measurement of inclusive W and Z boson production cross sections in pp collisions at $\sqrt{s} = 8$ TeV”, *Phys. Rev. Lett.* **112** (2014) 191802, doi:10.1103/PhysRevLett.112.191802, arXiv:1402.0923.
- [34] M. Cacciari and G. P. Salam, “Pileup subtraction using jet areas”, *Phys. Lett. B* **659** (2008) 119, doi:10.1016/j.physletb.2007.09.077, arXiv:0707.1378.
- [35] CMS Collaboration, “Performance of electron reconstruction and selection with the CMS detector in proton-proton collisions at $\sqrt{s} = 8$ TeV”, *JINST* **10** (2015) P06005, doi:10.1088/1748-0221/10/06/P06005, arXiv:1502.02701.
- [36] CMS Collaboration, “Jet energy scale and resolution in the CMS experiment in pp collisions at 8 TeV”, (2016). arXiv:1607.03663. Submitted to *JINST*.
- [37] CMS Collaboration, “Identification of b quark jets at the CMS Experiment in the LHC Run 2”, CMS Physics Analysis Summary CMS-PAS-BTV-15-001, 2016.
- [38] B. A. Betchart, R. Demina, and A. Harel, “Analytic solutions for neutrino momenta in decay of top quarks”, *Nucl. Instrum. Meth. A* **736** (2014) 169, doi:10.1016/j.nima.2013.10.039, arXiv:1305.1878.
- [39] G. D’Agostini, “A multidimensional unfolding method based on Bayes’ theorem”, *Nucl. Instrum. Meth. A* **362** (1995) 487, doi:10.1016/0168-9002(95)00274-X.
- [40] M. Guzzi, K. Lipka, and S.-O. Moch, “Top-quark pair production at hadron colliders: differential cross section and phenomenological applications with DiffTop”, *JHEP* **01** (2015) 082, doi:10.1007/JHEP01(2015)082, arXiv:1406.0386.
- [41] S. Dulat et al., “New parton distribution functions from a global analysis of quantum chromodynamics”, *Phys. Rev. D* **93** (2016) 033006, doi:10.1103/PhysRevD.93.033006, arXiv:1506.07443.
- [42] N. Kidonakis, “NNNLO soft-gluon corrections for the top-antitop pair production cross section”, *Phys. Rev. D* **90** (2014) 014006, doi:10.1103/PhysRevD.90.014006, arXiv:1405.7046.
- [43] N. Kidonakis, “NNNLO soft-gluon corrections for the top-quark p_T and rapidity distributions”, *Phys. Rev. D* **91** (2015) 031501, doi:10.1103/PhysRevD.91.031501, arXiv:1411.2633.

-
- [44] A. D. Martin, W. J. Stirling, R. S. Thorne, and G. Watt, "Parton distributions for the LHC", *Eur. Phys. J. C* **63** (2009) 189, doi:10.1140/epjc/s10052-009-1072-5, arXiv:0901.0002.
- [45] B. Pecjak, D. Scott, X. Wang, and L. L. Yang, "Resummed Differential Cross Sections for Top-Quark Pairs at the LHC", *Phys. Rev. Lett.* **116** (2016) 202001, doi:10.1103/PhysRevLett.116.202001, arXiv:1601.07020.
- [46] M. Czakon, D. Heymes, and A. Mitov, "High-Precision Differential Predictions for Top-Quark Pairs at the LHC", *Phys. Rev. Lett.* **116** (2016) 082003, doi:10.1103/PhysRevLett.116.082003, arXiv:1511.00549.

A Tables of parton level cross sections.

Table 4: Differential cross section at parton level as a function of $p_T(t_h)$. The values are shown together with their statistical and systematic uncertainties.

$p_T(t_h)$ [GeV]	$\frac{d\sigma}{dp_T(t_h)}$ [fb GeV ⁻¹]	$p_T(t_h)$ [GeV]	$\frac{d\sigma}{dp_T(t_h)}$ [fb GeV ⁻¹]
0–45	680±20±180	225–270	228± 6 ±32
45–90	1500±20±190	270–315	119± 5 ±18
90–135	1290±20±160	315–400	46± 2 ±7
135–180	790±10±100	400–800	5.1±0.3±0.8
180–225	420± 9 ±59		—

Table 5: Differential cross section at parton level as a function of $|y(t_h)|$. The values are shown together with their statistical and systematic uncertainties.

$ y(t_h) $	$\frac{d\sigma}{d y(t_h) }$ [pb]	$ y(t_h) $	$\frac{d\sigma}{d y(t_h) }$ [pb]
0–0.2	142±2±14	1–1.3	100± 2 ±11
0.2–0.4	135±2±13	1.3–1.6	82± 2 ±11
0.4–0.7	129±2±13	1.6–2.5	44.0±0.9±6.4
0.7–1	114±2±12		—

Table 6: Differential cross section at parton level as a function of $p_T(t_\ell)$. The values are shown together with their statistical and systematic uncertainties.

$p_T(t_\ell)$ [GeV]	$\frac{d\sigma}{dp_T(t_\ell)}$ [fb GeV ⁻¹]	$p_T(t_\ell)$ [GeV]	$\frac{d\sigma}{dp_T(t_\ell)}$ [fb GeV ⁻¹]
0–45	690±10±100	225–270	218± 4 ±20
45–90	1470±20±190	270–315	115± 3 ±14
90–135	1300±10±150	315–400	47± 1 ±6
135–180	810±10±91	400–800	4.8±0.2±0.5
180–225	432± 7 ±44		—

Table 7: Differential cross section at parton level as a function of $|y(t_\ell)|$. The values are shown together with their statistical and systematic uncertainties.

$ y(t_\ell) $	$\frac{d\sigma}{d y(t_\ell) }$ [pb]	$ y(t_\ell) $	$\frac{d\sigma}{d y(t_\ell) }$ [pb]
0–0.2	$135 \pm 2 \pm 14$	1–1.3	$101 \pm 1 \pm 11$
0.2–0.4	$133 \pm 1 \pm 14$	1.3–1.6	$82 \pm 1 \pm 9$
0.4–0.7	$128 \pm 1 \pm 14$	1.6–2.5	$45.5 \pm 0.9 \pm 5.1$
0.7–1	$118 \pm 1 \pm 13$	—	—

Table 8: Differential cross section at parton level as a function of $p_T(\bar{t}\bar{t})$. The values are shown together with their statistical and systematic uncertainties.

$p_T(\bar{t}\bar{t})$ [GeV]	$\frac{d\sigma}{dp_T(\bar{t}\bar{t})}$ [fb GeV ⁻¹]	$p_T(\bar{t}\bar{t})$ [GeV]	$\frac{d\sigma}{dp_T(\bar{t}\bar{t})}$ [fb GeV ⁻¹]
0–35	$3050 \pm 70 \pm 870$	140–200	$220 \pm 10 \pm 30$
35–80	$1470 \pm 50 \pm 370$	200–500	$39 \pm 1 \pm 5$
80–140	$570 \pm 20 \pm 90$	—	—

Table 9: Differential cross section at parton level as a function of $M(\bar{t}\bar{t})$. The values are shown together with their statistical and systematic uncertainties.

$M(\bar{t}\bar{t})$ [GeV]	$\frac{d\sigma}{dM(\bar{t}\bar{t})}$ [fb GeV ⁻¹]	$M(\bar{t}\bar{t})$ [GeV]	$\frac{d\sigma}{dM(\bar{t}\bar{t})}$ [fb GeV ⁻¹]
300–375	$360 \pm 10 \pm 160$	625–740	$192 \pm 6 \pm 31$
375–450	$990 \pm 20 \pm 130$	740–850	$84 \pm 4 \pm 10$
450–530	$620 \pm 10 \pm 110$	850–1100	$35 \pm 2 \pm 6$
530–625	$373 \pm 9 \pm 48$	1100–2000	$3.6 \pm 0.3 \pm 0.4$

Table 10: Differential cross section at parton level as a function of $|y(\bar{t}\bar{t})|$. The values are shown together with their statistical and systematic uncertainties.

$ y(\bar{t}\bar{t}) $	$\frac{d\sigma}{d y(\bar{t}\bar{t}) }$ [pb]	$ y(\bar{t}\bar{t}) $	$\frac{d\sigma}{d y(\bar{t}\bar{t}) }$ [pb]
0–0.2	$166 \pm 3 \pm 17$	0.6–0.9	$137 \pm 2 \pm 15$
0.2–0.4	$157 \pm 3 \pm 17$	0.9–1.3	$103 \pm 2 \pm 12$
0.4–0.6	$149 \pm 3 \pm 16$	1.3–2.3	$48 \pm 1 \pm 6$

Table 11: Cross sections at parton level in bins of the number of additional jets. The values are shown together with their statistical and systematic uncertainties.

Additional jets	σ [pb]	Additional jets	σ [pb]
0	$97 \pm 2 \pm 7$	3	$12.7 \pm 0.6 \pm 3.1$
1	$77 \pm 2 \pm 11$	≥ 4	$5.9 \pm 0.2 \pm 2.1$
2	$36 \pm 1 \pm 6$	—	—

Table 12: Differential cross sections at parton level as a function of $p_T(t_h)$ in bins of the number of additional jets. The values are shown together with their statistical and systematic uncertainties.

$p_T(t_h)$ [GeV]	$\frac{d\sigma}{dp_T(t_h)}$ [fb GeV ⁻¹]	$p_T(t_h)$ [GeV]	$\frac{d\sigma}{dp_T(t_h)}$ [fb GeV ⁻¹]
Additional jets: 0			
0–45	340±20±100	225–270	71± 4 ±9
45–90	750±20±110	270–315	29± 3 ±5
90–135	610±20±70	315–400	11± 1 ±2
135–180	310±10±20	400–800	1.0±0.2±0.1
180–225	157± 7 ±16		—
Additional jets: 1			
0–45	206± 6 ±30	225–270	79± 4 ±11
45–90	458± 9 ±60	270–315	42± 3 ±7
90–135	408± 8 ±69	315–400	17± 1 ±2
135–180	267± 6 ±52	400–800	1.8±0.2±0.4
180–225	138± 5 ±24		—
Additional jets: 2			
0–45	92± 3 ±17	225–270	50± 2 ±9
45–90	210± 5 ±37	270–315	29± 2 ±6
90–135	196± 4 ±35	315–400	10.6±1.0±1.7
135–180	136± 4 ±25	400–800	1.1±0.2±0.2
180–225	82± 3 ±17		—
Additional jets: ≥3			
0–45	40± 2 ±8	225–270	28± 2 ±8
45–90	90± 3 ±20	270–315	18± 1 ±5
90–135	94± 3 ±25	315–400	8.4±0.8±3.1
135–180	69± 2 ±21	400–800	1.2±0.2±0.3
180–225	45± 2 ±14		—

Table 13: Differential cross sections at parton level as a function of $p_T(\bar{t}t)$ in bins of the number of additional jets. The values are shown together with their statistical and systematic uncertainties.

$p_T(\bar{t}t)$ [GeV]	$\frac{d\sigma}{dp_T(\bar{t}t)}$ [fb GeV ⁻¹]	$p_T(\bar{t}t)$ [GeV]	$\frac{d\sigma}{dp_T(\bar{t}t)}$ [fb GeV ⁻¹]
Additional jets: 0			
0–35	2220±60±530	140–200	14± 5 ±6
35–80	420±40±210	200–500	0.1±0.2±0.1
80–140	50±10±40		—
Additional jets: 1			
0–35	610±40±160	140–200	100± 10 ±20
35–80	670±30±90	200–500	9± 1 ±2
80–140	260±20±40		—
Additional jets: 2			
0–35	150±10±40	140–200	68± 8 ±12
35–80	240±10±60	200–500	18± 1 ±3
80–140	180±10±40		—
Additional jets: ≥3			
0–35	42± 6 ±22	140–200	54± 6 ±13
35–80	95± 8 ±29	200–500	14.3±0.8±3.4
80–140	77± 6 ±23		—

Table 14: Double-differential cross section at parton level as a function of $|y(t_h)|$ vs. $p_T(t_h)$. The values are shown together with their statistical and systematic uncertainties.

$p_T(t_h)$ [GeV]	$\frac{d^2\sigma}{dp_T(t_h)dy(t_h)}$ [fb GeV ⁻¹]	$p_T(t_h)$ [GeV]	$\frac{d^2\sigma}{dp_T(t_h)dy(t_h)}$ [fb GeV ⁻¹]
$0 < y(t_h) < 0.5$			
0–45	370± 8 ±74	225–270	149± 4 ±19
45–90	830±10±120	270–315	81± 3 ±11
90–135	770±10±80	315–400	36± 2 ±6
135–180	493± 8 ±59	400–800	4.4± 0.3 ±0.6
180–225	268± 6 ±36		—
$0.5 < y(t_h) < 1$			
0–45	340± 7 ±56	225–270	127± 4 ±22
45–90	730±10±110	270–315	65± 3 ±11
90–135	669±10±73	315–400	26± 1 ±3
135–180	425± 8 ±49	400–800	3.3± 0.3 ±0.6
180–225	238± 6 ±34		—
$1 < y(t_h) < 1.5$			
0–45	278± 7 ±44	225–270	88± 3 ±11
45–90	600±10±70	270–315	48± 2 ±8
90–135	528± 9 ±65	315–400	19± 1 ±3
135–180	334± 7 ±46	400–800	1.5± 0.2 ±0.2
180–225	173± 5 ±25		—
$1.5 < y(t_h) < 2.5$			
0–45	188± 7 ±24	225–270	46± 2 ±8
45–90	385± 9 ±50	270–315	20± 1 ±4
90–135	318± 7 ±44	315–400	6.3± 0.6 ±1.0
135–180	175± 5 ±22	400–800	0.50±0.09±0.09
180–225	91± 3 ±12		—

Table 15: Double-differential cross section at parton level as a function of $M(\bar{t}t)$ vs. $|y(\bar{t}t)|$. The values are shown together with their statistical and systematic uncertainties.

$ y(\bar{t}t) $	$\frac{d^2\sigma}{dM(\bar{t}t)d y(\bar{t}t) }$ [fb GeV ⁻¹]	$ y(\bar{t}t) $	$\frac{d^2\sigma}{dM(\bar{t}t)d y(\bar{t}t) }$ [fb GeV ⁻¹]
$300 < M(\bar{t}t) < 450 \text{ GeV}$			
0–0.2	$418 \pm 10 \pm 67$	0.6–0.9	$374 \pm 7 \pm 53$
0.2–0.4	$418 \pm 8 \pm 63$	0.9–1.3	$307 \pm 7 \pm 46$
0.4–0.6	$409 \pm 8 \pm 56$	1.3–2.3	$162 \pm 5 \pm 25$
$450 < M(\bar{t}t) < 625 \text{ GeV}$			
0–0.2	$359 \pm 7 \pm 45$	0.6–0.9	$303 \pm 6 \pm 43$
0.2–0.4	$343 \pm 6 \pm 45$	0.9–1.3	$224 \pm 5 \pm 36$
0.4–0.6	$331 \pm 7 \pm 46$	1.3–2.3	$99 \pm 3 \pm 15$
$625 < M(\bar{t}t) < 850 \text{ GeV}$			
0–0.2	$123 \pm 4 \pm 18$	0.6–0.9	$87 \pm 3 \pm 13$
0.2–0.4	$108 \pm 3 \pm 17$	0.9–1.3	$62 \pm 3 \pm 13$
0.4–0.6	$92 \pm 3 \pm 13$	1.3–2.3	$24 \pm 2 \pm 5$
$850 < M(\bar{t}t) < 2000 \text{ GeV}$			
0–0.2	$10.0 \pm 0.6 \pm 1.5$	0.6–0.9	$6.9 \pm 0.5 \pm 0.8$
0.2–0.4	$10.1 \pm 0.6 \pm 1.4$	0.9–1.3	$3.7 \pm 0.4 \pm 0.5$
0.4–0.6	$9.1 \pm 0.6 \pm 1.5$	1.3–2.3	$1.0 \pm 0.2 \pm 0.2$

Table 16: Double-differential cross section at parton level as a function of $p_T(\bar{t}\bar{t})$ vs. $M(\bar{t}\bar{t})$. The values are shown together with their statistical and systematic uncertainties.

$M(\bar{t}\bar{t})$ [GeV]	$\frac{d^2\sigma}{dp_T(\bar{t}\bar{t})dM(\bar{t}\bar{t})}$ [fb GeV ⁻²]	$M(\bar{t}\bar{t})$ [GeV]	$\frac{d^2\sigma}{dp_T(\bar{t}\bar{t})dM(\bar{t}\bar{t})}$ [fb GeV ⁻²]
$0 < p_T(\bar{t}\bar{t}) < 35 \text{ GeV}$			
300–375	$4.8 \pm 0.2 \pm 2.0$	625–740	$2.18 \pm 0.09 \pm 0.63$
375–450	$13.7 \pm 0.3 \pm 3.0$	740–850	$0.92 \pm 0.06 \pm 0.18$
450–530	$8.5 \pm 0.2 \pm 3.8$	850–1100	$0.36 \pm 0.03 \pm 0.12$
530–625	$4.4 \pm 0.1 \pm 1.3$	1100–2000	$0.039 \pm 0.005 \pm 0.012$
$35 < p_T(\bar{t}\bar{t}) < 80 \text{ GeV}$			
300–375	$2.25 \pm 0.07 \pm 1.20$	625–740	$1.32 \pm 0.04 \pm 0.22$
375–450	$6.6 \pm 0.1 \pm 1.6$	740–850	$0.60 \pm 0.03 \pm 0.07$
450–530	$4.30 \pm 0.08 \pm 0.60$	850–1100	$0.23 \pm 0.01 \pm 0.03$
530–625	$2.53 \pm 0.06 \pm 0.29$	1100–2000	$0.022 \pm 0.002 \pm 0.005$
$80 < p_T(\bar{t}\bar{t}) < 140 \text{ GeV}$			
300–375	$0.76 \pm 0.03 \pm 0.30$	625–740	$0.51 \pm 0.02 \pm 0.07$
375–450	$2.24 \pm 0.05 \pm 0.50$	740–850	$0.25 \pm 0.01 \pm 0.04$
450–530	$1.52 \pm 0.04 \pm 0.19$	850–1100	$0.100 \pm 0.008 \pm 0.026$
530–625	$0.96 \pm 0.03 \pm 0.10$	1100–2000	$0.011 \pm 0.002 \pm 0.002$
$140 < p_T(\bar{t}\bar{t}) < 500 \text{ GeV}$			
300–375	$0.095 \pm 0.005 \pm 0.025$	625–740	$0.068 \pm 0.003 \pm 0.017$
375–450	$0.258 \pm 0.008 \pm 0.032$	740–850	$0.036 \pm 0.002 \pm 0.004$
450–530	$0.185 \pm 0.006 \pm 0.024$	850–1100	$0.016 \pm 0.001 \pm 0.003$
530–625	$0.122 \pm 0.005 \pm 0.034$	1100–2000	$0.0018 \pm 0.0003 \pm 0.0003$

B Tables of particle level cross sections.

Table 17: Differential cross section at particle level as a function of $p_T(t_h)$. The values are shown together with their statistical and systematic uncertainties.

$p_T(t_h)$ [GeV]	$\frac{d\sigma}{dp_T(t_h)}$ [fb GeV ⁻¹]	$p_T(t_h)$ [GeV]	$\frac{d\sigma}{dp_T(t_h)}$ [fb GeV ⁻¹]
0–45	204±4±18	225–270	106± 2 ±9
45–90	461±5±40	270–315	61± 2 ±6
90–135	430±5±41	315–400	27.4±0.9±2.5
135–180	292±4±27	400–800	3.2±0.2±0.3
180–225	179±3±17		—

Table 18: Differential cross section at particle level as a function of $|y(t_h)|$. The values are shown together with their statistical and systematic uncertainties.

$ y(t_h) $	$\frac{d\sigma}{d y(t_h) }$ [pb]	$ y(t_h) $	$\frac{d\sigma}{d y(t_h) }$ [pb]
0–0.2	61.3±0.7±5.2	1–1.3	38.6±0.4±3.7
0.2–0.4	59.4±0.6±4.9	1.3–1.6	27.8±0.4±3.1
0.4–0.7	55.1±0.5±4.7	1.6–2.5	7.3±0.1±0.8
0.7–1	47.6±0.5±4.2		—

Table 19: Differential cross section at particle level as a function of $p_T(t_\ell)$. The values are shown together with their statistical and systematic uncertainties.

$p_T(t_\ell)$ [GeV]	$\frac{d\sigma}{dp_T(t_\ell)}$ [fb GeV ⁻¹]	$p_T(t_\ell)$ [GeV]	$\frac{d\sigma}{dp_T(t_\ell)}$ [fb GeV ⁻¹]
0–45	185±3±17	225–270	113± 2 ±9
45–90	425±4±41	270–315	67± 2 ±5
90–135	429±4±41	315–400	30.6±0.9±2.4
135–180	310±4±28	400–800	3.7±0.2±0.4
180–225	194±3±16		—

Table 20: Differential cross section at particle level as a function of $|y(t_\ell)|$. The values are shown together with their statistical and systematic uncertainties.

$ y(t_\ell) $	$\frac{d\sigma}{d y(t_\ell) }$ [pb]	$ y(t_\ell) $	$\frac{d\sigma}{d y(t_\ell) }$ [pb]
0–0.2	$55.7 \pm 0.7 \pm 5.0$	1–1.3	$38.9 \pm 0.5 \pm 3.6$
0.2–0.4	$54.6 \pm 0.6 \pm 5.1$	1.3–1.6	$29.3 \pm 0.4 \pm 2.7$
0.4–0.7	$52.0 \pm 0.5 \pm 4.9$	1.6–2.5	$10.2 \pm 0.2 \pm 0.9$
0.7–1	$47.2 \pm 0.5 \pm 4.4$	—	—

Table 21: Differential cross section at particle level as a function of $p_T(\bar{t}\bar{t})$. The values are shown together with their statistical and systematic uncertainties.

$p_T(\bar{t}\bar{t})$ [GeV]	$\frac{d\sigma}{dp_T(\bar{t}\bar{t})}$ [fb GeV ⁻¹]	$p_T(\bar{t}\bar{t})$ [GeV]	$\frac{d\sigma}{dp_T(\bar{t}\bar{t})}$ [fb GeV ⁻¹]
0–35	$890 \pm 10 \pm 140$	140–200	$92 \pm 3 \pm 10$
35–80	$577 \pm 10 \pm 62$	200–500	$18.4 \pm 0.5 \pm 1.7$
80–140	$219 \pm 5 \pm 22$	—	—

Table 22: Differential cross section at particle level as a function of $M(\bar{t}\bar{t})$. The values are shown together with their statistical and systematic uncertainties.

$M(\bar{t}\bar{t})$ [GeV]	$\frac{d\sigma}{dM(\bar{t}\bar{t})}$ [fb GeV ⁻¹]	$M(\bar{t}\bar{t})$ [GeV]	$\frac{d\sigma}{dM(\bar{t}\bar{t})}$ [fb GeV ⁻¹]
300–375	$124 \pm 4 \pm 14$	625–740	$91 \pm 2 \pm 8$
375–450	$247 \pm 4 \pm 27$	740–850	$47 \pm 2 \pm 4$
450–530	$200 \pm 4 \pm 22$	850–1100	$22.3 \pm 0.8 \pm 2.1$
530–625	$144 \pm 3 \pm 13$	1100–2000	$2.7 \pm 0.2 \pm 0.4$

Table 23: Differential cross section at particle level as a function of $|y(\bar{t}\bar{t})|$. The values are shown together with their statistical and systematic uncertainties.

$ y(\bar{t}\bar{t}) $	$\frac{d\sigma}{d y(\bar{t}\bar{t}) }$ [pb]	$ y(\bar{t}\bar{t}) $	$\frac{d\sigma}{d y(\bar{t}\bar{t}) }$ [pb]
0–0.2	$76.2 \pm 0.9 \pm 6.6$	0.6–0.9	$55.0 \pm 0.6 \pm 4.9$
0.2–0.4	$71.8 \pm 0.7 \pm 6.3$	0.9–1.3	$35.8 \pm 0.5 \pm 3.5$
0.4–0.6	$66.1 \pm 0.7 \pm 6.1$	1.3–2.3	$7.7 \pm 0.2 \pm 0.8$

Table 24: Cross sections at particle level in bins of the number of additional jets. The values are shown together with their statistical and systematic uncertainties.

Additional jets	σ [pb]	Additional jets	σ [pb]
0	$39.9 \pm 0.4 \pm 3.0$	3	$3.8 \pm 0.1 \pm 0.6$
1	$25.6 \pm 0.3 \pm 2.7$	≥ 4	$1.75 \pm 0.07 \pm 0.36$
2	$10.6 \pm 0.2 \pm 1.3$	—	—

Table 25: Differential cross sections at particle level as a function of $p_T(t_h)$ in bins of the number of additional jets. The values are shown together with their statistical and systematic uncertainties.

$p_T(t_h)$ [GeV]	$\frac{d\sigma}{dp_T(t_h)}$ [fb GeV ⁻¹]	$p_T(t_h)$ [GeV]	$\frac{d\sigma}{dp_T(t_h)}$ [fb GeV ⁻¹]
Additional jets: 0			
0–45	108 ± 3 ± 7	225–270	44 ± 1 ± 4
45–90	241 ± 4 ± 16	270–315	22.7 ± 0.9 ± 2.0
90–135	226 ± 3 ± 16	315–400	9.7 ± 0.5 ± 1.3
135–180	146 ± 3 ± 10	400–800	1.09 ± 0.09 ± 0.15
180–225	84 ± 2 ± 7		—
Additional jets: 1			
0–45	60 ± 1 ± 7	225–270	34.8 ± 0.9 ± 3.6
45–90	136 ± 2 ± 16	270–315	20.9 ± 0.7 ± 2.6
90–135	129 ± 2 ± 13	315–400	9.4 ± 0.4 ± 0.8
135–180	92 ± 1 ± 9	400–800	1.06 ± 0.08 ± 0.14
180–225	57 ± 1 ± 6		—
Additional jets: 2			
0–45	24.7 ± 0.5 ± 3.5	225–270	17.1 ± 0.5 ± 2.1
45–90	55.8 ± 0.9 ± 7.7	270–315	10.7 ± 0.4 ± 1.3
90–135	52.7 ± 0.8 ± 6.9	315–400	4.9 ± 0.3 ± 0.6
135–180	38.4 ± 0.7 ± 4.6	400–800	0.60 ± 0.05 ± 0.08
180–225	26.0 ± 0.6 ± 3.1		—
Additional jets: ≥ 3			
0–45	11.6 ± 0.3 ± 2.0	225–270	9.4 ± 0.4 ± 1.4
45–90	25.9 ± 0.6 ± 4.4	270–315	6.5 ± 0.3 ± 1.0
90–135	26.0 ± 0.6 ± 4.3	315–400	3.5 ± 0.2 ± 0.6
135–180	19.2 ± 0.5 ± 2.8	400–800	0.47 ± 0.05 ± 0.07
180–225	13.5 ± 0.4 ± 1.8		—

Table 26: Differential cross sections at particle level as a function of $p_T(\bar{t}\bar{t})$ in bins of the number of additional jets. The values are shown together with their statistical and systematic uncertainties.

$p_T(\bar{t}\bar{t})$ [GeV]	$\frac{d\sigma}{dp_T(\bar{t}\bar{t})}$ [fb GeV ⁻¹]	$p_T(\bar{t}\bar{t})$ [GeV]	$\frac{d\sigma}{dp_T(\bar{t}\bar{t})}$ [fb GeV ⁻¹]
Additional jets: 0			
0–35	730 ± 10 ± 100	140–200	7 ± 1 ± 2
35–80	268 ± 8 ± 31	200–500	0.19 ± 0.09 ± 0.07
80–140	33 ± 3 ± 8		—
Additional jets: 1			
0–35	118 ± 5 ± 19	140–200	45 ± 3 ± 5
35–80	222 ± 5 ± 26	200–500	6.6 ± 0.4 ± 0.7
80–140	112 ± 4 ± 12		—
Additional jets: 2			
0–35	25 ± 2 ± 5	140–200	26 ± 2 ± 3
35–80	59 ± 3 ± 10	200–500	6.8 ± 0.4 ± 0.7
80–140	55 ± 2 ± 8		—
Additional jets: ≥3			
0–35	8.1 ± 1.0 ± 2.0	140–200	17 ± 1 ± 4
35–80	23 ± 2 ± 5	200–500	5.4 ± 0.3 ± 0.8
80–140	22 ± 1 ± 4		—

Table 27: Double-differential cross section at particle level as a function of $|y(t_h)|$ vs. $p_T(t_h)$. The values are shown together with their statistical and systematic uncertainties.

$p_T(t_h)$ [GeV]	$\frac{d^2\sigma}{dp_T(t_h)d y(t_h) }$ [fb GeV ⁻¹]	$p_T(t_h)$ [GeV]	$\frac{d^2\sigma}{dp_T(t_h)d y(t_h) }$ [fb GeV ⁻¹]
$0 < y(t_h) < 0.5$			
0–45	146 ± 2 ± 12	225–270	78 ± 2 ± 6
45–90	330 ± 4 ± 28	270–315	46 ± 1 ± 4
90–135	316 ± 4 ± 26	315–400	21.8 ± 0.8 ± 2.0
135–180	217 ± 3 ± 18	400–800	2.7 ± 0.2 ± 0.3
180–225	129 ± 2 ± 11		—
$0.5 < y(t_h) < 1$			
0–45	126 ± 2 ± 13	225–270	63 ± 2 ± 6
45–90	281 ± 3 ± 25	270–315	36 ± 1 ± 3
90–135	267 ± 3 ± 23	315–400	16.4 ± 0.7 ± 1.4
135–180	182 ± 3 ± 15	400–800	2.2 ± 0.1 ± 0.3
180–225	112 ± 2 ± 10		—
$1 < y(t_h) < 1.5$			
0–45	88 ± 2 ± 9	225–270	44 ± 1 ± 4
45–90	198 ± 3 ± 21	270–315	25.3 ± 1.0 ± 2.3
90–135	186 ± 3 ± 18	315–400	11.1 ± 0.6 ± 1.2
135–180	130 ± 2 ± 12	400–800	0.99 ± 0.09 ± 0.11
180–225	77 ± 2 ± 7		—
$1.5 < y(t_h) < 2.5$			
0–45	21.9 ± 0.8 ± 3.3	225–270	12.9 ± 0.5 ± 1.4
45–90	49 ± 1 ± 6	270–315	7.0 ± 0.4 ± 0.8
90–135	48 ± 1 ± 5	315–400	2.9 ± 0.2 ± 0.3
135–180	32.2 ± 0.9 ± 3.2	400–800	0.25 ± 0.03 ± 0.04
180–225	21.3 ± 0.7 ± 2.0		—

Table 28: Double-differential cross section at particle level as a function of $M(\text{t}\bar{\text{t}})$ vs. $|y(\text{t}\bar{\text{t}})|$. The values are shown together with their statistical and systematic uncertainties.

$ y(\text{t}\bar{\text{t}}) $	$\frac{d^2\sigma}{dM(\text{t}\bar{\text{t}})d y(\text{t}\bar{\text{t}}) }$ [fb GeV ⁻¹]	$ y(\text{t}\bar{\text{t}}) $	$\frac{d^2\sigma}{dM(\text{t}\bar{\text{t}})d y(\text{t}\bar{\text{t}}) }$ [fb GeV ⁻¹]
$300 < M(\text{t}\bar{\text{t}}) < 450 \text{ GeV}$			
0–0.2	$143 \pm 3 \pm 12$	0.6–0.9	$124 \pm 3 \pm 11$
0.2–0.4	$142 \pm 3 \pm 12$	0.9–1.3	$96 \pm 2 \pm 9$
0.4–0.6	$140 \pm 3 \pm 12$	1.3–2.3	$25.7 \pm 0.9 \pm 2.5$
$450 < M(\text{t}\bar{\text{t}}) < 625 \text{ GeV}$			
0–0.2	$158 \pm 3 \pm 15$	0.6–0.9	$118 \pm 2 \pm 12$
0.2–0.4	$148 \pm 3 \pm 15$	0.9–1.3	$75 \pm 2 \pm 9$
0.4–0.6	$142 \pm 3 \pm 14$	1.3–2.3	$15.5 \pm 0.6 \pm 1.7$
$625 < M(\text{t}\bar{\text{t}}) < 850 \text{ GeV}$			
0–0.2	$77 \pm 2 \pm 6$	0.6–0.9	$47 \pm 1 \pm 4$
0.2–0.4	$67 \pm 2 \pm 6$	0.9–1.3	$27 \pm 1 \pm 3$
0.4–0.6	$57 \pm 2 \pm 5$	1.3–2.3	$4.3 \pm 0.3 \pm 0.4$
$850 < M(\text{t}\bar{\text{t}}) < 2000 \text{ GeV}$			
0–0.2	$8.4 \pm 0.4 \pm 0.9$	0.6–0.9	$4.7 \pm 0.3 \pm 0.4$
0.2–0.4	$8.5 \pm 0.4 \pm 1.0$	0.9–1.3	$1.9 \pm 0.1 \pm 0.2$
0.4–0.6	$6.7 \pm 0.3 \pm 0.7$	1.3–2.3	$0.20 \pm 0.03 \pm 0.03$

Table 29: Double-differential cross section at particle level as a function of $p_T(\bar{t}\bar{t})$ vs. $M(\bar{t}\bar{t})$. The values are shown together with their statistical and systematic uncertainties.

$M(\bar{t}\bar{t})$ [GeV]	$\frac{d^2\sigma}{dp_T(\bar{t}\bar{t})dM(\bar{t}\bar{t})}$ [fb GeV ⁻²]	$M(\bar{t}\bar{t})$ [GeV]	$\frac{d^2\sigma}{dp_T(\bar{t}\bar{t})dM(\bar{t}\bar{t})}$ [fb GeV ⁻²]
$0 < p_T(\bar{t}\bar{t}) < 35$ GeV			
300–375	$1.44 \pm 0.05 \pm 0.09$	625–740	$0.88 \pm 0.02 \pm 0.11$
375–450	$2.85 \pm 0.06 \pm 0.41$	740–850	$0.48 \pm 0.02 \pm 0.05$
450–530	$2.26 \pm 0.05 \pm 0.40$	850–1100	$0.215 \pm 0.010 \pm 0.040$
530–625	$1.47 \pm 0.03 \pm 0.22$	1100–2000	$0.030 \pm 0.003 \pm 0.012$
$35 < p_T(\bar{t}\bar{t}) < 80$ GeV			
300–375	$0.89 \pm 0.02 \pm 0.09$	625–740	$0.66 \pm 0.01 \pm 0.06$
375–450	$1.76 \pm 0.03 \pm 0.20$	740–850	$0.36 \pm 0.01 \pm 0.03$
450–530	$1.44 \pm 0.02 \pm 0.16$	850–1100	$0.158 \pm 0.006 \pm 0.020$
530–625	$1.03 \pm 0.02 \pm 0.09$	1100–2000	$0.018 \pm 0.001 \pm 0.004$
$80 < p_T(\bar{t}\bar{t}) < 140$ GeV			
300–375	$0.31 \pm 0.01 \pm 0.03$	625–740	$0.249 \pm 0.007 \pm 0.021$
375–450	$0.67 \pm 0.02 \pm 0.08$	740–850	$0.137 \pm 0.005 \pm 0.016$
450–530	$0.55 \pm 0.01 \pm 0.06$	850–1100	$0.059 \pm 0.003 \pm 0.007$
530–625	$0.395 \pm 0.010 \pm 0.036$	1100–2000	$0.0066 \pm 0.0007 \pm 0.0018$
$140 < p_T(\bar{t}\bar{t}) < 500$ GeV			
300–375	$0.035 \pm 0.002 \pm 0.007$	625–740	$0.039 \pm 0.001 \pm 0.004$
375–450	$0.081 \pm 0.002 \pm 0.009$	740–850	$0.022 \pm 0.001 \pm 0.003$
450–530	$0.077 \pm 0.002 \pm 0.008$	850–1100	$0.0107 \pm 0.0006 \pm 0.0009$
530–625	$0.061 \pm 0.002 \pm 0.008$	1100–2000	$0.0016 \pm 0.0002 \pm 0.0002$

C The CMS Collaboration

Yerevan Physics Institute, Yerevan, Armenia

V. Khachatryan, A.M. Sirunyan, A. Tumasyan

Institut für Hochenergiephysik, Wien, Austria

W. Adam, E. Asilar, T. Bergauer, J. Brandstetter, E. Brondolin, M. Dragicevic, J. Erö, M. Flechl, M. Friedl, R. Frühwirth¹, V.M. Ghete, C. Hartl, N. Hörmann, J. Hrubec, M. Jeitler¹, A. König, I. Krätschmer, D. Liko, T. Matsushita, I. Mikulec, D. Rabadý, N. Rad, B. Rahbaran, H. Rohringer, J. Schieck¹, J. Strauss, W. Waltenberger, C.-E. Wulz¹

Institute for Nuclear Problems, Minsk, Belarus

O. Dvornikov, V. Makarenko, V. Zykunov

National Centre for Particle and High Energy Physics, Minsk, Belarus

V. Mossolov, N. Shumeiko, J. Suarez Gonzalez

Universiteit Antwerpen, Antwerpen, Belgium

S. Alderweireldt, E.A. De Wolf, X. Janssen, J. Lauwers, M. Van De Klundert, H. Van Haevermaet, P. Van Mechelen, N. Van Remortel, A. Van Spilbeeck

Vrije Universiteit Brussel, Brussel, Belgium

S. Abu Zeid, F. Blekman, J. D'Hondt, N. Daci, I. De Bruyn, K. Deroover, S. Lowette, S. Moortgat, L. Moreels, A. Olbrechts, Q. Python, S. Tavernier, W. Van Doninck, P. Van Mulders, I. Van Parijs

Université Libre de Bruxelles, Bruxelles, Belgium

H. Brun, B. Clerbaux, G. De Lentdecker, H. Delannoy, G. Fasanella, L. Favart, R. Goldouzian, A. Grebenyuk, G. Karapostoli, T. Lenzi, A. Léonard, J. Luetic, T. Maerschalk, A. Marinov, A. Randle-conde, T. Seva, C. Vander Velde, P. Vanlaer, R. Yonamine, F. Zenoni, F. Zhang²

Ghent University, Ghent, Belgium

A. Cimmino, T. Cornelis, D. Dobur, A. Fagot, G. Garcia, M. Gul, I. Khvastunov, D. Poyraz, S. Salva, R. Schöfbeck, A. Sharma, M. Tytgat, W. Van Driessche, E. Yazgan, N. Zaganidis

Université Catholique de Louvain, Louvain-la-Neuve, Belgium

H. Bakhshiansohi, C. Beluffi³, O. Bondu, S. Brochet, G. Bruno, A. Caudron, S. De Visscher, C. Delaere, M. Delcourt, B. Francois, A. Giammanco, A. Jafari, P. Jez, M. Komm, V. Lemaitre, A. Magitteri, A. Mertens, M. Musich, C. Nuttens, K. Piotrkowski, L. Quertenmont, M. Selvaggi, M. Vidal Marono, S. Wertz

Université de Mons, Mons, Belgium

N. Bely

Centro Brasileiro de Pesquisas Físicas, Rio de Janeiro, Brazil

W.L. Aldá Júnior, F.L. Alves, G.A. Alves, L. Brito, C. Hensel, A. Moraes, M.E. Pol, P. Rebello Teles

Universidade do Estado do Rio de Janeiro, Rio de Janeiro, Brazil

E. Belchior Batista Das Chagas, W. Carvalho, J. Chinellato⁴, A. Custódio, E.M. Da Costa, G.G. Da Silveira⁵, D. De Jesus Damiao, C. De Oliveira Martins, S. Fonseca De Souza, L.M. Huertas Guativa, H. Malbouisson, D. Matos Figueiredo, C. Mora Herrera, L. Mundim, H. Nogima, W.L. Prado Da Silva, A. Santoro, A. Sznajder, E.J. Tonelli Manganote⁴, A. Vilela Pereira

Universidade Estadual Paulista ^a, Universidade Federal do ABC ^b, São Paulo, Brazil

S. Ahuja^a, C.A. Bernardes^b, S. Dogra^a, T.R. Fernandez Perez Tomei^a, E.M. Gregores^b,

P.G. Mercadante^b, C.S. Moon^a, S.F. Novaes^a, Sandra S. Padula^a, D. Romero Abad^b, J.C. Ruiz Vargas

Institute for Nuclear Research and Nuclear Energy, Sofia, Bulgaria

A. Aleksandrov, R. Hadjiiska, P. Iaydjiev, M. Rodozov, S. Stoykova, G. Sultanov, M. Vutova

University of Sofia, Sofia, Bulgaria

A. Dimitrov, I. Glushkov, L. Litov, B. Pavlov, P. Petkov

Beihang University, Beijing, China

W. Fang⁶

Institute of High Energy Physics, Beijing, China

M. Ahmad, J.G. Bian, G.M. Chen, H.S. Chen, M. Chen, Y. Chen⁷, T. Cheng, C.H. Jiang, D. Leggat, Z. Liu, F. Romeo, S.M. Shaheen, A. Spiezia, J. Tao, C. Wang, Z. Wang, H. Zhang, J. Zhao

State Key Laboratory of Nuclear Physics and Technology, Peking University, Beijing, China

Y. Ban, G. Chen, Q. Li, S. Liu, Y. Mao, S.J. Qian, D. Wang, Z. Xu

Universidad de Los Andes, Bogota, Colombia

C. Avila, A. Cabrera, L.F. Chaparro Sierra, C. Florez, J.P. Gomez, C.F. González Hernández, J.D. Ruiz Alvarez, J.C. Sanabria

University of Split, Faculty of Electrical Engineering, Mechanical Engineering and Naval Architecture, Split, Croatia

N. Godinovic, D. Lelas, I. Puljak, P.M. Ribeiro Cipriano, T. Sculac

University of Split, Faculty of Science, Split, Croatia

Z. Antunovic, M. Kovac

Institute Rudjer Boskovic, Zagreb, Croatia

V. Brigljevic, D. Ferencek, K. Kadija, S. Micanovic, L. Sudic, T. Susa

University of Cyprus, Nicosia, Cyprus

A. Attikis, G. Mavromanolakis, J. Mousa, C. Nicolaou, F. Ptochos, P.A. Razis, H. Rykaczewski, D. Tsiakkouri

Charles University, Prague, Czech Republic

M. Finger⁸, M. Finger Jr.⁸

Universidad San Francisco de Quito, Quito, Ecuador

E. Carrera Jarrin

Academy of Scientific Research and Technology of the Arab Republic of Egypt, Egyptian Network of High Energy Physics, Cairo, Egypt

Y. Assran^{9,10}, T. Elkafrawy¹¹, A. Mahrous¹²

National Institute of Chemical Physics and Biophysics, Tallinn, Estonia

B. Calpas, M. Kadastik, M. Murumaa, L. Perrini, M. Raidal, A. Tiko, C. Veelken

Department of Physics, University of Helsinki, Helsinki, Finland

P. Eerola, J. Pekkanen, M. Voutilainen

Helsinki Institute of Physics, Helsinki, Finland

J. Härkönen, T. Järvinen, V. Karimäki, R. Kinnunen, T. Lampén, K. Lassila-Perini, S. Lehti, T. Lindén, P. Luukka, J. Tuominiemi, E. Tuovinen, L. Wendland

Lappeenranta University of Technology, Lappeenranta, Finland

J. Talvitie, T. Tuuva

IRFU, CEA, Université Paris-Saclay, Gif-sur-Yvette, France

M. Besancon, F. Couderc, M. Dejardin, D. Denegri, B. Fabbro, J.L. Faure, C. Favaro, F. Ferri, S. Ganjour, S. Ghosh, A. Givernaud, P. Gras, G. Hamel de Monchenault, P. Jarry, I. Kucher, E. Locci, M. Machet, J. Malcles, J. Rander, A. Rosowsky, M. Titov, A. Zghiche

Laboratoire Leprince-Ringuet, Ecole Polytechnique, IN2P3-CNRS, Palaiseau, France

A. Abdulsalam, I. Antropov, S. Baffioni, F. Beaudette, P. Busson, L. Cadamuro, E. Chapon, C. Charlot, O. Davignon, R. Granier de Cassagnac, M. Jo, S. Lisniak, P. Miné, M. Nguyen, C. Ochando, G. Ortona, P. Paganini, P. Pigard, S. Regnard, R. Salerno, Y. Sirois, T. Strebler, Y. Yilmaz, A. Zabi

Institut Pluridisciplinaire Hubert Curien, Université de Strasbourg, Université de Haute Alsace Mulhouse, CNRS/IN2P3, Strasbourg, France

J.-L. Agram¹³, J. Andrea, A. Aubin, D. Bloch, J.-M. Brom, M. Buttignol, E.C. Chabert, N. Chanon, C. Collard, E. Conte¹³, X. Coubez, J.-C. Fontaine¹³, D. Gelé, U. Goerlach, A.-C. Le Bihan, K. Skovpen, P. Van Hove

Centre de Calcul de l'Institut National de Physique Nucleaire et de Physique des Particules, CNRS/IN2P3, Villeurbanne, France

S. Gadrat

Université de Lyon, Université Claude Bernard Lyon 1, CNRS-IN2P3, Institut de Physique Nucléaire de Lyon, Villeurbanne, France

S. Beauceron, C. Bernet, G. Boudoul, E. Bouvier, C.A. Carrillo Montoya, R. Chierici, D. Contardo, B. Courbon, P. Depasse, H. El Mamouni, J. Fan, J. Fay, S. Gascon, M. Gouzevitch, G. Grenier, B. Ille, F. Lagarde, I.B. Laktineh, M. Lethuillier, L. Mirabito, A.L. Pequegnot, S. Perries, A. Popov¹⁴, D. Sabes, V. Sordini, M. Vander Donckt, P. Verdier, S. Viret

Georgian Technical University, Tbilisi, Georgia

T. Toriashvili¹⁵

Tbilisi State University, Tbilisi, Georgia

D. Lomidze

RWTH Aachen University, I. Physikalisches Institut, Aachen, Germany

C. Autermann, S. Beranek, L. Feld, A. Heister, M.K. Kiesel, K. Klein, M. Lipinski, A. Ostapchuk, M. Preuten, F. Raupach, S. Schael, C. Schomakers, J. Schulz, T. Verlage, H. Weber

RWTH Aachen University, III. Physikalisches Institut A, Aachen, Germany

A. Albert, M. Brodski, E. Dietz-Laursonn, D. Duchardt, M. Endres, M. Erdmann, S. Erdweg, T. Esch, R. Fischer, A. Güth, M. Hamer, T. Hebbeker, C. Heidemann, K. Hoepfner, S. Knutzen, M. Merschmeyer, A. Meyer, P. Millet, S. Mukherjee, M. Olschewski, K. Padeken, T. Pook, M. Radziej, H. Reithler, M. Rieger, F. Scheuch, L. Sonnenschein, D. Teyssier, S. Thüer

RWTH Aachen University, III. Physikalisches Institut B, Aachen, Germany

V. Cherepanov, G. Flügge, F. Hoehle, B. Kargoll, T. Kress, A. Künsken, J. Lingemann, T. Müller, A. Nehr Korn, A. Nowack, I.M. Nugent, C. Pistone, O. Pooth, A. Stahl¹⁶

Deutsches Elektronen-Synchrotron, Hamburg, Germany

M. Aldaya Martin, T. Arndt, C. Asawatangtrakuldee, K. Beernaert, O. Behnke, U. Behrens, A.A. Bin Anuar, K. Borrás¹⁷, A. Campbell, P. Connor, C. Contreras-Campana, F. Costanza, C. Diez Pardos, G. Dolinska, G. Eckerlin, D. Eckstein, T. Eichhorn, E. Eren, E. Gallo¹⁸,

J. Garay Garcia, A. Geiser, A. Gizhko, J.M. Grados Luyando, P. Gunnellini, A. Harb, J. Hauk, M. Hempel¹⁹, H. Jung, A. Kalogeropoulos, O. Karacheban¹⁹, M. Kasemann, J. Keaveney, C. Kleinwort, I. Korol, D. Krücker, W. Lange, A. Lelek, J. Leonard, K. Lipka, A. Lobanov, W. Lohmann¹⁹, R. Mankel, I.-A. Melzer-Pellmann, A.B. Meyer, G. Mittag, J. Mnich, A. Mussgiller, E. Ntomari, D. Pitzl, R. Placakyte, A. Raspereza, B. Roland, M.Ö. Sahin, P. Saxena, T. Schoerner-Sadenius, C. Seitz, S. Spannagel, N. Stefaniuk, G.P. Van Onsem, R. Walsh, C. Wissing

University of Hamburg, Hamburg, Germany

V. Blobel, M. Centis Vignali, A.R. Draeger, T. Dreyer, E. Garutti, D. Gonzalez, J. Haller, M. Hoffmann, A. Junkes, R. Klanner, R. Kogler, N. Kovalchuk, T. Lapsien, T. Lenz, I. Marchesini, D. Marconi, M. Meyer, M. Niedziela, D. Nowatschin, F. Pantaleo¹⁶, T. Peiffer, A. Perieanu, J. Poehlsen, C. Sander, C. Scharf, P. Schleper, A. Schmidt, S. Schumann, J. Schwandt, H. Stadie, G. Steinbrück, F.M. Stober, M. Stöver, H. Tholen, D. Troendle, E. Usai, L. Vanelderen, A. Vanhoefer, B. Vormwald

Institut für Experimentelle Kernphysik, Karlsruhe, Germany

M. Akbiyik, C. Barth, S. Baur, C. Baus, J. Berger, E. Butz, R. Caspart, T. Chwalek, F. Colombo, W. De Boer, A. Dierlamm, S. Fink, B. Freund, R. Friese, M. Giffels, A. Gilbert, P. Goldenzweig, D. Haitz, F. Hartmann¹⁶, S.M. Heindl, U. Husemann, I. Katkov¹⁴, S. Kudella, P. Lobelle Pardo, H. Mildner, M.U. Mozer, Th. Müller, M. Plagge, G. Quast, K. Rabbertz, S. Röcker, F. Roscher, M. Schröder, I. Shvetsov, G. Sieber, H.J. Simonis, R. Ulrich, J. Wagner-Kuhr, S. Wayand, M. Weber, T. Weiler, S. Williamson, C. Wöhrmann, R. Wolf

Institute of Nuclear and Particle Physics (INPP), NCSR Demokritos, Aghia Paraskevi, Greece

G. Anagnostou, G. Daskalakis, T. Gerasis, V.A. Giakoumopoulou, A. Kyriakis, D. Loukas, I. Topsis-Giotis

National and Kapodistrian University of Athens, Athens, Greece

S. Kesisoglou, A. Panagiotou, N. Saoulidou, E. Tziaferi

University of Ioánnina, Ioánnina, Greece

I. Evangelou, G. Flouris, C. Foudas, P. Kokkas, N. Loukas, N. Manthos, I. Papadopoulos, E. Paradis

MTA-ELTE Lendület CMS Particle and Nuclear Physics Group, Eötvös Loránd University, Budapest, Hungary

N. Filipovic

Wigner Research Centre for Physics, Budapest, Hungary

G. Bencze, C. Hajdu, P. Hidas, D. Horvath²⁰, F. Sikler, V. Veszpremi, G. Vesztergombi²¹, A.J. Zsigmond

Institute of Nuclear Research ATOMKI, Debrecen, Hungary

N. Beni, S. Czellar, J. Karancsi²², A. Makovec, J. Molnar, Z. Szillasi

University of Debrecen, Debrecen, Hungary

M. Bartók²¹, P. Raics, Z.L. Trocsanyi, B. Ujvari

National Institute of Science Education and Research, Bhubaneswar, India

S. Bahinipati, S. Choudhury²³, P. Mal, K. Mandal, A. Nayak²⁴, D.K. Sahoo, N. Sahoo, S.K. Swain

Panjab University, Chandigarh, India

S. Bansal, S.B. Beri, V. Bhatnagar, R. Chawla, U. Bhawandeep, A.K. Kalsi, A. Kaur, M. Kaur, R. Kumar, P. Kumari, A. Mehta, M. Mittal, J.B. Singh, G. Walia

University of Delhi, Delhi, India

Ashok Kumar, A. Bhardwaj, B.C. Choudhary, R.B. Garg, S. Keshri, S. Malhotra, M. Naimuddin, N. Nishu, K. Ranjan, R. Sharma, V. Sharma

Saha Institute of Nuclear Physics, Kolkata, India

R. Bhattacharya, S. Bhattacharya, K. Chatterjee, S. Dey, S. Dutt, S. Dutta, S. Ghosh, N. Majumdar, A. Modak, K. Mondal, S. Mukhopadhyay, S. Nandan, A. Purohit, A. Roy, D. Roy, S. Roy Chowdhury, S. Sarkar, M. Sharan, S. Thakur

Indian Institute of Technology Madras, Madras, India

P.K. Behera

Bhabha Atomic Research Centre, Mumbai, India

R. Chudasama, D. Dutta, V. Jha, V. Kumar, A.K. Mohanty¹⁶, P.K. Netrakanti, L.M. Pant, P. Shukla, A. Topkar

Tata Institute of Fundamental Research-A, Mumbai, India

T. Aziz, S. Dugad, G. Kole, B. Mahakud, S. Mitra, G.B. Mohanty, B. Parida, N. Sur, B. Sutar

Tata Institute of Fundamental Research-B, Mumbai, India

S. Banerjee, S. Bhowmik²⁵, R.K. Dewanjee, S. Ganguly, M. Guchait, Sa. Jain, S. Kumar, M. Maity²⁵, G. Majumder, K. Mazumdar, T. Sarkar²⁵, N. Wickramage²⁶

Indian Institute of Science Education and Research (IISER), Pune, India

S. Chauhan, S. Dube, V. Hegde, A. Kapoor, K. Kotheekar, A. Rane, S. Sharma

Institute for Research in Fundamental Sciences (IPM), Tehran, Iran

H. Behnamian, S. Chenarani²⁷, E. Eskandari Tadavani, S.M. Etesami²⁷, A. Fahim²⁸, M. Khakzad, M. Mohammadi Najafabadi, M. Naseri, S. Paktinat Mehdiabadi²⁹, F. Rezaei Hosseinabadi, B. Safarzadeh³⁰, M. Zeinali

University College Dublin, Dublin, Ireland

M. Felcini, M. Grunewald

INFN Sezione di Bari ^a, Università di Bari ^b, Politecnico di Bari ^c, Bari, Italy

M. Abbrescia^{a,b}, C. Calabria^{a,b}, C. Caputo^{a,b}, A. Colaleo^a, D. Creanza^{a,c}, L. Cristella^{a,b}, N. De Filippis^{a,c}, M. De Palma^{a,b}, L. Fiore^a, G. Iaselli^{a,c}, G. Maggi^{a,c}, M. Maggi^a, G. Miniello^{a,b}, S. My^{a,b}, S. Nuzzo^{a,b}, A. Pompili^{a,b}, G. Pugliese^{a,c}, R. Radogna^{a,b}, A. Ranieri^a, G. Selvaggi^{a,b}, L. Silvestris^{a,16}, R. Venditti^{a,b}, P. Verwilligen^a

INFN Sezione di Bologna ^a, Università di Bologna ^b, Bologna, Italy

G. Abbiendi^a, C. Battilana, D. Bonacorsi^{a,b}, S. Braibant-Giacomelli^{a,b}, L. Brigliadori^{a,b}, R. Campanini^{a,b}, P. Capiluppi^{a,b}, A. Castro^{a,b}, F.R. Cavallo^a, S.S. Chhibra^{a,b}, G. Codispoti^{a,b}, M. Cuffiani^{a,b}, G.M. Dallavalle^a, F. Fabbri^a, A. Fanfani^{a,b}, D. Fasanella^{a,b}, P. Giacomelli^a, C. Grandi^a, L. Guiducci^{a,b}, S. Marcellini^a, G. Masetti^a, A. Montanari^a, F.L. Navarria^{a,b}, A. Perrotta^a, A.M. Rossi^{a,b}, T. Rovelli^{a,b}, G.P. Siroli^{a,b}, N. Tosi^{a,b,16}

INFN Sezione di Catania ^a, Università di Catania ^b, Catania, Italy

S. Albergo^{a,b}, M. Chiorboli^{a,b}, S. Costa^{a,b}, A. Di Mattia^a, F. Giordano^{a,b}, R. Potenza^{a,b}, A. Tricomi^{a,b}, C. Tuve^{a,b}

INFN Sezione di Firenze ^a, Università di Firenze ^b, Firenze, Italy

G. Barbagli^a, V. Ciulli^{a,b}, C. Civinini^a, R. D'Alessandro^{a,b}, E. Focardi^{a,b}, V. Gori^{a,b}, P. Lenzi^{a,b}, M. Meschini^a, S. Paoletti^a, G. Sguazzoni^a, L. Viliani^{a,b,16}

INFN Laboratori Nazionali di Frascati, Frascati, Italy

L. Benussi, S. Bianco, F. Fabbri, D. Piccolo, F. Primavera¹⁶

INFN Sezione di Genova ^a, Università di Genova ^b, Genova, Italy

V. Calvelli^{a,b}, F. Ferro^a, M. Lo Vetere^{a,b}, M.R. Monge^{a,b}, E. Robutti^a, S. Tosi^{a,b}

INFN Sezione di Milano-Bicocca ^a, Università di Milano-Bicocca ^b, Milano, Italy

L. Brianza¹⁶, M.E. Dinardo^{a,b}, S. Fiorendi^{a,b}, S. Gennai^a, A. Ghezzi^{a,b}, P. Govoni^{a,b}, M. Malberti, S. Malvezzi^a, R.A. Manzoni^{a,b,16}, D. Menasce^a, L. Moroni^a, M. Paganoni^{a,b}, D. Pedrini^a, S. Pigazzini, S. Ragazzi^{a,b}, T. Tabarelli de Fatis^{a,b}

INFN Sezione di Napoli ^a, Università di Napoli 'Federico II' ^b, Napoli, Italy, Università della Basilicata ^c, Potenza, Italy, Università G. Marconi ^d, Roma, Italy

S. Buontempo^a, N. Cavallo^{a,c}, G. De Nardo, S. Di Guida^{a,d,16}, M. Esposito^{a,b}, F. Fabozzi^{a,c}, F. Fienga^{a,b}, A.O.M. Iorio^{a,b}, G. Lanza^a, L. Lista^a, S. Meola^{a,d,16}, P. Paolucci^{a,16}, C. Sciacca^{a,b}, F. Thyssen

INFN Sezione di Padova ^a, Università di Padova ^b, Padova, Italy, Università di Trento ^c, Trento, Italy

P. Azzi^{a,16}, N. Bacchetta^a, L. Benato^{a,b}, D. Bisello^{a,b}, A. Boletti^{a,b}, R. Carlin^{a,b}, A. Carvalho Antunes De Oliveira^{a,b}, P. Checchia^a, M. Dall'Osso^{a,b}, T. Dorigo^a, U. Dosselli^a, F. Gasparini^{a,b}, U. Gasparini^{a,b}, A. Gozzelino^a, M. Gulmini^{a,31}, S. Lacaprara^a, M. Margoni^{a,b}, A.T. Meneguzzo^{a,b}, J. Pazzini^{a,b}, N. Pozzobon^{a,b}, P. Ronchese^{a,b}, F. Simonetto^{a,b}, E. Torassa^a, S. Ventura^a, M. Zanetti, P. Zotto^{a,b}

INFN Sezione di Pavia ^a, Università di Pavia ^b, Pavia, Italy

A. Braghieri^a, A. Magnani^{a,b}, P. Montagna^{a,b}, S.P. Ratti^{a,b}, V. Re^a, C. Riccardi^{a,b}, P. Salvini^a, I. Vai^{a,b}, P. Vitulo^{a,b}

INFN Sezione di Perugia ^a, Università di Perugia ^b, Perugia, Italy

L. Alunni Solestizi^{a,b}, G.M. Bilei^a, D. Ciangottini^{a,b}, L. Fanò^{a,b}, P. Lariccia^{a,b}, R. Leonardi^{a,b}, G. Mantovani^{a,b}, M. Menichelli^a, A. Saha^a, A. Santocchia^{a,b}

INFN Sezione di Pisa ^a, Università di Pisa ^b, Scuola Normale Superiore di Pisa ^c, Pisa, Italy

K. Androsov^{a,32}, P. Azzurri^{a,16}, G. Bagliesi^a, J. Bernardini^a, T. Boccali^a, R. Castaldi^a, M.A. Ciocci^{a,32}, R. Dell'Orso^a, S. Donato^{a,c}, G. Fedi, A. Giassi^a, M.T. Grippo^{a,32}, F. Ligabue^{a,c}, T. Lomtadze^a, L. Martini^{a,b}, A. Messineo^{a,b}, F. Palla^a, A. Rizzi^{a,b}, A. Savoy-Navarro^{a,33}, P. Spagnolo^a, R. Tenchini^a, G. Tonelli^{a,b}, A. Venturi^a, P.G. Verdini^a

INFN Sezione di Roma ^a, Università di Roma ^b, Roma, Italy

L. Barone^{a,b}, F. Cavallari^a, M. Cipriani^{a,b}, D. Del Re^{a,b,16}, M. Diemoz^a, S. Gelli^{a,b}, E. Longo^{a,b}, F. Margaroli^{a,b}, B. Marzocchi^{a,b}, P. Meridiani^a, G. Organtini^{a,b}, R. Paramatti^a, F. Preiato^{a,b}, S. Rahatlou^{a,b}, C. Rovelli^a, F. Santanastasio^{a,b}

INFN Sezione di Torino ^a, Università di Torino ^b, Torino, Italy, Università del Piemonte Orientale ^c, Novara, Italy

N. Amapane^{a,b}, R. Arcidiacono^{a,c,16}, S. Argiro^{a,b}, M. Arneodo^{a,c}, N. Bartosik^a, R. Bellan^{a,b}, C. Biino^a, N. Cartiglia^a, F. Cenna^{a,b}, M. Costa^{a,b}, R. Covarelli^{a,b}, A. Degano^{a,b}, N. Demaria^a, L. Finco^{a,b}, B. Kiani^{a,b}, C. Mariotti^a, S. Maselli^a, E. Migliore^{a,b}, V. Monaco^{a,b}, E. Monteil^{a,b}, M.M. Obertino^{a,b}, L. Pacher^{a,b}, N. Pastrone^a, M. Pelliccioni^a, G.L. Pinna Angioni^{a,b}, F. Ravera^{a,b}

A. Romero^{a,b}, M. Ruspa^{a,c}, R. Sacchi^{a,b}, K. Shchelina^{a,b}, V. Sola^a, A. Solano^{a,b}, A. Staiano^a, P. Traczyk^{a,b}

INFN Sezione di Trieste^a, Università di Trieste^b, Trieste, Italy

S. Belforte^a, M. Casarsa^a, F. Cossutti^a, G. Della Ricca^{a,b}, A. Zanetti^a

Kyungpook National University, Daegu, Korea

D.H. Kim, G.N. Kim, M.S. Kim, S. Lee, S.W. Lee, Y.D. Oh, S. Sekmen, D.C. Son, Y.C. Yang

Chonbuk National University, Jeonju, Korea

A. Lee

Chonnam National University, Institute for Universe and Elementary Particles, Kwangju, Korea

H. Kim

Hanyang University, Seoul, Korea

J.A. Brochero Cifuentes, T.J. Kim

Korea University, Seoul, Korea

S. Cho, S. Choi, Y. Go, D. Gyun, S. Ha, B. Hong, Y. Jo, Y. Kim, B. Lee, K. Lee, K.S. Lee, S. Lee, J. Lim, S.K. Park, Y. Roh

Seoul National University, Seoul, Korea

J. Almond, J. Kim, H. Lee, S.B. Oh, B.C. Radburn-Smith, S.h. Seo, U.K. Yang, H.D. Yoo, G.B. Yu

University of Seoul, Seoul, Korea

M. Choi, H. Kim, J.H. Kim, J.S.H. Lee, I.C. Park, G. Ryu, M.S. Ryu

Sungkyunkwan University, Suwon, Korea

Y. Choi, J. Goh, C. Hwang, J. Lee, I. Yu

Vilnius University, Vilnius, Lithuania

V. Dudenas, A. Juodagalvis, J. Vaitkus

National Centre for Particle Physics, Universiti Malaya, Kuala Lumpur, Malaysia

I. Ahmed, Z.A. Ibrahim, J.R. Komaragiri, M.A.B. Md Ali³⁴, F. Mohamad Idris³⁵, W.A.T. Wan Abdullah, M.N. Yusli, Z. Zolkapli

Centro de Investigacion y de Estudios Avanzados del IPN, Mexico City, Mexico

H. Castilla-Valdez, E. De La Cruz-Burelo, I. Heredia-De La Cruz³⁶, A. Hernandez-Almada, R. Lopez-Fernandez, R. Magaña Villalba, J. Mejia Guisao, A. Sanchez-Hernandez

Universidad Iberoamericana, Mexico City, Mexico

S. Carrillo Moreno, C. Oropeza Barrera, F. Vazquez Valencia

Benemerita Universidad Autonoma de Puebla, Puebla, Mexico

S. Carpinteyro, I. Pedraza, H.A. Salazar Ibarguen, C. Uribe Estrada

Universidad Autónoma de San Luis Potosí, San Luis Potosí, Mexico

A. Morelos Pineda

University of Auckland, Auckland, New Zealand

D. Krofcheck

University of Canterbury, Christchurch, New Zealand

P.H. Butler

National Centre for Physics, Quaid-I-Azam University, Islamabad, Pakistan

A. Ahmad, M. Ahmad, Q. Hassan, H.R. Hoorani, W.A. Khan, A. Saddique, M.A. Shah, M. Shoaib, M. Waqas

National Centre for Nuclear Research, Swierk, Poland

H. Bialkowska, M. Bluj, B. Boimska, T. Frueboes, M. Górski, M. Kazana, K. Nawrocki, K. Romanowska-Rybinska, M. Szleper, P. Zalewski

Institute of Experimental Physics, Faculty of Physics, University of Warsaw, Warsaw, Poland

K. Bunkowski, A. Byszuk³⁷, K. Doroba, A. Kalinowski, M. Konecki, J. Krolikowski, M. Misiura, M. Olszewski, M. Walczak

Laboratório de Instrumentação e Física Experimental de Partículas, Lisboa, Portugal

P. Bargassa, C. Beirão Da Cruz E Silva, A. Di Francesco, P. Faccioli, P.G. Ferreira Parracho, M. Gallinaro, J. Hollar, N. Leonardo, L. Lloret Iglesias, M.V. Nemallapudi, J. Rodrigues Antunes, J. Seixas, O. Toldaiev, D. Vadrucchio, J. Varela, P. Vischia

Joint Institute for Nuclear Research, Dubna, Russia

V. Alexakhin, A. Golunov, I. Golutvin, N. Gorbounov, A. Kamenev, V. Karjavin, V. Korenkov, A. Lanev, A. Malakhov, V. Matveev^{38,39}, V.V. Mitsyn, V. Palichik, V. Perelygin, S. Shmatov, N. Skatchkov, V. Smirnov, E. Tikhonenko, A. Zarubin

Petersburg Nuclear Physics Institute, Gatchina (St. Petersburg), Russia

L. Chtchypounov, V. Golovtsov, Y. Ivanov, V. Kim⁴⁰, E. Kuznetsova⁴¹, V. Murzin, V. Oreshkin, V. Sulimov, A. Vorobyev

Institute for Nuclear Research, Moscow, Russia

Yu. Andreev, A. Dermenev, S. Gninenko, N. Golubev, A. Karneyeu, M. Kirsanov, N. Krasnikov, A. Pashenkov, D. Tlisov, A. Toropin

Institute for Theoretical and Experimental Physics, Moscow, Russia

V. Epshteyn, V. Gavrilov, N. Lychkovskaya, V. Popov, I. Pozdnyakov, G. Safronov, A. Spiridonov, M. Toms, E. Vlasov, A. Zhokin

Moscow Institute of Physics and Technology

A. Bylinkin³⁹

National Research Nuclear University 'Moscow Engineering Physics Institute' (MEPhI), Moscow, Russia

O. Markin, E. Popova, E. Tarkovskii

P.N. Lebedev Physical Institute, Moscow, Russia

V. Andreev, M. Azarkin³⁹, I. Dremin³⁹, M. Kirakosyan, A. Leonidov³⁹, S.V. Rusakov, A. Terkulov

Skobeltsyn Institute of Nuclear Physics, Lomonosov Moscow State University, Moscow, Russia

A. Baskakov, A. Belyaev, E. Boos, V. Bunichev, M. Dubinin⁴², L. Dudko, A. Ershov, V. Klyukhin, O. Kodolova, N. Korneeva, I. Lokhtin, I. Miagkov, S. Obraztsov, M. Perfilov, V. Savrin

Novosibirsk State University (NSU), Novosibirsk, Russia

V. Blinov⁴³, Y. Skovpen⁴³

State Research Center of Russian Federation, Institute for High Energy Physics, Protvino, Russia

I. Azhgirey, I. Bayshev, S. Bitioukov, D. Elumakhov, V. Kachanov, A. Kalinin, D. Konstantinov, V. Krychkine, V. Petrov, R. Ryutin, A. Sobol, S. Troshin, N. Tyurin, A. Uzunian, A. Volkov

University of Belgrade, Faculty of Physics and Vinca Institute of Nuclear Sciences, Belgrade, Serbia

P. Adzic⁴⁴, P. Cirkovic, D. Devetak, M. Dordevic, J. Milosevic, V. Rekovic

Centro de Investigaciones Energéticas Medioambientales y Tecnológicas (CIEMAT), Madrid, Spain

J. Alcaraz Maestre, M. Barrio Luna, E. Calvo, M. Cerrada, M. Chamizo Llatas, N. Colino, B. De La Cruz, A. Delgado Peris, A. Escalante Del Valle, C. Fernandez Bedoya, J.P. Fernández Ramos, J. Flix, M.C. Fouz, P. Garcia-Abia, O. Gonzalez Lopez, S. Goy Lopez, J.M. Hernandez, M.I. Josa, E. Navarro De Martino, A. Pérez-Calero Yzquierdo, J. Puerta Pelayo, A. Quintario Olmeda, I. Redondo, L. Romero, M.S. Soares

Universidad Autónoma de Madrid, Madrid, Spain

J.F. de Trocóniz, M. Missiroli, D. Moran

Universidad de Oviedo, Oviedo, Spain

J. Cuevas, J. Fernandez Menendez, I. Gonzalez Caballero, J.R. González Fernández, E. Palencia Cortezon, S. Sanchez Cruz, I. Suárez Andrés, J.M. Vizán Garcia

Instituto de Física de Cantabria (IFCA), CSIC-Universidad de Cantabria, Santander, Spain

I.J. Cabrillo, A. Calderon, J.R. Castiñeiras De Saa, E. Curras, M. Fernandez, J. Garcia-Ferrero, G. Gomez, A. Lopez Virto, J. Marco, C. Martinez Rivero, F. Matorras, J. Piedra Gomez, T. Rodrigo, A. Ruiz-Jimeno, L. Scodellaro, N. Trevisani, I. Vila, R. Vilar Cortabitarte

CERN, European Organization for Nuclear Research, Geneva, Switzerland

D. Abbaneo, E. Auffray, G. Auzinger, M. Bachtis, P. Baillon, A.H. Ball, D. Barney, P. Bloch, A. Bocci, A. Bonato, C. Botta, T. Camporesi, R. Castello, M. Cepeda, G. Cerminara, M. D'Alfonso, D. d'Enterria, A. Dabrowski, V. Daponte, A. David, M. De Gruttola, A. De Roeck, E. Di Marco⁴⁵, M. Dobson, B. Dorney, T. du Pree, D. Duggan, M. Dünser, N. Dupont, A. Elliott-Peisert, S. Fartoukh, G. Franzoni, J. Fulcher, W. Funk, D. Gigi, K. Gill, M. Girone, F. Glege, D. Gulhan, S. Gundacker, M. Guthoff, J. Hammer, P. Harris, J. Hegeman, V. Innocente, P. Janot, J. Kieseler, H. Kirschenmann, V. Knünz, A. Kornmayer¹⁶, M.J. Kortelainen, K. Kousouris, M. Krammer¹, C. Lange, P. Lecoq, C. Lourenço, M.T. Lucchini, L. Malgeri, M. Mannelli, A. Martelli, F. Meijers, J.A. Merlin, S. Mersi, E. Meschi, F. Moortgat, S. Morovic, M. Mulders, H. Neugebauer, S. Orfanelli, L. Orsini, L. Pape, E. Perez, M. Peruzzi, A. Petrilli, G. Petrucciani, A. Pfeiffer, M. Pierini, A. Racz, T. Reis, G. Rolandi⁴⁶, M. Rovere, M. Ruan, H. Sakulin, J.B. Sauvan, C. Schäfer, C. Schwick, M. Seidel, A. Sharma, P. Silva, P. Sphicas⁴⁷, J. Steggemann, M. Stoye, Y. Takahashi, M. Tosi, D. Treille, A. Triossi, A. Tsirou, V. Veckalns⁴⁸, G.I. Veres²¹, N. Wardle, A. Zagozdinska³⁷, W.D. Zeuner

Paul Scherrer Institut, Villigen, Switzerland

W. Bertl, K. Deiters, W. Erdmann, R. Horisberger, Q. Ingram, H.C. Kaestli, D. Kotlinski, U. Langenegger, T. Rohe

Institute for Particle Physics, ETH Zurich, Zurich, Switzerland

F. Bachmair, L. Bäni, L. Bianchini, B. Casal, G. Dissertori, M. Dittmar, M. Donegà, C. Grab, C. Heidegger, D. Hits, J. Hoss, G. Kasieczka, P. Lecomte[†], W. Lustermann, B. Mangano, M. Marionneau, P. Martinez Ruiz del Arbol, M. Masciovecchio, M.T. Meinhard, D. Meister,

F. Micheli, P. Musella, F. Nessi-Tedaldi, F. Pandolfi, J. Pata, F. Pauss, G. Perrin, L. Perrozzi, M. Quitnat, M. Rossini, M. Schönenberger, A. Starodumov⁴⁹, V.R. Tavolaro, K. Theofilatos, R. Wallny

Universität Zürich, Zurich, Switzerland

T.K. Aarrestad, C. AMSler⁵⁰, L. Caminada, M.F. Canelli, A. De Cosa, C. Galloni, A. Hinzmann, T. Hreus, B. Kilminster, J. Ngadiuba, D. Pinna, G. Rauco, P. Robmann, D. Salerno, Y. Yang, A. Zucchetta

National Central University, Chung-Li, Taiwan

V. Candelise, T.H. Doan, Sh. Jain, R. Khurana, M. Konyushikhin, C.M. Kuo, W. Lin, Y.J. Lu, A. Pozdnyakov, S.S. Yu

National Taiwan University (NTU), Taipei, Taiwan

Arun Kumar, P. Chang, Y.H. Chang, Y.W. Chang, Y. Chao, K.F. Chen, P.H. Chen, C. Dietz, F. Fiori, W.-S. Hou, Y. Hsiung, Y.F. Liu, R.-S. Lu, M. Miñano Moya, E. Paganis, A. Psallidas, J.f. Tsai, Y.M. Tzeng

Chulalongkorn University, Faculty of Science, Department of Physics, Bangkok, Thailand

B. Asavapibhop, G. Singh, N. Srimanobhas, N. Suwonjandee

Cukurova University, Adana, Turkey

A. Adiguzel, M.N. Bakirci⁵¹, S. Cerci⁵², S. Damarseckin, Z.S. Demiroglu, C. Dozen, I. Dumanoglu, S. Girgis, G. Gokbulut, Y. Guler, I. Hos, E.E. Kangal⁵³, O. Kara, A. Kayis Topaksu, U. Kiminsu, M. Oglakci, G. Onengut⁵⁴, K. Ozdemir⁵⁵, B. Tali⁵², S. Turkcapar, I.S. Zorbakir, C. Zorbilmez

Middle East Technical University, Physics Department, Ankara, Turkey

B. Bilin, S. Bilmis, B. Isildak⁵⁶, G. Karapinar⁵⁷, M. Yalvac, M. Zeyrek

Bogazici University, Istanbul, Turkey

E. Gülmez, M. Kaya⁵⁸, O. Kaya⁵⁹, E.A. Yetkin⁶⁰, T. Yetkin⁶¹

Istanbul Technical University, Istanbul, Turkey

A. Cakir, K. Cankocak, S. Sen⁶²

Institute for Scintillation Materials of National Academy of Science of Ukraine, Kharkov, Ukraine

B. Grynyov

National Scientific Center, Kharkov Institute of Physics and Technology, Kharkov, Ukraine

L. Levchuk, P. Sorokin

University of Bristol, Bristol, United Kingdom

R. Aggleton, F. Ball, L. Beck, J.J. Brooke, D. Burns, E. Clement, D. Cussans, H. Flacher, J. Goldstein, M. Grimes, G.P. Heath, H.F. Heath, J. Jacob, L. Kreczko, C. Lucas, D.M. Newbold⁶³, S. Paramesvaran, A. Poll, T. Sakuma, S. Seif El Nasr-storey, D. Smith, V.J. Smith

Rutherford Appleton Laboratory, Didcot, United Kingdom

K.W. Bell, A. Belyaev⁶⁴, C. Brew, R.M. Brown, L. Calligaris, D. Cieri, D.J.A. Cockerill, J.A. Coughlan, K. Harder, S. Harper, E. Olaiya, D. Petyt, C.H. Shepherd-Themistocleous, A. Thea, I.R. Tomalin, T. Williams

Imperial College, London, United Kingdom

M. Baber, R. Bainbridge, O. Buchmuller, A. Bundock, D. Burton, S. Casasso, M. Citron, D. Colling, L. Corpe, P. Dauncey, G. Davies, A. De Wit, M. Della Negra, R. Di Maria, P. Dunne,

A. Elwood, D. Futyan, Y. Haddad, G. Hall, G. Iles, T. James, R. Lane, C. Laner, R. Lucas⁶³, L. Lyons, A.-M. Magnan, S. Malik, L. Mastrolorenzo, J. Nash, A. Nikitenko⁴⁹, J. Pela, B. Penning, M. Pesaresi, D.M. Raymond, A. Richards, A. Rose, C. Seez, S. Summers, A. Tapper, K. Uchida, M. Vazquez Acosta⁶⁵, T. Virdee¹⁶, J. Wright, S.C. Zenz

Brunel University, Uxbridge, United Kingdom

J.E. Cole, P.R. Hobson, A. Khan, P. Kyberd, D. Leslie, I.D. Reid, P. Symonds, L. Teodorescu, M. Turner

Baylor University, Waco, USA

A. Borzou, K. Call, J. Dittmann, K. Hatakeyama, H. Liu, N. Pastika

The University of Alabama, Tuscaloosa, USA

O. Charaf, S.I. Cooper, C. Henderson, P. Rumerio, C. West

Boston University, Boston, USA

D. Arcaro, A. Avetisyan, T. Bose, D. Gastler, D. Rankin, C. Richardson, J. Rohlf, L. Sulak, D. Zou

Brown University, Providence, USA

G. Benelli, E. Berry, D. Cutts, A. Garabedian, J. Hakala, U. Heintz, J.M. Hogan, O. Jesus, K.H.M. Kwok, E. Laird, G. Landsberg, Z. Mao, M. Narain, S. Piperov, S. Sagir, E. Spencer, R. Syarif

University of California, Davis, Davis, USA

R. Breedon, G. Breto, D. Burns, M. Calderon De La Barca Sanchez, S. Chauhan, M. Chertok, J. Conway, R. Conway, P.T. Cox, R. Erbacher, C. Flores, G. Funk, M. Gardner, W. Ko, R. Lander, C. Mclean, M. Mulhearn, D. Pellett, J. Pilot, S. Shalhout, J. Smith, M. Squires, D. Stolp, M. Tripathi, S. Wilbur, R. Yohay

University of California, Los Angeles, USA

C. Bravo, R. Cousins, P. Everaerts, A. Florent, J. Hauser, M. Ignatenko, N. Mccoll, D. Saltzberg, C. Schnaible, E. Takasugi, V. Valuev, M. Weber

University of California, Riverside, Riverside, USA

K. Burt, R. Clare, J. Ellison, J.W. Gary, S.M.A. Ghiasi Shirazi, G. Hanson, J. Heilman, P. Jandir, E. Kennedy, F. Lacroix, O.R. Long, M. Olmedo Negrete, M.I. Paneva, A. Shrinivas, W. Si, H. Wei, S. Wimpenny, B. R. Yates

University of California, San Diego, La Jolla, USA

J.G. Branson, G.B. Cerati, S. Cittolin, M. Derdzinski, R. Gerosa, A. Holzner, D. Klein, V. Krutelyov, J. Letts, I. Macneill, D. Olivito, S. Padhi, M. Pieri, M. Sani, V. Sharma, S. Simon, M. Tadel, A. Vartak, S. Wasserbaech⁶⁶, C. Welke, J. Wood, F. Würthwein, A. Yagil, G. Zevi Della Porta

University of California, Santa Barbara - Department of Physics, Santa Barbara, USA

N. Amin, R. Bhandari, J. Bradmiller-Feld, C. Campagnari, A. Dishaw, V. Dutta, K. Flowers, M. Franco Sevilla, P. Geffert, C. George, F. Golf, L. Gouskos, J. Gran, R. Heller, J. Incandela, S.D. Mullin, A. Ovcharova, J. Richman, D. Stuart, I. Suarez, J. Yoo

California Institute of Technology, Pasadena, USA

D. Anderson, A. Apresyan, J. Bendavid, A. Bornheim, J. Bunn, Y. Chen, J. Duarte, J.M. Lawhorn, A. Mott, H.B. Newman, C. Pena, M. Spiropulu, J.R. Vlimant, S. Xie, R.Y. Zhu

Carnegie Mellon University, Pittsburgh, USA

M.B. Andrews, V. Azzolini, T. Ferguson, M. Paulini, J. Russ, M. Sun, H. Vogel, I. Vorobiev, M. Weinberg

University of Colorado Boulder, Boulder, USA

J.P. Cumalat, W.T. Ford, F. Jensen, A. Johnson, M. Krohn, T. Mulholland, K. Stenson, S.R. Wagner

Cornell University, Ithaca, USA

J. Alexander, J. Chaves, J. Chu, S. Dittmer, K. Mcdermott, N. Mirman, G. Nicolas Kaufman, J.R. Patterson, A. Rinkevicius, A. Ryd, L. Skinnari, L. Soffi, S.M. Tan, Z. Tao, J. Thom, J. Tucker, P. Wittich, M. Zientek

Fairfield University, Fairfield, USA

D. Winn

Fermi National Accelerator Laboratory, Batavia, USA

S. Abdullin, M. Albrow, G. Apollinari, S. Banerjee, L.A.T. Bauerdick, A. Beretvas, J. Berryhill, P.C. Bhat, G. Bolla, K. Burkett, J.N. Butler, H.W.K. Cheung, F. Chlebana, S. Cihangir[†], M. Cremonesi, V.D. Elvira, I. Fisk, J. Freeman, E. Gottschalk, L. Gray, D. Green, S. Grünendahl, O. Gutsche, D. Hare, R.M. Harris, S. Hasegawa, J. Hirschauer, Z. Hu, B. Jayatilaka, S. Jindariani, M. Johnson, U. Joshi, B. Klima, B. Kreis, S. Lammel, J. Linacre, D. Lincoln, R. Lipton, T. Liu, R. Lopes De Sá, J. Lykken, K. Maeshima, N. Magini, J.M. Marraffino, S. Maruyama, D. Mason, P. McBride, P. Merkel, S. Mrenna, S. Nahn, C. Newman-Holmes[†], V. O'Dell, K. Pedro, O. Prokofyev, G. Rakness, L. Ristori, E. Sexton-Kennedy, A. Soha, W.J. Spalding, L. Spiegel, S. Stoynev, N. Strobbe, L. Taylor, S. Tkaczyk, N.V. Tran, L. Uplegger, E.W. Vaandering, C. Vernieri, M. Verzocchi, R. Vidal, M. Wang, H.A. Weber, A. Whitbeck

University of Florida, Gainesville, USA

D. Acosta, P. Avery, P. Bortignon, D. Bourilkov, A. Brinkerhoff, A. Carnes, M. Carver, D. Curry, S. Das, R.D. Field, I.K. Furic, J. Konigsberg, A. Korytov, P. Ma, K. Matchev, H. Mei, P. Milenovic⁶⁷, G. Mitselmakher, D. Rank, L. Shchutska, D. Sperka, L. Thomas, J. Wang, S. Wang, J. Yelton

Florida International University, Miami, USA

S. Linn, P. Markowitz, G. Martinez, J.L. Rodriguez

Florida State University, Tallahassee, USA

A. Ackert, J.R. Adams, T. Adams, A. Askew, S. Bein, B. Diamond, S. Hagopian, V. Hagopian, K.F. Johnson, A. Khatiwada, H. Prosper, A. Santra

Florida Institute of Technology, Melbourne, USA

M.M. Baarmand, V. Bhopatkar, S. Colafranceschi⁶⁸, M. Hohlmann, D. Noonan, T. Roy, F. Yumiceva

University of Illinois at Chicago (UIC), Chicago, USA

M.R. Adams, L. Apanasevich, D. Berry, R.R. Betts, I. Bucinskaite, R. Cavanaugh, O. Evdokimov, L. Gauthier, C.E. Gerber, D.J. Hofman, K. Jung, P. Kurt, C. O'Brien, I.D. Sandoval Gonzalez, P. Turner, N. Varelas, H. Wang, Z. Wu, M. Zakaria, J. Zhang

The University of Iowa, Iowa City, USA

B. Bilki⁶⁹, W. Clarida, K. Dilsiz, S. Durgut, R.P. Gandrajula, M. Haytmyradov, V. Khristenko, J.-P. Merlo, H. Mermerkaya⁷⁰, A. Mestvirishvili, A. Moeller, J. Nachtman, H. Ogul, Y. Onel, F. Ozok⁷¹, A. Penzo, C. Snyder, E. Tiras, J. Wetzel, K. Yi

Johns Hopkins University, Baltimore, USA

I. Anderson, B. Blumenfeld, A. Cocoros, N. Eminizer, D. Fehling, L. Feng, A.V. Gritsan, P. Maksimovic, C. Martin, M. Osherson, J. Roskes, U. Sarica, M. Swartz, M. Xiao, Y. Xin, C. You

The University of Kansas, Lawrence, USA

A. Al-bataineh, P. Baringer, A. Bean, S. Boren, J. Bowen, C. Bruner, J. Castle, L. Forthomme, R.P. Kenny III, A. Kropivnitskaya, D. Majumder, W. Mcbrayer, M. Murray, S. Sanders, R. Stringer, J.D. Tapia Takaki, Q. Wang

Kansas State University, Manhattan, USA

A. Ivanov, K. Kaadze, S. Khalil, Y. Maravin, A. Mohammadi, L.K. Saini, N. Skhirtladze, S. Toda

Lawrence Livermore National Laboratory, Livermore, USA

F. Rebassoo, D. Wright

University of Maryland, College Park, USA

C. Anelli, A. Baden, O. Baron, A. Belloni, B. Calvert, S.C. Eno, C. Ferraioli, J.A. Gomez, N.J. Hadley, S. Jabeen, R.G. Kellogg, T. Kolberg, J. Kunkle, Y. Lu, A.C. Mignerey, F. Ricci-Tam, Y.H. Shin, A. Skuja, M.B. Tonjes, S.C. Tonwar

Massachusetts Institute of Technology, Cambridge, USA

D. Abercrombie, B. Allen, A. Apyan, R. Barbieri, A. Baty, R. Bi, K. Bierwagen, S. Brandt, W. Busza, I.A. Cali, Z. Demiragli, L. Di Matteo, G. Gomez Ceballos, M. Goncharov, D. Hsu, Y. Iiyama, G.M. Innocenti, M. Klute, D. Kovalskyi, K. Krajczar, Y.S. Lai, Y.-J. Lee, A. Levin, P.D. Luckey, B. Maier, A.C. Marini, C. McGinn, C. Mironov, S. Narayanan, X. Niu, C. Paus, C. Roland, G. Roland, J. Salfeld-Nebgen, G.S.F. Stephans, K. Sumorok, K. Tatar, M. Varma, D. Velicanu, J. Veverka, J. Wang, T.W. Wang, B. Wyslouch, M. Yang, V. Zhukova

University of Minnesota, Minneapolis, USA

A.C. Benvenuti, R.M. Chatterjee, A. Evans, A. Finkel, A. Gude, P. Hansen, S. Kalafut, S.C. Kao, Y. Kubota, Z. Lesko, J. Mans, S. Nourbakhsh, N. Ruckstuhl, R. Rusack, N. Tambe, J. Turkewitz

University of Mississippi, Oxford, USA

J.G. Acosta, S. Oliveros

University of Nebraska-Lincoln, Lincoln, USA

E. Avdeeva, R. Bartek, K. Bloom, D.R. Claes, A. Dominguez, C. Fangmeier, R. Gonzalez Suarez, R. Kamalieddin, I. Kravchenko, A. Malta Rodrigues, F. Meier, J. Monroy, J.E. Siado, G.R. Snow, B. Stieger

State University of New York at Buffalo, Buffalo, USA

M. Alyari, J. Dolen, J. George, A. Godshalk, C. Harrington, I. Iashvili, J. Kaisen, A. Kharchilava, A. Kumar, A. Parker, S. Rappoccio, B. Roozbahani

Northeastern University, Boston, USA

G. Alverson, E. Barberis, A. Hortiangtham, A. Massironi, D.M. Morse, D. Nash, T. Orimoto, R. Teixeira De Lima, D. Trocino, R.-J. Wang, D. Wood

Northwestern University, Evanston, USA

S. Bhattacharya, K.A. Hahn, A. Kubik, A. Kumar, J.F. Low, N. Mucia, N. Odell, B. Pollack, M.H. Schmitt, K. Sung, M. Trovato, M. Velasco

University of Notre Dame, Notre Dame, USA

N. Dev, M. Hildreth, K. Hurtado Anampa, C. Jessop, D.J. Karmgard, N. Kellams, K. Lannon,

N. Marinelli, F. Meng, C. Mueller, Y. Musienko³⁸, M. Planer, A. Reinsvold, R. Ruchti, G. Smith, S. Taroni, M. Wayne, M. Wolf, A. Woodard

The Ohio State University, Columbus, USA

J. Alimena, L. Antonelli, J. Brinson, B. Bylsma, L.S. Durkin, S. Flowers, B. Francis, A. Hart, C. Hill, R. Hughes, W. Ji, B. Liu, W. Luo, D. Puigh, B.L. Winer, H.W. Wulsin

Princeton University, Princeton, USA

S. Cooperstein, O. Driga, P. Elmer, J. Hardenbrook, P. Hebda, D. Lange, J. Luo, D. Marlow, J. McDonald, T. Medvedeva, K. Mei, M. Mooney, J. Olsen, C. Palmer, P. Piroué, D. Stickland, C. Tully, A. Zuranski

University of Puerto Rico, Mayaguez, USA

S. Malik

Purdue University, West Lafayette, USA

A. Barker, V.E. Barnes, S. Folgueras, L. Gutay, M.K. Jha, M. Jones, A.W. Jung, D.H. Miller, N. Neumeister, J.F. Schulte, X. Shi, J. Sun, A. Svyatkovskiy, F. Wang, W. Xie, L. Xu

Purdue University Calumet, Hammond, USA

N. Parashar, J. Stupak

Rice University, Houston, USA

A. Adair, B. Akgun, Z. Chen, K.M. Ecklund, F.J.M. Geurts, M. Guilbaud, W. Li, B. Michlin, M. Northup, B.P. Padley, R. Redjimi, J. Roberts, J. Rorie, Z. Tu, J. Zabel

University of Rochester, Rochester, USA

B. Betchart, A. Bodek, P. de Barbaro, R. Demina, Y.t. Duh, T. Ferbel, M. Galanti, A. Garcia-Bellido, J. Han, O. Hindrichs, A. Khukhunaishvili, K.H. Lo, P. Tan, M. Verzetti

Rutgers, The State University of New Jersey, Piscataway, USA

A. Agapitos, J.P. Chou, E. Contreras-Campana, Y. Gershtein, T.A. Gómez Espinosa, E. Halkiadakis, M. Heindl, D. Hidas, E. Hughes, S. Kaplan, R. Kunnawalkam Elayavalli, S. Kyriacou, A. Lath, K. Nash, H. Saka, S. Salur, S. Schnetzer, D. Sheffield, S. Somalwar, R. Stone, S. Thomas, P. Thomassen, M. Walker

University of Tennessee, Knoxville, USA

A.G. Delannoy, M. Foerster, J. Heideman, G. Riley, K. Rose, S. Spanier, K. Thapa

Texas A&M University, College Station, USA

O. Bouhali⁷², A. Celik, M. Dalchenko, M. De Mattia, A. Delgado, S. Dildick, R. Eusebi, J. Gilmore, T. Huang, E. Juska, T. Kamon⁷³, R. Mueller, Y. Pakhotin, R. Patel, A. Perloff, L. Perniè, D. Rathjens, A. Rose, A. Safonov, A. Tatarinov, K.A. Ulmer

Texas Tech University, Lubbock, USA

N. Akchurin, C. Cowden, J. Damgov, F. De Guio, C. Dragoiu, P.R. Duderod, J. Faulkner, E. Gурpinar, S. Kunori, K. Lamichhane, S.W. Lee, T. Libeiro, T. Peltola, S. Undleeb, I. Volobouev, Z. Wang

Vanderbilt University, Nashville, USA

S. Greene, A. Gurrola, R. Janjam, W. Johns, C. Maguire, A. Melo, H. Ni, P. Sheldon, S. Tuo, J. Velkovska, Q. Xu

University of Virginia, Charlottesville, USA

M.W. Arenton, P. Barria, B. Cox, J. Goodell, R. Hirosky, A. Ledovskoy, H. Li, C. Neu, T. Sinthuprasith, X. Sun, Y. Wang, E. Wolfe, F. Xia

Wayne State University, Detroit, USA

C. Clarke, R. Harr, P.E. Karchin, J. Sturdy

University of Wisconsin - Madison, Madison, WI, USA

D.A. Belknap, C. Caillol, S. Dasu, L. Dodd, S. Duric, B. Gomber, M. Grothe, M. Herndon, A. Hervé, P. Klabbbers, A. Lanaro, A. Levine, K. Long, R. Loveless, I. Ojalvo, T. Perry, G.A. Pierro, G. Polese, T. Ruggles, A. Savin, N. Smith, W.H. Smith, D. Taylor, N. Woods

†: Deceased

1: Also at Vienna University of Technology, Vienna, Austria

2: Also at State Key Laboratory of Nuclear Physics and Technology, Peking University, Beijing, China

3: Also at Institut Pluridisciplinaire Hubert Curien, Université de Strasbourg, Université de Haute Alsace Mulhouse, CNRS/IN2P3, Strasbourg, France

4: Also at Universidade Estadual de Campinas, Campinas, Brazil

5: Also at Universidade Federal de Pelotas, Pelotas, Brazil

6: Also at Université Libre de Bruxelles, Bruxelles, Belgium

7: Also at Deutsches Elektronen-Synchrotron, Hamburg, Germany

8: Also at Joint Institute for Nuclear Research, Dubna, Russia

9: Also at Suez University, Suez, Egypt

10: Now at British University in Egypt, Cairo, Egypt

11: Also at Ain Shams University, Cairo, Egypt

12: Now at Helwan University, Cairo, Egypt

13: Also at Université de Haute Alsace, Mulhouse, France

14: Also at Skobeltsyn Institute of Nuclear Physics, Lomonosov Moscow State University, Moscow, Russia

15: Also at Tbilisi State University, Tbilisi, Georgia

16: Also at CERN, European Organization for Nuclear Research, Geneva, Switzerland

17: Also at RWTH Aachen University, III. Physikalisches Institut A, Aachen, Germany

18: Also at University of Hamburg, Hamburg, Germany

19: Also at Brandenburg University of Technology, Cottbus, Germany

20: Also at Institute of Nuclear Research ATOMKI, Debrecen, Hungary

21: Also at MTA-ELTE Lendület CMS Particle and Nuclear Physics Group, Eötvös Loránd University, Budapest, Hungary

22: Also at University of Debrecen, Debrecen, Hungary

23: Also at Indian Institute of Science Education and Research, Bhopal, India

24: Also at Institute of Physics, Bhubaneswar, India

25: Also at University of Visva-Bharati, Santiniketan, India

26: Also at University of Ruhuna, Matara, Sri Lanka

27: Also at Isfahan University of Technology, Isfahan, Iran

28: Also at University of Tehran, Department of Engineering Science, Tehran, Iran

29: Also at Yazd University, Yazd, Iran

30: Also at Plasma Physics Research Center, Science and Research Branch, Islamic Azad University, Tehran, Iran

31: Also at Laboratori Nazionali di Legnaro dell'INFN, Legnaro, Italy

32: Also at Università degli Studi di Siena, Siena, Italy

33: Also at Purdue University, West Lafayette, USA

34: Also at International Islamic University of Malaysia, Kuala Lumpur, Malaysia

35: Also at Malaysian Nuclear Agency, MOSTI, Kajang, Malaysia

36: Also at Consejo Nacional de Ciencia y Tecnología, Mexico city, Mexico

- 37: Also at Warsaw University of Technology, Institute of Electronic Systems, Warsaw, Poland
- 38: Also at Institute for Nuclear Research, Moscow, Russia
- 39: Now at National Research Nuclear University 'Moscow Engineering Physics Institute' (MEPhI), Moscow, Russia
- 40: Also at St. Petersburg State Polytechnical University, St. Petersburg, Russia
- 41: Also at University of Florida, Gainesville, USA
- 42: Also at California Institute of Technology, Pasadena, USA
- 43: Also at Budker Institute of Nuclear Physics, Novosibirsk, Russia
- 44: Also at Faculty of Physics, University of Belgrade, Belgrade, Serbia
- 45: Also at INFN Sezione di Roma; Università di Roma, Roma, Italy
- 46: Also at Scuola Normale e Sezione dell'INFN, Pisa, Italy
- 47: Also at National and Kapodistrian University of Athens, Athens, Greece
- 48: Also at Riga Technical University, Riga, Latvia
- 49: Also at Institute for Theoretical and Experimental Physics, Moscow, Russia
- 50: Also at Albert Einstein Center for Fundamental Physics, Bern, Switzerland
- 51: Also at Gaziosmanpasa University, Tokat, Turkey
- 52: Also at Adiyaman University, Adiyaman, Turkey
- 53: Also at Mersin University, Mersin, Turkey
- 54: Also at Cag University, Mersin, Turkey
- 55: Also at Piri Reis University, Istanbul, Turkey
- 56: Also at Ozyegin University, Istanbul, Turkey
- 57: Also at Izmir Institute of Technology, Izmir, Turkey
- 58: Also at Marmara University, Istanbul, Turkey
- 59: Also at Kafkas University, Kars, Turkey
- 60: Also at Istanbul Bilgi University, Istanbul, Turkey
- 61: Also at Yildiz Technical University, Istanbul, Turkey
- 62: Also at Hacettepe University, Ankara, Turkey
- 63: Also at Rutherford Appleton Laboratory, Didcot, United Kingdom
- 64: Also at School of Physics and Astronomy, University of Southampton, Southampton, United Kingdom
- 65: Also at Instituto de Astrofísica de Canarias, La Laguna, Spain
- 66: Also at Utah Valley University, Orem, USA
- 67: Also at University of Belgrade, Faculty of Physics and Vinca Institute of Nuclear Sciences, Belgrade, Serbia
- 68: Also at Facoltà Ingegneria, Università di Roma, Roma, Italy
- 69: Also at Argonne National Laboratory, Argonne, USA
- 70: Also at Erzincan University, Erzincan, Turkey
- 71: Also at Mimar Sinan University, Istanbul, Istanbul, Turkey
- 72: Also at Texas A&M University at Qatar, Doha, Qatar
- 73: Also at Kyungpook National University, Daegu, Korea